

A Robin-Robin splitting method for the Stokes-Biot fluid-poroelastic structure interaction model

Aashi Dalal*

Rebecca Durst^{†‡}

Annalisa Quaini[§]

Ivan Yotov[¶]

April 15, 2025

Abstract

We develop and analyze a splitting method for fluid-poroelastic structure interaction. The fluid is described using the Stokes equations and the poroelastic structure is described using the Biot equations. The transmission conditions on the interface are mass conservation, balance of stresses, and the Beavers-Joseph-Saffman condition. The splitting method involves single and decoupled Stokes and Biot solves at each time step. The subdomain problems use Robin boundary conditions on the interface, which are obtained from the transmission conditions. The Robin data is represented by an auxiliary interface variable. We prove that the method is unconditionally stable and establish that the time discretization error is $\mathcal{O}(\sqrt{T}\Delta t)$, where T is the final time and Δt is the time step. We further study the iterative version of the algorithm, which involves an iteration between the Stokes and Biot sub-problems at each time step. We prove that the iteration converges to a monolithic scheme with a Robin Lagrange multiplier used to impose the continuity of the velocity. Numerical experiments are presented to illustrate the theoretical results.

Keywords: Stokes-Biot; fluid-poroelastic structure interaction; domain decomposition; Robin interface condition.

1 Introduction

We consider the interaction of an incompressible, viscous, and Newtonian fluid with a poroelastic medium, referred to as fluid-poroelastic structure interaction (FPSI). This phenomenon occurs in a wide range of applications, including surface-groundwater flows, geomechanics, reservoir engineering, filter design, seabed-wave interaction, and arterial blood flows. The modeling leads to coupled problems that present significant mathematical and computational challenges.

We model the incompressible flow with the Stokes equations and the poroelastic medium with the Biot system [8]. In the latter, the equation describing the deformation of the elastic porous matrix is complemented with the Darcy equations that describe the average velocity and pressure of the fluid in

*Department of Mathematics, University of Pittsburgh, Pittsburgh, PA 15260, USA; email: aad100@pitt.edu.

[†]Argonne National Laboratory, Lemont, IL 60439, USA; email: rdurst@anl.gov; partially supported by the U.S. Department of Energy, Office of Science, Office of Advanced Scientific Computing Research (ASCR) program under Contract DE-AC02-06CH11357.

[‡]Department of Mathematics, University of Pittsburgh, Pittsburgh, PA 15260, USA.

[§]Department of Mathematics, University of Houston, Houston, TX 77204, USA; email: aquaini@central.uh.edu; partially supported by NSF grant DMS-1953535.

[¶]Department of Mathematics, University of Pittsburgh, Pittsburgh, PA 15260, USA; email: yotov@math.pitt.edu; partially supported by NSF grants DMS-2111129 and DMS-2410686.

the pores. The Stokes and Biot problems are coupled at the interface between the fluid and porous regions through dynamic and kinematic transmission conditions. The Stokes-Biot model combines two classical well-studied kinds of coupling: the fluid-(elastic)structure interaction (FSI) with thick structure and the Stokes–Darcy coupling. While historically the Stokes-Biot and Navier-Stokes-Biot couplings have been less studied, they have received increasing attention in recent years.

Early works on the coupled Stokes-Biot problem include [37, 44]. Well posedness of the fully dynamic model was established in [44]. In [5], both monolithic solvers and partitioned approaches based on domain decomposition methods [39] were applied to the Navier-Stokes-Biot problem, whose well-posedness with a non-mixed Darcy formulation is established in [21]. A non-iterative partitioned method based on operator splitting for the Navier-Stokes-Biot problem with non-mixed Darcy formulation was introduced in [14] and extended in [13]. The model with a mixed Darcy formulation was studied in [12]. In this formulation, the continuity of flux across the interface is a condition of essential type, which is enforced with the Nitsche’s interior penalty method. A mixed formulation for the Darcy problem in the Stokes-Biot coupling was also adopted in [3], where the the continuity of flux is imposed via a Lagrange multiplier method. A more complex Stokes-Biot problem involving a non-Newtonian fluid is considered in [1]. A finite element method for the four-field Stokes velocity-pressure and Biot displacement-pressure formulation is presented in [22]. A total pressure formulation for the Stokes-Biot problem is introduced in [40], a stress-displacement mixed elasticity formulation is studied in [35], a fully mixed formulation is developed in [19], and a HDG method is presented in [24]. An augmented finite element method for the fully mixed Navier-Stokes-Biot problem is developed in [34]. Several interesting extensions of the Stokes-Biot problem have also been proposed, including a dimensionally-reduced model for flow through fractures [15], coupling with transport [2, 45], multi-layered porous media [9], and porohyperelastic media [43]. An optimization-based decoupling method is presented in [23]. Second order in time split schemes are developed in [32, 38]. Parameter-robust preconditioners are studied in [11].

In this paper, we study a new Robin-Robin partitioned method for the Stokes-Biot problem. We employ a velocity-pressure Stokes formulation, a displacement-based elasticity formulation, and a mixed velocity-pressure Darcy formulation. The starting point is a rewriting of the coupling conditions for the Stokes-Biot problem, which state mass conservation, balance of stresses, and slip with friction (Beavers-Joseph-Saffman condition). These conditions are combined to generate two sets of Robin boundary conditions on the interface - one for the Stokes problem and the other for the Biot problem. Such approach was first utilized for FPSI in [5] and later used in [38, 43] with the motivation to alleviate the difficulty of the so-called added-mass-effect, which has been observed in FSI for certain parameter regimes [20]. This effect may cause classical Neumann-Dirichlet split methods to become unstable or the convergence of their iterative versions to deteriorate [5, 20], see also [6, 27, 28, 30, 36] for partitioned FSI schemes that address this issue. It has been shown that Robin-Robin schemes are more robust for wider ranges of physical parameters [4, 5]. The algorithm developed in this paper differs from the methods in [5, 38, 43]. It is inspired by a sequential Robin-Robin domain decomposition method for the Stokes-Darcy coupling introduced in [26]. The key ingredient in the design of the algorithm is an auxiliary vector variable used to approximate the interface Robin data, which is modeled in a suitable norm. This avoids the explicit appearance of the normal stress in the interface terms, which does not have sufficient regularity for the stability of the subdomain problems and lead to suboptimal approximation in space and time. In its non-iterative form, our FPSI algorithm requires the sequential solution of one Stokes problem and one Biot problem per time step. The appealing features of this algorithm are modularity (one can use their favorite Stokes and Biot finite element approximations), the option to use non-matching meshes, and the reduced computational cost that comes from the lack of sub-iterations. It is not unusual for non-iterative partitioned methods to have stability issues or suffer

from a loss of accuracy. We prove that our non-iterative method is unconditionally stable and establish an error estimate for the quasistatic model showing that the time discretization error is $\mathcal{O}(\sqrt{T}\Delta t)$, where T is the final time and Δt is the time step. We remark that in [5] the Robin-Robin method is only studied computationally, while in [38, 43] only stability analysis is performed. Thus, to the best of our knowledge, this is the first result in the literature on both unconditional stability and optimal time discretization error for a non-iterative Robin-Robin split scheme for FPSI.

We also present the iterative version of the algorithm, i.e., at every time step one iterates over the Stokes and Biot sub-problems until convergence. We prove that the solution of the iterative method converges to the solution of a monolithic scheme. The auxiliary interface variable converges to a Robin Lagrange multiplier used to impose weakly the velocity continuity condition. To the best of our knowledge, the resulting monolithic scheme has not been studied in the literature. We prove that a unique and stable solution to the monolithic scheme exists. While the iterative FPSI algorithm has an increased computational cost, it has the advantage of not introducing a splitting error while still allowing to recycle existing fluid and structure solvers. For the monolithic scheme instead, one needs to implement a coupled solver. We assess the convergence, robustness, and accuracy of the non-iterative and iterative Robin-Robin methods and the monolithic scheme with two benchmarks: a test that features an exact solution and a simplified blood flow problem.

We further remark that the FPSI problem is a generalization of FSI with thick structure. Therefore, the techniques developed in this paper apply to the corresponding Robin-Robin algorithm for FSI, which is also new. In recent years, alternative unconditionally stable Robin-Robin methods for FSI have been developed in [17, 18, 42], where discretization error of order $\mathcal{O}(\sqrt{\Delta t})$ is established. An improved convergence of order $\mathcal{O}(\Delta t\sqrt{T + \log \frac{1}{\Delta t}})$ is obtained in [16] for a related model in a specific geometry. Our work provides a generalization and improvement of these results.

The remaining of the paper is structured as follows. Sec. 2 describes the coupled Stokes-Biot problems. Sec. 3 presents the non-iterative Robin-Robin algorithm, whose stability analysis is carried out in Sec. 4. The time discretization error analysis for the quasistatic model is presented in Sec. 5. The iterative version of the algorithm is developed in Sec. 6. The numerical results are discussed in Sec. 7. Finally, conclusions are drawn in Sec. 8.

2 Problem setting

We consider a multiphysics model problem studied in [3] that describes the interaction of a free fluid with a flow in a deformable porous media. The spatial domain $\Omega \subset \mathbf{R}^d$, $d = 2, 3$ is the union of non-overlapping regions Ω_f and Ω_p , see Figure 1. Here, Ω_f is a free fluid region with flow governed by the Stokes equations and Ω_p is a poroelastic material governed by the Biot system. For simplicity of notation, we assume that each region is connected. The extension to non-connected regions is straightforward. Let $\Gamma_{fp} = \partial\Omega_f \cap \partial\Omega_p$ be the interface. Let (\mathbf{u}_*, p_*) be the velocity-pressure pair in Ω_* , $*$ = f , p , and let $\boldsymbol{\eta}_p$ be the displacement in Ω_p . Let $\mu_f > 0$ be the fluid viscosity, let \mathbf{f}_* be the body force terms, and let q_* be external source or sink terms. Finally, let $\mathbf{D}(\mathbf{u}_f)$ and $\boldsymbol{\sigma}_f(\mathbf{u}_f, p_f)$ denote, respectively, the deformation rate tensor and the Cauchy stress tensor:

$$\mathbf{D}(\mathbf{u}_f) = \frac{1}{2}(\nabla \mathbf{u}_f + \nabla \mathbf{u}_f^T), \quad \boldsymbol{\sigma}_f(\mathbf{u}_f, p_f) = -p_f \mathbf{I} + 2\mu_f \mathbf{D}(\mathbf{u}_f). \quad (2.1)$$

In the free fluid region Ω_f , (\mathbf{u}_f, p_f) satisfy the Stokes equations

$$\rho_f \partial_t \mathbf{u}_f - \nabla \cdot \boldsymbol{\sigma}_f(\mathbf{u}_f, p_f) = \mathbf{f}_f \quad \text{in } \Omega_f \times (0, T] \quad (2.2)$$

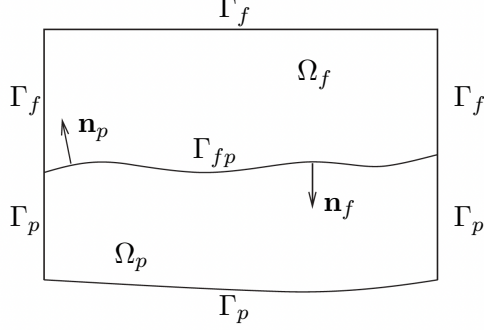


Figure 1: Schematic representation of a 2D computational domain.

$$\nabla \cdot \mathbf{u}_f = q_f \quad \text{in } \Omega_f \times (0, T], \quad (2.3)$$

where $\partial_t = \frac{\partial}{\partial t}$ and $T > 0$ is the end of the time interval of interest. Let $\boldsymbol{\sigma}_e(\boldsymbol{\eta}_p)$ and $\boldsymbol{\sigma}_p(\boldsymbol{\eta}_p, p_p)$ be the elastic and poroelastic stress tensors, respectively:

$$\boldsymbol{\sigma}_e(\boldsymbol{\eta}_p) = \lambda_p(\nabla \cdot \boldsymbol{\eta}_p)\mathbf{I} + 2\mu_p\mathbf{D}(\boldsymbol{\eta}_p), \quad \boldsymbol{\sigma}_p(\boldsymbol{\eta}_p, p_p) = \boldsymbol{\sigma}_e(\boldsymbol{\eta}_p) - \alpha p_p \mathbf{I}, \quad (2.4)$$

where $0 < \lambda_{min} \leq \lambda_p(\mathbf{x}) \leq \lambda_{max}$ and $0 < \mu_{min} \leq \mu_p(\mathbf{x}) \leq \mu_{max}$ are the Lamé parameters and $0 \leq \alpha \leq 1$ is the Biot-Willis constant. The poroelasticity region Ω_p is governed by the Biot system [8]

$$\rho_p \partial_{tt} \boldsymbol{\eta} - \nabla \cdot \boldsymbol{\sigma}_p(\boldsymbol{\eta}_p, p_p) = \mathbf{f}_p \quad \text{in } \Omega_p \times (0, T], \quad (2.5)$$

$$\mu_f K^{-1} \mathbf{u}_p + \nabla p_p = 0 \quad \text{in } \Omega_p \times (0, T], \quad (2.6)$$

$$\partial_t(s_0 p_p + \alpha \nabla \cdot \boldsymbol{\eta}_p) + \nabla \cdot \mathbf{u}_p = q_p \quad \text{in } \Omega_p \times (0, T], \quad (2.7)$$

where $\partial_{tt} = \frac{\partial^2}{\partial t^2}$, $s_0 > 0$ is a storage coefficient and K the symmetric and uniformly positive definite permeability tensor, satisfying, for some constants $0 < k_{min} \leq k_{max}$,

$$\forall \boldsymbol{\xi} \in \mathbf{R}^d, \quad k_{min} \boldsymbol{\xi}^T \boldsymbol{\xi} \leq \boldsymbol{\xi}^T K(\mathbf{x}) \boldsymbol{\xi} \leq k_{max} \boldsymbol{\xi}^T \boldsymbol{\xi}, \quad \forall \mathbf{x} \in \Omega_p.$$

Following [5, 44], the *interface conditions* on the fluid-poroelasticity interface Γ_{fp} are *mass conservation, balance of stresses*, and the Beavers-Joseph-Saffman (BJS) condition [7, 41] modeling *slip with friction*:

$$\mathbf{u}_f \cdot \mathbf{n}_f + (\partial_t \boldsymbol{\eta}_p + \mathbf{u}_p) \cdot \mathbf{n}_p = 0 \quad \text{on } \Gamma_{fp} \times (0, T], \quad (2.8)$$

$$-(\boldsymbol{\sigma}_f \mathbf{n}_f) \cdot \mathbf{n}_f = p_p, \quad \boldsymbol{\sigma}_f \mathbf{n}_f + \boldsymbol{\sigma}_p \mathbf{n}_p = 0 \quad \text{on } \Gamma_{fp} \times (0, T], \quad (2.9)$$

$$-(\boldsymbol{\sigma}_f \mathbf{n}_f) \cdot \boldsymbol{\tau}_{f,j} = \mu_f \alpha_{BJS} \sqrt{K_j^{-1}} (\mathbf{u}_f - \partial_t \boldsymbol{\eta}_p) \cdot \boldsymbol{\tau}_{f,j} \quad \text{on } \Gamma_{fp} \times (0, T], \quad (2.10)$$

where \mathbf{n}_f and \mathbf{n}_p are the outward unit normal vectors to $\partial\Omega_f$, and $\partial\Omega_p$, respectively, $\boldsymbol{\tau}_{f,j}$, $1 \leq j \leq d-1$, is an orthogonal system of unit tangent vectors on Γ_{fp} , $K_j = (K \boldsymbol{\tau}_{f,j}) \cdot \boldsymbol{\tau}_{f,j}$, and $\alpha_{BJS} \geq 0$ is an experimentally determined friction coefficient. We note that the continuity of flux (2.8) constrains the normal velocity of the solid skeleton, while the BJS condition (2.10) accounts for its tangential velocity.

The above system of equations needs to be complemented by a set of boundary and initial conditions. Let $\Gamma_f = \partial\Omega_f \cap \partial\Omega$ and $\Gamma_p = \partial\Omega_p \cap \partial\Omega$, see Figure 1. Let $\Gamma_f = \Gamma_f^D \cup \Gamma_f^N$ with $|\Gamma_f^D| > 0$ and

$\Gamma_p = \Gamma_p^D \cup \Gamma_p^N = \tilde{\Gamma}_p^D \cup \tilde{\Gamma}_p^N$. We assume for simplicity homogeneous boundary conditions: for every $t \in [0, T]$,

$$\mathbf{u}_f = \mathbf{0} \text{ on } \Gamma_f^D, \quad \boldsymbol{\sigma}_f \mathbf{n}_f = \mathbf{0} \text{ on } \Gamma_f^N, \quad \boldsymbol{\eta}_p = \mathbf{0} \text{ on } \Gamma_p^D, \quad \boldsymbol{\sigma}_p \mathbf{n}_p = \mathbf{0} \text{ on } \Gamma_p^N, \quad p_p = 0 \text{ on } \tilde{\Gamma}_p^D, \quad \mathbf{u}_p \cdot \mathbf{n}_p = 0 \text{ on } \tilde{\Gamma}_p^N.$$

To simplify the characterization of the space for the trace $\mathbf{u}_f|_{\Gamma_{fp}}$, we assume that Γ_f^D is not adjacent to Γ_{fp} . In the case when they touch, the boundary condition $\mathbf{u}_f = \mathbf{0}$ on Γ_f^D needs to be imposed weakly by introducing a Lagrange multiplier $\varphi = \boldsymbol{\sigma}_f \mathbf{n}_f$ on Γ_f^D . We omit further details for this case. Finally, we set the initial conditions

$$\mathbf{u}_f(\mathbf{x}, 0) = \mathbf{u}_{f,0} \text{ in } \Omega_f, \quad p_p(\mathbf{x}, 0) = p_{p,0}(\mathbf{x}), \quad \boldsymbol{\eta}_p(\mathbf{x}, 0) = \boldsymbol{\eta}_{p,0}(\mathbf{x}), \quad \partial_t \boldsymbol{\eta}_p(\mathbf{x}, 0) = \mathbf{u}_{s,0}(\mathbf{x}) \text{ in } \Omega_p. \quad (2.11)$$

Compatible initial data $p_{f,0}$ for $p_f(0)$ and $\mathbf{u}_{p,0}$ for $\mathbf{u}_p(0)$ can be obtained by solving at $t = 0$ a sequence of single-physics sub-problems satisfying the interface conditions (2.8)–(2.10), see [1].

The solvability of the fully dynamic Stokes-Biot system with compressible Stokes fluid was discussed in [44]. The well posedness analysis of the incompressible quasistatic system has been carried out in [1]. The proof extends easily to the fully dynamic incompressible system (2.2)–(2.10) considered here.

Let $(\cdot, \cdot)_S$, $S \subset \mathbf{R}^d$, be the $L^2(S)$ inner product and let $\langle \cdot, \cdot \rangle_F$, $F \subset \mathbf{R}^{d-1}$, be the $L^2(F)$ inner product or duality pairing. We will use the standard notation for Sobolev spaces, see, e.g. [25]. Let

$$\begin{aligned} \mathbf{V}_f &= \{\mathbf{v}_f \in (H^1(\Omega_f))^d : \mathbf{v}_f = \mathbf{0} \text{ on } \Gamma_f^D\}, & W_f &= L^2(\Omega_f), \\ \mathbf{V}_p &= \{\mathbf{v}_p \in H(\text{div}; \Omega_p) : \mathbf{v}_p \cdot \mathbf{n}_p|_{\Gamma_{fp}} \in L^2(\Gamma_{fp}) \text{ and } \mathbf{v}_p \cdot \mathbf{n}_p = 0 \text{ on } \tilde{\Gamma}_p^N\}, & W_p &= L^2(\Omega_p), \\ \mathbf{X}_p &= \{\boldsymbol{\xi}_p \in H^1(\Omega_p)^d : \boldsymbol{\xi}_p = \mathbf{0} \text{ on } \Gamma_p^D\}, \end{aligned} \quad (2.12)$$

where $H(\text{div}; \Omega_p)$ is the space of $(L^2(\Omega_p))^d$ -vectors with divergence in $L^2(\Omega_p)$ with a norm

$$\|\mathbf{v}\|_{H(\text{div}; \Omega_p)}^2 = \|\mathbf{v}\|_{L^2(\Omega_p)}^2 + \|\nabla \cdot \mathbf{v}\|_{L^2(\Omega_p)}^2,$$

and the space \mathbf{V}_p is equipped with the norm

$$\|\mathbf{v}\|_{\mathbf{V}_p}^2 = \|\mathbf{v}\|_{H(\text{div}; \Omega_p)}^2 + \|\mathbf{v} \cdot \mathbf{n}_p\|_{L^2(\Gamma_{fp})}^2. \quad (2.13)$$

3 Robin-Robin non-iterative partitioned algorithm

For the solution of the coupled problem presented in Section 2, we consider a Robin-Robin splitting algorithm motivated by the method proposed in [5]. For this, we rewrite the coupling conditions (2.8)–(2.10) in the equivalent form of Robin conditions. To simplify the notation, consider a single tangential vector $\boldsymbol{\tau}$ and let $\gamma_{BJS} = \sqrt{K_\tau}/(\mu_f \alpha_{BJS})$. Let $\gamma_f > 0$ and $\gamma_p > 0$ be given combination parameters. For the fluid subproblem, we consider the following Robin transmission conditions

$$\gamma_f \mathbf{u}_f \cdot \mathbf{n}_f + (\boldsymbol{\sigma}_f \mathbf{n}_f) \cdot \mathbf{n}_f = -\gamma_f (\partial_t \boldsymbol{\eta}_p + \mathbf{u}_p) \cdot \mathbf{n}_p + (\boldsymbol{\sigma}_p \mathbf{n}_p) \cdot \mathbf{n}_p, \quad (3.1a)$$

$$\gamma_f \mathbf{u}_f \cdot \boldsymbol{\tau}_f + (1 + \gamma_f \gamma_{BJS}) (\boldsymbol{\sigma}_f \mathbf{n}_f) \cdot \boldsymbol{\tau}_f = -\gamma_f \partial_t \boldsymbol{\eta}_p \cdot \boldsymbol{\tau}_p + (\boldsymbol{\sigma}_p \mathbf{n}_p) \cdot \boldsymbol{\tau}_p, \quad (3.1b)$$

while the transmission conditions for the poroelastic structure are

$$\gamma_p (\mathbf{u}_p + \partial_t \boldsymbol{\eta}_p) \cdot \mathbf{n}_p + (\boldsymbol{\sigma}_p \mathbf{n}_p) \cdot \mathbf{n}_p = -\gamma_p \mathbf{u}_f \cdot \mathbf{n}_f + (\boldsymbol{\sigma}_f \mathbf{n}_f) \cdot \mathbf{n}_f, \quad (3.2a)$$

$$\gamma_p \partial_t \boldsymbol{\eta}_p \cdot \boldsymbol{\tau}_p + (\boldsymbol{\sigma}_p \mathbf{n}_p) \cdot \boldsymbol{\tau}_p = -\gamma_p \mathbf{u}_f \cdot \boldsymbol{\tau}_f + (1 - \gamma_p \gamma_{BJS}) (\boldsymbol{\sigma}_f \mathbf{n}_f) \cdot \boldsymbol{\tau}_f, \quad (3.2b)$$

$$\gamma_p(\mathbf{u}_p + \partial_t \boldsymbol{\eta}_p) \cdot \mathbf{n}_p - p_p = -\gamma_p \mathbf{u}_f \cdot \mathbf{n}_f + (\boldsymbol{\sigma}_f \mathbf{n}_f) \cdot \mathbf{n}_f. \quad (3.2c)$$

To simplify the notation, let

$$\begin{aligned} a_f(\mathbf{u}_f, \mathbf{v}_f) &= (2\mu_f \mathbf{D}(\mathbf{u}_f), \mathbf{D}(\mathbf{v}_f))_{\Omega_f}, \\ a_p^d(\mathbf{u}_p, \mathbf{v}_p) &= (\mu_f K^{-1} \mathbf{u}_p, \mathbf{v}_p)_{\Omega_p}, \\ a_p^e(\boldsymbol{\eta}_p, \boldsymbol{\xi}_p) &= (2\mu_p \mathbf{D}(\boldsymbol{\eta}_p), \mathbf{D}(\boldsymbol{\xi}_p))_{\Omega_p} + (\lambda_p \nabla \cdot \boldsymbol{\eta}_p, \nabla \cdot \boldsymbol{\xi}_p)_{\Omega_p} \end{aligned}$$

be the bilinear forms related to Stokes, Darcy, and the elasticity operators, respectively. Let

$$b_*(\mathbf{v}, w) = -(\nabla \cdot \mathbf{v}, w)_{\Omega_*}.$$

Using standard techniques involving multiplication by suitable test functions and integration by parts, as well as the interface transmission conditions (3.1)–(3.2), we obtain that the solution of the system (2.2)–(2.10), $(\mathbf{u}_f, p_f, \boldsymbol{\eta}_p, \mathbf{u}_p, p_p) : [0, T] \rightarrow \mathbf{V}_f \times W_f \times \mathbf{X}_p \times \mathbf{V}_p \times W_p$ satisfies the following variational formulation for each $t \in (0, T]$ and for all $(\mathbf{v}_f, w_f, \boldsymbol{\xi}_p, \mathbf{v}_p, w_p) \in \mathbf{V}_f \times W_f \times \mathbf{X}_p \times \mathbf{V}_p \times W_p$:

$$\begin{aligned} &(\rho_f \partial_t \mathbf{u}_f, \mathbf{v}_f)_{\Omega_f} + a_f(\mathbf{u}_f, \mathbf{v}_f) + b_f(\mathbf{v}_f, p_f) + \gamma_f \langle \mathbf{u}_f \cdot \mathbf{n}_f, \mathbf{v}_f \cdot \mathbf{n}_f \rangle_{\Gamma_{fp}} + \gamma_f \langle \mathbf{u}_f \cdot \boldsymbol{\tau}_f, \mathbf{v}_f \cdot \boldsymbol{\tau}_f \rangle_{\Gamma_{fp}} \\ &= (\mathbf{f}_f, \mathbf{v}_f)_{\Omega_f} - \gamma_f \langle (\partial_t \boldsymbol{\eta}_p + \mathbf{u}_p) \cdot \mathbf{n}_p, \mathbf{v}_f \cdot \mathbf{n}_f \rangle_{\Gamma_{fp}} + \langle (\boldsymbol{\sigma}_p \mathbf{n}_p) \cdot \mathbf{n}_p, \mathbf{v}_f \cdot \mathbf{n}_f \rangle_{\Gamma_{fp}} \\ &\quad - \gamma_f \langle \partial_t \boldsymbol{\eta}_p \cdot \boldsymbol{\tau}_p, \mathbf{v}_f \cdot \boldsymbol{\tau}_f \rangle_{\Gamma_{fp}} + \langle (\boldsymbol{\sigma}_p \mathbf{n}_p) \cdot \boldsymbol{\tau}_p, \mathbf{v}_f \cdot \boldsymbol{\tau}_f \rangle_{\Gamma_{fp}} - \gamma_f \gamma_{BJS} \langle (\boldsymbol{\sigma}_f \mathbf{n}_f) \cdot \boldsymbol{\tau}_f, \mathbf{v}_f \cdot \boldsymbol{\tau}_f \rangle_{\Gamma_{fp}}, \quad (3.3) \end{aligned}$$

$$- b_f(\mathbf{u}_f, w_f) = (q_f, w_f)_{\Omega_f}, \quad (3.4)$$

$$\begin{aligned} &(\rho_p \partial_{tt} \boldsymbol{\eta}_p, \boldsymbol{\xi}_p)_{\Omega_p} + a_p^e(\boldsymbol{\eta}_p, \boldsymbol{\xi}_p) + a_p^d(\mathbf{u}_p, \mathbf{v}_p) + \alpha b_p(\boldsymbol{\xi}_p, p_p) + b_p(\mathbf{v}_p, p_p) \\ &\quad + \gamma_p \langle (\mathbf{u}_p + \partial_t \boldsymbol{\eta}_p) \cdot \mathbf{n}_p, (\mathbf{v}_p + \boldsymbol{\xi}_p) \cdot \mathbf{n}_p \rangle_{\Gamma_{fp}} + \gamma_p \langle \partial_t \boldsymbol{\eta}_p \cdot \boldsymbol{\tau}_p, \boldsymbol{\xi}_p \cdot \boldsymbol{\tau}_p \rangle_{\Gamma_{fp}} \\ &= (\mathbf{f}_p, \boldsymbol{\xi}_p)_{\Omega_p} + \langle (-\gamma_p \mathbf{u}_f + \boldsymbol{\sigma}_f \mathbf{n}_f) \cdot \mathbf{n}_f, (\mathbf{v}_p + \boldsymbol{\xi}_p) \cdot \mathbf{n}_p \rangle_{\Gamma_{fp}} \\ &\quad - \gamma_p \langle \mathbf{u}_f \cdot \boldsymbol{\tau}_f, \boldsymbol{\xi}_p \cdot \boldsymbol{\tau}_p \rangle_{\Gamma_{fp}} + (1 - \gamma_p \gamma_{BJS}) \langle (\boldsymbol{\sigma}_f \mathbf{n}_f) \cdot \boldsymbol{\tau}_f, \boldsymbol{\xi}_p \cdot \boldsymbol{\tau}_p \rangle_{\Gamma_{fp}}, \quad (3.5) \end{aligned}$$

$$s_0(\partial_t p_p, w_p)_{\Omega_p} - \alpha b_p(\partial_t \boldsymbol{\eta}_p, w_p) - b_p(\mathbf{u}_p, w_p) = (q_p, w_p)_{\Omega_p}. \quad (3.6)$$

In the above, we assume that the solution to (2.2)–(2.10) is sufficiently smooth, so that all interface bilinear forms are continuous.

Let $\mathcal{T}_{f,h}$ and $\mathcal{T}_{p,h}$ be shape-regular finite element partitions of Ω_f and Ω_p , respectively, consisting of affine elements with maximal diameter h . The two meshes may not match along Γ_{fp} . For the space discretization we consider a stable Stokes finite element pair $\mathbf{V}_{f,h} \times W_{f,h} \subset \mathbf{V}_f \times W_f$, a finite element space $\mathbf{X}_{p,h} \subset \mathbf{X}_p$ for the displacement, and any stable Darcy pair $\mathbf{V}_{p,h} \times W_{p,h} \subset \mathbf{V}_p \times W_p$. Examples include the Taylor-Hood or the MINI elements for $\mathbf{V}_{f,h} \times W_{f,h}$, continuous piecewise polynomials for $\mathbf{X}_{p,h}$ and the Raviart-Thomas or the Brezzi-Douglas-Marini elements for $\mathbf{V}_{p,h} \times W_{p,h}$. See [10] for further details.

Remark 3.1. In the following, in order to simplify the notation, we suppress the subscript h from the variables.

For the time discretization, we consider a uniform partition of $[0, T]$ with time step $\Delta t = T/N$ and $t_n = n\Delta t$, $n = 0, \dots, N$. Let $\varphi^n = \varphi(t_n)$. For $n \geq 0$, let $d_t \varphi^{n+1} := (\varphi^{n+1} - \varphi^n)/\Delta t$. Let $d_{tt} \boldsymbol{\eta}_p^{n+1} := d_t d_t \boldsymbol{\eta}_p^{n+1} = (d_t \boldsymbol{\eta}_p^{n+1} - d_t \boldsymbol{\eta}_p^n)/\Delta t$ for $n \geq 0$. Note that $d_{tt} \boldsymbol{\eta}_p^{n+1} = (\boldsymbol{\eta}_p^{n+1} - 2\boldsymbol{\eta}_p^n + \boldsymbol{\eta}_p^{n-1})/\Delta t^2$ for $n \geq 1$, while for $n = 0$, $d_t \boldsymbol{\eta}_p^0 := P_X \mathbf{u}_{s,0}$, using the initial condition (2.11), where $P_X : (L^2(\Omega_p))^d \rightarrow \mathbf{X}_p$ is the L^2 -orthogonal projection.

Next, we present a time-splitting Robin-Robin algorithm that is similar to the iterative scheme introduced in [5]. At every time t^{n+1} , $n = 0, \dots, N - 1$, the Robin-Robin algorithm involves solving decoupled fluid and poroelastic structure sub-problems:

1. Stokes problem: find $(\mathbf{u}_f^{n+1}, p_f^{n+1}) \in \mathbf{V}_{f,h} \times W_{f,h}$ such that for all $(\mathbf{v}_f, w_f) \in \mathbf{V}_{f,h} \times W_{f,h}$,

$$\begin{aligned} & (\rho_f d_t \mathbf{u}_f^{n+1}, \mathbf{v}_f)_{\Omega_f} + a_f(\mathbf{u}_f^{n+1}, \mathbf{v}_f) + b_f(\mathbf{v}_f, p_f^{n+1}) + \gamma_f \langle \mathbf{u}_f^{n+1} \cdot \mathbf{n}_f, \mathbf{v}_f \cdot \mathbf{n}_f \rangle_{\Gamma_{fp}} + \gamma_f \langle \mathbf{u}_f^{n+1} \cdot \boldsymbol{\tau}_f, \mathbf{v}_f \cdot \boldsymbol{\tau}_f \rangle_{\Gamma_{fp}} \\ &= (\mathbf{f}_f, \mathbf{v}_f)_{\Omega_f} - \gamma_f \langle (d_t \boldsymbol{\eta}_p^n + \mathbf{u}_p^n) \cdot \mathbf{n}_p, \mathbf{v}_f \cdot \mathbf{n}_f \rangle_{\Gamma_{fp}} + \langle (\boldsymbol{\sigma}_p^n \mathbf{n}_p) \cdot \mathbf{n}_p, \mathbf{v}_f \cdot \mathbf{n}_f \rangle_{\Gamma_{fp}} \\ &\quad - \gamma_f \langle d_t \boldsymbol{\eta}_p^n \cdot \boldsymbol{\tau}_p, \mathbf{v}_f \cdot \boldsymbol{\tau}_f \rangle_{\Gamma_{fp}} + \langle (\boldsymbol{\sigma}_p^n \mathbf{n}_p) \cdot \boldsymbol{\tau}_p, \mathbf{v}_f \cdot \boldsymbol{\tau}_f \rangle_{\Gamma_{fp}} - \gamma_f \gamma_{BJS} \langle (\boldsymbol{\sigma}_f^n \mathbf{n}_f) \cdot \boldsymbol{\tau}_f, \mathbf{v}_f \cdot \boldsymbol{\tau}_f \rangle_{\Gamma_{fp}}, \end{aligned} \quad (3.7)$$

$$- b_f(\mathbf{u}_f^{n+1}, w_f) = (q_f, w_f)_{\Omega_f}, \quad (3.8)$$

which corresponds to the finite element approximation of the weak formulation of problem (2.2)–(2.3) supplemented with the following Robin boundary conditions on Γ_{fp} :

$$\gamma_f \mathbf{u}_f^{n+1} \cdot \mathbf{n}_f + (\boldsymbol{\sigma}_f^{n+1} \mathbf{n}_f) \cdot \mathbf{n}_f = -\gamma_f (d_t \boldsymbol{\eta}_p^n + \mathbf{u}_p^n) \cdot \mathbf{n}_p + (\boldsymbol{\sigma}_p^n \mathbf{n}_p) \cdot \mathbf{n}_p, \quad (3.9a)$$

$$\gamma_f \mathbf{u}_f^{n+1} \cdot \boldsymbol{\tau}_f + (\boldsymbol{\sigma}_f^{n+1} \mathbf{n}_f) \cdot \boldsymbol{\tau}_f + \gamma_f \gamma_{BJS} (\boldsymbol{\sigma}_f^n \mathbf{n}_f) \cdot \boldsymbol{\tau}_f = -\gamma_f d_t \boldsymbol{\eta}_p^n \cdot \boldsymbol{\tau}_p + (\boldsymbol{\sigma}_p^n \mathbf{n}_p) \cdot \boldsymbol{\tau}_p. \quad (3.9b)$$

It is obtained by applying the backward Euler time discretization to (3.3)–(3.4) and time-lagging the interface quantities from the Biot region as well as the term $\gamma_f \gamma_{BJS} (\boldsymbol{\sigma}_f \mathbf{n}_f) \cdot \boldsymbol{\tau}_f$.

Using the initial conditions (2.11), at $n = 0$ we set $\phi^0 := P_\phi \phi_0$ for any variable ϕ , where P_ϕ is the L^2 -orthogonal projection onto the corresponding finite element space and $\boldsymbol{\sigma}_f^0$ and $\boldsymbol{\sigma}_p^0$ are obtained from (2.1) and (2.4), respectively. We also recall that $d_t \boldsymbol{\eta}_p^0 = P_X \mathbf{u}_{s,0}$.

2. Biot problem: find $(\boldsymbol{\eta}_p^{n+1}, \mathbf{u}_p^{n+1}, p_p^{n+1}) \in \mathbf{X}_{p,h} \times \mathbf{V}_{p,h} \times W_{p,h}$ such that for all $(\boldsymbol{\xi}_p, \mathbf{v}_p, w_p) \in \mathbf{X}_{p,h} \times \mathbf{V}_{p,h} \times W_{p,h}$,

$$\begin{aligned} & (\rho_p d_{tt} \boldsymbol{\eta}_p^{n+1}, \boldsymbol{\xi}_p)_{\Omega_p} + a_p^e(\boldsymbol{\eta}_p^{n+1}, \boldsymbol{\xi}_p) + a_p^d(\mathbf{u}_p^{n+1}, \mathbf{v}_p) + \alpha b_p(\boldsymbol{\xi}_p, p_p^{n+1}) + b_p(\mathbf{v}_p, p_p^{n+1}) \\ &\quad + \gamma_p \langle (\mathbf{u}_p^{n+1} + d_t \boldsymbol{\eta}_p^{n+1}) \cdot \mathbf{n}_p, (\mathbf{v}_p + \boldsymbol{\xi}_p) \cdot \mathbf{n}_p \rangle_{\Gamma_{fp}} + \gamma_p \langle d_t \boldsymbol{\eta}_p^{n+1} \cdot \boldsymbol{\tau}_p, \boldsymbol{\xi}_p \cdot \boldsymbol{\tau}_p \rangle_{\Gamma_{fp}} \\ &= (\mathbf{f}_p, \boldsymbol{\xi}_p)_{\Omega_p} + \langle (-\gamma_p \mathbf{u}_f^{n+1} + \boldsymbol{\sigma}_f^{n+1} \mathbf{n}_f) \cdot \mathbf{n}_f, (\mathbf{v}_p + \boldsymbol{\xi}_p) \cdot \mathbf{n}_p \rangle_{\Gamma_{fp}} \\ &\quad - \gamma_p \langle \mathbf{u}_f^{n+1} \cdot \boldsymbol{\tau}_f, \boldsymbol{\xi}_p \cdot \boldsymbol{\tau}_p \rangle_{\Gamma_{fp}} + (1 - \gamma_p \gamma_{BJS}) \langle (\boldsymbol{\sigma}_f^{n+1} \mathbf{n}_f) \cdot \boldsymbol{\tau}_f, \boldsymbol{\xi}_p \cdot \boldsymbol{\tau}_p \rangle_{\Gamma_{fp}}, \end{aligned} \quad (3.10)$$

$$s_0(d_t p_p^{n+1}, w_p)_{\Omega_p} - \alpha b_p(d_t \boldsymbol{\eta}_p^{n+1}, w_p) - b_p(\mathbf{u}_p^{n+1}, w_p) = (q_p, w_p)_{\Omega_p}, \quad (3.11)$$

which corresponds to the finite element approximation of the weak formulation of problem (2.6)–(2.7) supplemented with the following Robin boundary conditions on Γ_{fp} :

$$\gamma_p (\mathbf{u}_p^{n+1} + d_t \boldsymbol{\eta}_p^{n+1}) \cdot \mathbf{n}_p + (\boldsymbol{\sigma}_p^{n+1} \mathbf{n}_p) \cdot \mathbf{n}_p = -\gamma_p \mathbf{u}_f^{n+1} \cdot \mathbf{n}_f + (\boldsymbol{\sigma}_f^{n+1} \mathbf{n}_f) \cdot \mathbf{n}_f, \quad (3.12a)$$

$$\gamma_p d_t \boldsymbol{\eta}_p^{n+1} \cdot \boldsymbol{\tau}_p + (\boldsymbol{\sigma}_p^{n+1} \mathbf{n}_p) \cdot \boldsymbol{\tau}_p = -\gamma_p \mathbf{u}_f^{n+1} \cdot \boldsymbol{\tau}_f + (1 - \gamma_p \gamma_{BJS}) (\boldsymbol{\sigma}_f^{n+1} \mathbf{n}_f) \cdot \boldsymbol{\tau}_f, \quad (3.12b)$$

$$\gamma_p (\mathbf{u}_p^{n+1} + d_t \boldsymbol{\eta}_p^{n+1}) \cdot \mathbf{n}_p - p_p^{n+1} = -\gamma_p \mathbf{u}_f^{n+1} \cdot \mathbf{n}_f + (\boldsymbol{\sigma}_f^{n+1} \mathbf{n}_f) \cdot \mathbf{n}_f. \quad (3.12c)$$

It is obtained by applying the backward Euler time discretization to (3.5)–(3.6) and using the interface quantities from the Stokes region obtained in the previous Stokes solve.

We note that the above algorithm involves $\boldsymbol{\sigma}_f \mathbf{n}_f$ and $\boldsymbol{\sigma}_p \mathbf{n}_p$ on Γ_{fp} , which in the continuous setting may not belong to $L^2(\Gamma_{fp})$, while in the finite element method they require postprocessing from the primary variables and may result in loss of accuracy. Moreover, the algorithm is difficult to analyze in this form. Motivated by the Robin-Robin iterative algorithm for the coupled Stokes-Darcy flow problem developed in [26], we consider the following modified algorithm.

Let $\mathcal{T}_{fp,h}$ be the partition of Γ_{fp} obtained from the trace of $\mathcal{T}_{f,h}$. Let $\Lambda_h \subset (L^2(\Gamma_{fp}))^d$ be a finite element space on $\mathcal{T}_{fp,h}$ defined as

$$\Lambda_h := \mathbf{V}_{f,h}|_{\Gamma_{fp}}. \quad (3.13)$$

For $0 \leq n \leq N$, we introduce an auxiliary interface variable $\mu^n = (\mu_n^n, \mu_\tau^n) \in \Lambda_h$, where $\mu_n^n = \mu^n \cdot \mathbf{n}_f$ and $\mu_\tau^n = \mu^n \cdot \boldsymbol{\tau}_f$ are used to approximate the Robin data on Γ_{fp} . In particular,

$$\mu_n^n \simeq -\gamma_f (d_t \boldsymbol{\eta}_p^n + \mathbf{u}_p^n) \cdot \mathbf{n}_p + (\boldsymbol{\sigma}_p^n \mathbf{n}_p) \cdot \mathbf{n}_p, \quad (3.14a)$$

$$\mu_\tau^n \simeq -\gamma_f d_t \boldsymbol{\eta}_p^n \cdot \boldsymbol{\tau}_p + (\boldsymbol{\sigma}_p^n \mathbf{n}_p) \cdot \boldsymbol{\tau}_p - \gamma_f \gamma_{BJS} (\boldsymbol{\sigma}_f^n \mathbf{n}_f) \cdot \boldsymbol{\tau}_f. \quad (3.14b)$$

The Robin-Robin non-iterative partitioned algorithm is as follows.

Algorithm 1.

Let, for all $\chi \in \Lambda_h$,

$$\begin{aligned} \langle \mu_n^0, \chi_n \rangle_{\Gamma_{fp}} &= \langle -\gamma_f (d_t \boldsymbol{\eta}_p^0 + \mathbf{u}_p^0) \cdot \mathbf{n}_p + \boldsymbol{\sigma}_p^0 \mathbf{n}_p \cdot \mathbf{n}_p, \chi_n \rangle_{\Gamma_{fp}}, \\ \langle \mu_\tau^0, \chi_\tau \rangle_{\Gamma_{fp}} &= \langle -\gamma_f d_t \boldsymbol{\eta}_p^0 \cdot \boldsymbol{\tau}_p + \boldsymbol{\sigma}_p^0 \mathbf{n}_p \cdot \boldsymbol{\tau}_p - \gamma_f \gamma_{BJS} (\boldsymbol{\sigma}_f^0 \mathbf{n}_f) \cdot \boldsymbol{\tau}_f, \chi_\tau \rangle_{\Gamma_{fp}}, \end{aligned}$$

where we assume that the initial data is sufficiently smooth.

In the above, and in the following, we write the two equations separately for clarity, with the understanding that they represent a single equation for μ^0 , i.e., the sum of the two equations holds.

For $n = 0, \dots, N-1$, solve

1. Stokes problem: find $(\mathbf{u}_f^{n+1}, p_f^{n+1}) \in \mathbf{V}_{f,h} \times W_{f,h}$ such that for all $(\mathbf{v}_f, w_f) \in \mathbf{V}_{f,h} \times W_{f,h}$,

$$\begin{aligned} &\left(\rho_f d_t \mathbf{u}_f^{n+1}, \mathbf{v}_f \right)_{\Omega_f} + a_f(\mathbf{u}_f^{n+1}, \mathbf{v}_f) + b_f(\mathbf{v}_f, p_f^{n+1}) + \gamma_f \langle \mathbf{u}_f^{n+1} \cdot \mathbf{n}_f, \mathbf{v}_f \cdot \mathbf{n}_f \rangle_{\Gamma_{fp}} \\ &+ \gamma_f \langle \mathbf{u}_f^{n+1} \cdot \boldsymbol{\tau}_f, \mathbf{v}_f \cdot \boldsymbol{\tau}_f \rangle_{\Gamma_{fp}} = (\mathbf{f}_f, \mathbf{v}_f)_{\Omega_f} + \langle \mu_n^n, \mathbf{v}_f \cdot \mathbf{n}_f \rangle_{\Gamma_{fp}} + \langle \mu_\tau^n, \mathbf{v}_f \cdot \boldsymbol{\tau}_f \rangle_{\Gamma_{fp}} \end{aligned} \quad (3.15)$$

$$- b_f(\mathbf{u}_f^{n+1}, w_f) = (q_f, w_f)_{\Omega_f}, \quad (3.16)$$

which corresponds to the weak imposition of the Robin boundary conditions on Γ_{fp} :

$$\gamma_f \mathbf{u}_f^{n+1} \cdot \mathbf{n}_f + (\boldsymbol{\sigma}_f^{n+1} \mathbf{n}_f) \cdot \mathbf{n}_f = \mu_n^n, \quad (3.17a)$$

$$\gamma_f \mathbf{u}_f^{n+1} \cdot \boldsymbol{\tau}_f + (\boldsymbol{\sigma}_f^{n+1} \mathbf{n}_f) \cdot \boldsymbol{\tau}_f = \mu_\tau^n. \quad (3.17b)$$

2. Biot problem: find $(\boldsymbol{\eta}_p^{n+1}, \mathbf{u}_p^{n+1}, p_p^{n+1}) \in \mathbf{X}_{p,h}, \mathbf{V}_{p,h}, W_{p,h}$ such that for all $(\boldsymbol{\xi}_p, \mathbf{v}_p, w_p) \in \mathbf{X}_{p,h} \times \mathbf{V}_{p,h} \times W_{p,h}$,

$$\begin{aligned} &\left(\rho_p d_{tt} \boldsymbol{\eta}_p^{n+1}, \boldsymbol{\xi}_p \right)_{\Omega_p} + a_p^e(\boldsymbol{\eta}_p^{n+1}, \boldsymbol{\xi}_p) + a_p^d(\mathbf{u}_p^{n+1}, \mathbf{v}_p) + \alpha b_p(\boldsymbol{\xi}_p, p_p^{n+1}) + b_p(\mathbf{v}_p, p_p^{n+1}) \\ &+ \gamma_p \langle (\mathbf{u}_p^{n+1} + d_t \boldsymbol{\eta}_p^{n+1}) \cdot \mathbf{n}_p, (\mathbf{v}_p + \boldsymbol{\xi}_p) \cdot \mathbf{n}_p \rangle_{\Gamma_{fp}} + \gamma_p \langle d_t \boldsymbol{\eta}_p^{n+1} \cdot \boldsymbol{\tau}_p, \boldsymbol{\xi}_p \cdot \boldsymbol{\tau}_p \rangle_{\Gamma_{fp}} \\ &= (\mathbf{f}_p, \boldsymbol{\xi}_p)_{\Omega_p} + \langle \mu_n^n - (\gamma_p + \gamma_f) \mathbf{u}_f^{n+1} \cdot \mathbf{n}_f, (\mathbf{v}_p + \boldsymbol{\xi}_p) \cdot \mathbf{n}_p \rangle_{\Gamma_{fp}} \\ &+ \left\langle \mu_\tau^n - (\gamma_p + \gamma_f) \mathbf{u}_f^{n+1} \cdot \boldsymbol{\tau}_f - \gamma_p \gamma_{BJS} (\boldsymbol{\sigma}_f^{n+1} \mathbf{n}_f) \cdot \boldsymbol{\tau}_f, \boldsymbol{\xi}_p \cdot \boldsymbol{\tau}_p \right\rangle_{\Gamma_{fp}}, \end{aligned} \quad (3.18)$$

$$s_0(d_t p_p^{n+1}, w_p)_{\Omega_p} - \alpha b_p(d_t \boldsymbol{\eta}_p^{n+1}, w_p) - b_p(\mathbf{u}_p^{n+1}, w_p) = (q_p, w_p)_{\Omega_p}, \quad (3.19)$$

which corresponds to the weak imposition of the Robin boundary conditions on Γ_{fp} :

$$\gamma_p (\mathbf{u}_p^{n+1} + d_t \boldsymbol{\eta}_p^{n+1}) \cdot \mathbf{n}_p + (\boldsymbol{\sigma}_p^{n+1} \mathbf{n}_p) \cdot \mathbf{n}_p = \mu_n^n - (\gamma_p + \gamma_f) \mathbf{u}_f^{n+1} \cdot \mathbf{n}_f$$

$$= -\gamma_p \mathbf{u}_f^{n+1} \cdot \mathbf{n}_f + (\boldsymbol{\sigma}_f^{n+1} \mathbf{n}_f) \cdot \mathbf{n}_f, \quad (3.20a)$$

$$\begin{aligned} \gamma_p d_t \boldsymbol{\eta}_p^{n+1} \cdot \boldsymbol{\tau}_p + (\boldsymbol{\sigma}_p^{n+1} \mathbf{n}_p) \cdot \boldsymbol{\tau}_p &= \mu_\tau^n - (\gamma_p + \gamma_f) \mathbf{u}_f^{n+1} \cdot \boldsymbol{\tau}_f - \gamma_p \gamma_{BJS} (\boldsymbol{\sigma}_f^{n+1} \mathbf{n}_f) \cdot \boldsymbol{\tau}_f \\ &= -\gamma_p \mathbf{u}_f^{n+1} \cdot \boldsymbol{\tau}_f + (1 - \gamma_p \gamma_{BJS}) (\boldsymbol{\sigma}_f^{n+1} \mathbf{n}_f) \cdot \boldsymbol{\tau}_f, \end{aligned} \quad (3.20b)$$

$$\begin{aligned} \gamma_p (\mathbf{u}_p^{n+1} + d_t \boldsymbol{\eta}_p^{n+1}) \cdot \mathbf{n}_p - p_p^{n+1} &= \mu_n^n - (\gamma_p + \gamma_f) \mathbf{u}_f^{n+1} \cdot \mathbf{n}_f \\ &= -\gamma_p \mathbf{u}_f^{n+1} \cdot \mathbf{n}_f + (\boldsymbol{\sigma}_f^{n+1} \mathbf{n}_f) \cdot \mathbf{n}_f, \end{aligned} \quad (3.20c)$$

where the second equalities in (3.20a) and (3.20c) are obtained from (3.17a) and the second equality in (3.20b) is obtained from (3.17b).

3. Update: for all $\chi \in \Lambda_h$,

$$\langle \mu_n^{n+1}, \chi_n \rangle_{\Gamma_{fp}} = \langle \mu_n^n - (\gamma_f + \gamma_p)((d_t \boldsymbol{\eta}_p^{n+1} + \mathbf{u}_p^{n+1}) \cdot \mathbf{n}_p + \mathbf{u}_f^{n+1} \cdot \mathbf{n}_f), \chi_n \rangle_{\Gamma_{fp}}, \quad (3.21a)$$

$$\langle \mu_\tau^{n+1}, \chi_\tau \rangle_{\Gamma_{fp}} = \langle \mu_\tau^n - (\gamma_f + \gamma_p)(d_t \boldsymbol{\eta}_p^{n+1} \cdot \boldsymbol{\tau}_p + \mathbf{u}_f^{n+1} \cdot \boldsymbol{\tau}_f + \gamma_{BJS} (\boldsymbol{\sigma}_f^{n+1} \mathbf{n}_f) \cdot \boldsymbol{\tau}_f), \chi_\tau \rangle_{\Gamma_{fp}}. \quad (3.21b)$$

End of Algorithm 1.

Remark 3.2. Equations (3.21), combined with the first equalities in (3.20a) and (3.20b), imply that

$$\mu_n^{n+1} \simeq -\gamma_f (d_t \boldsymbol{\eta}_p^{n+1} + \mathbf{u}_p^{n+1}) \cdot \mathbf{n}_p + (\boldsymbol{\sigma}_p^{n+1} \mathbf{n}_p) \cdot \mathbf{n}_p, \quad (3.22a)$$

$$\mu_\tau^{n+1} \simeq -\gamma_f d_t \boldsymbol{\eta}_p^{n+1} \cdot \boldsymbol{\tau}_p + (\boldsymbol{\sigma}_p^{n+1} \mathbf{n}_p) \cdot \boldsymbol{\tau}_p - \gamma_f \gamma_{BJS} (\boldsymbol{\sigma}_f^{n+1} \mathbf{n}_f) \cdot \boldsymbol{\tau}_f. \quad (3.22b)$$

Remark 3.3. The second equalities in (3.20) indicate that the Robin conditions (3.12) are weakly imposed in the Biot sub-problem. The expressions (3.22a), combined with (3.17) indicate that the Robin conditions (3.9) are weakly imposed in the Stokes sub-problem. We emphasize that (3.17), (3.20), and (3.22) are not used in the forthcoming analysis. Only (3.21) is used.

Remark 3.4. Assuming that $\mathbf{f}_f \in (L^2(\Omega_f))^d$, $q_f \in L^2(\Omega_f)$, $\mathbf{f}_p \in (L^2(\Omega_p))^d$, and $q_p \in L^2(\Omega_p)$, the well-posedness of the subdomain problems (3.15)–(3.16) and (3.18)–(3.19) can be shown using standard techniques for the Stokes and Biot systems, respectively, using the classical Babuska-Brezzi theory [10]. We emphasize the inclusion of the term $\|\mathbf{v} \cdot \mathbf{n}_p\|_{L^2(\Gamma_{fp})}$ in the norm of \mathbf{V}_p , cf. (2.13). Control of this term is obtained from the term $\gamma_p \langle (\mathbf{u}_p^{n+1} + d_t \boldsymbol{\eta}_p^{n+1}) \cdot \mathbf{n}_p, (\mathbf{v}_p + \boldsymbol{\xi}_p) \cdot \mathbf{n}_p \rangle_{\Gamma_{fp}}$ in (3.18). More precisely, this gives control on $\|(\mathbf{u}_p^{n+1} + \boldsymbol{\eta}_p^{n+1}) \cdot \mathbf{n}_p\|_{L^2(\Gamma_{fp})}$. Then, the bound on $\|\mathbf{u}_p^{n+1} \cdot \mathbf{n}_p\|_{L^2(\Gamma_{fp})}$ follows from the triangle inequality, the trace inequality, and the bound on $\|\boldsymbol{\eta}_p^{n+1}\|_{H^1(\Omega_p)}$.

4 Stability analysis

In the stability and error analysis we consider the case the case $\gamma_{BJS} = 0$, which corresponds to a no-slip condition as it is typical in fluid-structure interaction. Moreover, we assume that $\gamma_f = \gamma_p = \gamma$. Also, for simplicity, in the stability analysis presented in this section we consider no forcing terms, i.e., $\mathbf{f}_f = \mathbf{f}_p = \mathbf{0}$ and $q_f = q_p = 0$. In the analysis, we will use the identities

$$ab = \frac{1}{4} ((a+b)^2 - (a-b)^2), \quad (4.1)$$

$$a(a-b) = \frac{1}{2}(a^2 - b^2 + (a-b)^2). \quad (4.2)$$

We note that, due to the choice of $\mathbf{\Lambda}_h$ (3.13), (3.21) implies

$$\begin{pmatrix} \mu_n^{n+1} \\ \mu_\tau^{n+1} \end{pmatrix} = \begin{pmatrix} \mu_n^n \\ \mu_\tau^n \end{pmatrix} - 2\gamma \left(P_{\mathbf{\Lambda}_h} \begin{pmatrix} (d_t \boldsymbol{\eta}_p^{n+1} + \mathbf{u}_p^{n+1}) \cdot \mathbf{n}_p \\ d_t \boldsymbol{\eta}_p^{n+1} \cdot \boldsymbol{\tau}_p \end{pmatrix} + \begin{pmatrix} \mathbf{u}_f^{n+1} \cdot \mathbf{n}_f \\ \mathbf{u}_f^{n+1} \cdot \boldsymbol{\tau}_f \end{pmatrix} \right) \quad (4.3)$$

where $P_{\mathbf{\Lambda}_h} : (L^2(\Gamma_{fp}))^d \rightarrow \mathbf{\Lambda}_h$ is the L^2 -orthogonal projection satisfying, for any $\boldsymbol{\varphi} \in (L^2(\Gamma_{fp}))^d$,

$$\langle P_{\mathbf{\Lambda}_h} \boldsymbol{\varphi} - \boldsymbol{\varphi}, \boldsymbol{\chi} \rangle_{\Gamma_{fp}} = 0 \quad \forall \boldsymbol{\chi} \in \mathbf{\Lambda}_h. \quad (4.4)$$

A scaling argument similar to the one in [29, Lemma 5.1] shows that that $P_{\mathbf{\Lambda}_h}$ is stable in $\|\cdot\|_{H^{1/2}(\Gamma_{fp})}$:

$$\|P_{\mathbf{\Lambda}_h} \boldsymbol{\varphi}\|_{H^{1/2}(\Gamma_{fp})} \leq C_\Lambda \|\boldsymbol{\varphi}\|_{H^{1/2}(\Gamma_{fp})} \quad \forall \boldsymbol{\varphi} \in (H^{1/2}(\Gamma_{fp}))^d. \quad (4.5)$$

We define the following energy terms, which will be used in the stability estimate. Let

$$\begin{aligned} \mathcal{E}^n &= \frac{\rho_f}{2} \|\mathbf{u}_f^n\|_{L^2(\Omega_f)}^2 + \frac{\rho_p}{2} \|d_t \boldsymbol{\eta}_p^n\|_{L^2(\Omega_p)}^2 + \frac{1}{2} \|\boldsymbol{\eta}_p^n\|_e^2 + \frac{s_0}{2} \|p_p^n\|_{L^2(\Omega_p)}^2 \\ &\quad + \frac{\Delta t}{4\gamma} \|\mu_n^n\|_{L^2(\Gamma_{fp})}^2 + \frac{\Delta t}{4\gamma} \|\mu_\tau^n\|_{L^2(\Gamma_{fp})}^2, \end{aligned} \quad (4.6)$$

$$\mathcal{D}^n = \|\mathbf{u}_f^n\|_f^2 + \|\mathbf{u}_p^n\|_d^2, \quad (4.7)$$

$$\begin{aligned} \mathcal{S}^n &= \frac{\rho_p}{2} \|d_t \boldsymbol{\eta}_p^n - d_t \boldsymbol{\eta}_p^{n-1}\|_{L^2(\Omega_p)}^2 + \frac{\rho_f}{2} \|\mathbf{u}_f^n - \mathbf{u}_f^{n-1}\|_{L^2(\Omega_f)}^2 + \frac{1}{2} \|\boldsymbol{\eta}_p^n - \boldsymbol{\eta}_p^{n-1}\|_e^2 \\ &\quad + \frac{s_0}{2} \|p_p^n - p_p^{n-1}\|_{L^2(\Omega_p)}^2, \end{aligned} \quad (4.8)$$

where

$$\begin{aligned} \|\mathbf{v}_f\|_f^2 &:= a_f(\mathbf{v}_f, \mathbf{v}_f) = 2\mu_f \|\mathbf{D}(\mathbf{v}_f)\|_{\Omega_f}^2, \quad \|\mathbf{v}_p\|_d^2 = a_p^d(\mathbf{v}_p, \mathbf{v}_p) = \mu_f \|K^{-1/2} \mathbf{v}_p\|_{\Omega_p}^2, \\ \|\boldsymbol{\xi}_p\|_e^2 &:= a_p^e(\boldsymbol{\xi}_p, \boldsymbol{\xi}_p) = \|\mu_p^{1/2} \mathbf{D}(\boldsymbol{\xi}_p)\|_{\Omega_p}^2 + \|\lambda_p^{1/2} \nabla \cdot \boldsymbol{\xi}_p\|_{\Omega_p}^2. \end{aligned}$$

The assumptions on the coefficients imply that there exist positive constants c_f , c_d , and c_e such that

$$\begin{aligned} \|\mathbf{v}_f\|_f^2 &\geq c_f \|\mathbf{v}_f\|_{H^1(\Omega_f)}^2 \quad \forall \mathbf{v}_f \in H^1(\Omega_f), \quad \|\mathbf{v}_p\|_d^2 \geq c_d \|\mathbf{v}_p\|_{L^2(\Omega_p)}^2 \quad \forall \mathbf{v}_p \in L^2(\Omega_p), \\ \|\boldsymbol{\xi}_p\|_e^2 &\geq c_e \|\boldsymbol{\xi}_p\|_{H^1(\Omega_p)}^2 \quad \forall \boldsymbol{\xi}_p \in H^1(\Omega_p), \end{aligned} \quad (4.9)$$

where Korn's and Poincaré inequalities have been utilized in the first and third inequalities, using that $|\Gamma_f^D| > 0$.

Theorem 4.1. *The following energy inequality holds for :*

$$\mathcal{E}^N + \Delta t \sum_{n=1}^N \mathcal{D}^n + \sum_{n=1}^N \mathcal{S}^n \leq \mathcal{E}^0. \quad (4.10)$$

Proof. Taking $\mathbf{v}_f = \mathbf{u}_f^{n+1}$ and $w_f = p_f^{n+1}$ in (3.15)–(3.16), we obtain

$$\begin{aligned} &\frac{\rho_f}{\Delta t} (\mathbf{u}_f^{n+1} - \mathbf{u}_f^n, \mathbf{u}_f^{n+1})_{\Omega_f} + a_f(\mathbf{u}_f^{n+1}, \mathbf{u}_f^{n+1}) \\ &= \frac{1}{\gamma} \left\langle \mu_n^n - \gamma \mathbf{u}_f^{n+1} \cdot \mathbf{n}_f, \gamma \mathbf{u}_f^{n+1} \cdot \mathbf{n}_f \right\rangle_{\Gamma_{fp}} + \frac{1}{\gamma} \left\langle \mu_\tau^n - \gamma \mathbf{u}_f^{n+1} \cdot \boldsymbol{\tau}_f, \gamma \mathbf{u}_f^{n+1} \cdot \boldsymbol{\tau}_f \right\rangle_{\Gamma_{fp}} \end{aligned}$$

$$= \frac{1}{4\gamma} \int_{\Gamma_{fp}} (\mu_n^n)^2 - \frac{1}{4\gamma} \int_{\Gamma_{fp}} (\mu_n^n - 2\gamma \mathbf{u}_f^{n+1} \cdot \mathbf{n}_f)^2 + \frac{1}{4\gamma} \int_{\Gamma_{fp}} (\mu_\tau^n)^2 - \frac{1}{4\gamma} \int_{\Gamma_{fp}} (\mu_\tau^n - 2\gamma \mathbf{u}_f^{n+1} \cdot \boldsymbol{\tau}_f)^2, \quad (4.11)$$

where we used (4.1) in the last equality. Taking $\mathbf{v}_p = \mathbf{u}_p^{n+1}$, $w_p = p_p^{n+1}$, and $\boldsymbol{\xi}_p = d_t \boldsymbol{\eta}_p^{n+1}$ in (3.18)–(3.19), we obtain

$$\begin{aligned} & \frac{\rho_p}{\Delta t} (d_t \boldsymbol{\eta}_p^{n+1} - d_t \boldsymbol{\eta}_p^n, d_t \boldsymbol{\eta}_p^{n+1})_{\Omega_p} + \frac{1}{\Delta t} a_p^e(\boldsymbol{\eta}_p^{n+1}, \boldsymbol{\eta}_p^{n+1} - \boldsymbol{\eta}_p^n) + \frac{1}{\Delta t} s_0(p_p^{n+1} - p_p^n, p_p^{n+1})_{\Omega_p} + a_p^d(\mathbf{u}_p^{n+1}, \mathbf{u}_p^{n+1}) \\ &= \frac{1}{\gamma} \left\langle \mu_n^n - \gamma(\mathbf{u}_p^{n+1} + d_t \boldsymbol{\eta}_p^{n+1}) \cdot \mathbf{n}_p - 2\gamma \mathbf{u}_f^{n+1} \cdot \mathbf{n}_f, \gamma(\mathbf{u}_p^{n+1} + d_t \boldsymbol{\eta}_p^{n+1}) \cdot \mathbf{n}_p \right\rangle_{\Gamma_{fp}} \\ &\quad + \frac{1}{\gamma} \langle \mu_\tau^n - \gamma d_t \boldsymbol{\eta}_p^{n+1} \cdot \boldsymbol{\tau}_p - 2\gamma \mathbf{u}_f^{n+1} \cdot \boldsymbol{\tau}_f, \gamma d_t \boldsymbol{\eta}_p^{n+1} \cdot \boldsymbol{\tau}_p \rangle_{\Gamma_{fp}} \\ &= \frac{1}{\gamma} \left\langle \begin{pmatrix} \mu_n^n \\ \mu_\tau^n \end{pmatrix} - \gamma P_{\mathbf{A}_h} \begin{pmatrix} (d_t \boldsymbol{\eta}_p^{n+1} + \mathbf{u}_p^{n+1}) \cdot \mathbf{n}_p \\ d_t \boldsymbol{\eta}_p^{n+1} \cdot \boldsymbol{\tau}_p \end{pmatrix} - 2\gamma \begin{pmatrix} \mathbf{u}_f^{n+1} \cdot \mathbf{n}_f \\ \mathbf{u}_f^{n+1} \cdot \boldsymbol{\tau}_f \end{pmatrix}, \gamma P_{\mathbf{A}_h} \begin{pmatrix} (d_t \boldsymbol{\eta}_p^{n+1} + \mathbf{u}_p^{n+1}) \cdot \mathbf{n}_p \\ d_t \boldsymbol{\eta}_p^{n+1} \cdot \boldsymbol{\tau}_p \end{pmatrix} \right\rangle_{\Gamma_{fp}} \\ &\quad - \gamma \left\langle \begin{pmatrix} (d_t \boldsymbol{\eta}_p^{n+1} + \mathbf{u}_p^{n+1}) \cdot \mathbf{n}_p \\ d_t \boldsymbol{\eta}_p^{n+1} \cdot \boldsymbol{\tau}_p \end{pmatrix} - P_{\mathbf{A}_h} \begin{pmatrix} (d_t \boldsymbol{\eta}_p^{n+1} + \mathbf{u}_p^{n+1}) \cdot \mathbf{n}_p \\ d_t \boldsymbol{\eta}_p^{n+1} \cdot \boldsymbol{\tau}_p \end{pmatrix}, \begin{pmatrix} (d_t \boldsymbol{\eta}_p^{n+1} + \mathbf{u}_p^{n+1}) \cdot \mathbf{n}_p \\ d_t \boldsymbol{\eta}_p^{n+1} \cdot \boldsymbol{\tau}_p \end{pmatrix} - P_{\mathbf{A}_h} \begin{pmatrix} (d_t \boldsymbol{\eta}_p^{n+1} + \mathbf{u}_p^{n+1}) \cdot \mathbf{n}_p \\ d_t \boldsymbol{\eta}_p^{n+1} \cdot \boldsymbol{\tau}_p \end{pmatrix} \right\rangle_{\Gamma_{fp}}, \quad (4.12) \end{aligned}$$

where we used (4.4) in the last equality. Then, using (4.1) and (4.3), and dropping the last term in (4.12), we obtain

$$\begin{aligned} & \frac{\rho_p}{\Delta t} (d_t \boldsymbol{\eta}_p^{n+1} - d_t \boldsymbol{\eta}_p^n, d_t \boldsymbol{\eta}_p^{n+1})_{\Omega_p} + \frac{1}{\Delta t} a_p^e(\boldsymbol{\eta}_p^{n+1}, \boldsymbol{\eta}_p^{n+1} - \boldsymbol{\eta}_p^n) + \frac{1}{\Delta t} s_0(p_p^{n+1} - p_p^n, p_p^{n+1})_{\Omega_p} + a_p^d(\mathbf{u}_p^{n+1}, \mathbf{u}_p^{n+1}) \\ &\leq \frac{1}{4\gamma} \int_{\Gamma_{fp}} (\mu_n^n - 2\gamma \mathbf{u}_f^{n+1} \cdot \mathbf{n}_f)^2 - \frac{1}{4\gamma} \int_{\Gamma_{fp}} (\mu_n^{n+1})^2 + \frac{1}{4\gamma} \int_{\Gamma_{fp}} (\mu_\tau^n - 2\gamma \mathbf{u}_f^{n+1} \cdot \boldsymbol{\tau}_f)^2 - \frac{1}{4\gamma} \int_{\Gamma_{fp}} (\mu_\tau^{n+1})^2. \quad (4.13) \end{aligned}$$

Summing (4.11) and (4.13) and using (4.2) gives

$$\begin{aligned} & \frac{\rho_f}{2\Delta t} (\mathbf{u}_f^{n+1}, \mathbf{u}_f^{n+1})_{\Omega_f} + \frac{\rho_f}{2\Delta t} (\mathbf{u}_f^{n+1} - \mathbf{u}_f^n, \mathbf{u}_f^{n+1} - \mathbf{u}_f^n)_{\Omega_f} + a_f(\mathbf{u}_f^{n+1}, \mathbf{u}_f^{n+1}) \\ &\quad + \frac{\rho_p}{2\Delta t} (d_t \boldsymbol{\eta}_p^{n+1}, d_t \boldsymbol{\eta}_p^{n+1})_{\Omega_p} + \frac{\rho_p}{2\Delta t} (d_t \boldsymbol{\eta}_p^{n+1} - d_t \boldsymbol{\eta}_p^n, d_t \boldsymbol{\eta}_p^{n+1} - d_t \boldsymbol{\eta}_p^n)_{\Omega_p} + a_p^d(\mathbf{u}_p^{n+1}, \mathbf{u}_p^{n+1}) \\ &\quad + \frac{1}{2\Delta t} a_p^e(\boldsymbol{\eta}_p^{n+1}, \boldsymbol{\eta}_p^{n+1}) + \frac{1}{2\Delta t} a_p^e(\boldsymbol{\eta}_p^{n+1} - \boldsymbol{\eta}_p^n, \boldsymbol{\eta}_p^{n+1} - \boldsymbol{\eta}_p^n) + \frac{s_0}{2\Delta t} (p_p^{n+1}, p_p^{n+1})_{\Omega_p} \\ &\quad + \frac{s_0}{2\Delta t} (p_p^{n+1} - p_p^n, p_p^{n+1} - p_p^n)_{\Omega_p} + \frac{1}{4\gamma} \int_{\Gamma_{fp}} (\mu_n^{n+1})^2 + \frac{1}{4\gamma} \int_{\Gamma_{fp}} (\mu_\tau^{n+1})^2 \\ &\leq \frac{\rho_f}{2\Delta t} (\mathbf{u}_f^n, \mathbf{u}_f^n)_{\Omega_f} + \frac{\rho_p}{2\Delta t} (d_t \boldsymbol{\eta}_p^n, d_t \boldsymbol{\eta}_p^n)_{\Omega_p} + \frac{1}{2\Delta t} a_p^e(\boldsymbol{\eta}_p^n, \boldsymbol{\eta}_p^n) + \frac{s_0}{2\Delta t} (p_p^n, p_p^n)_{\Omega_p} \\ &\quad + \frac{1}{4\gamma} \int_{\Gamma_{fp}} (\mu_n^n)^2 + \frac{1}{4\gamma} \int_{\Gamma_{fp}} (\mu_\tau^n)^2. \end{aligned}$$

Finally, multiplying by Δt and summing over n implies

$$\frac{\rho_f}{2} (\mathbf{u}_f^N, \mathbf{u}_f^N)_{\Omega_f} + \frac{\rho_p}{2} (d_t \boldsymbol{\eta}_p^N, d_t \boldsymbol{\eta}_p^N)_{\Omega_p} + \frac{1}{2} a_p^e(\boldsymbol{\eta}_p^N, \boldsymbol{\eta}_p^N) + \frac{s_0}{2} (p_p^N, p_p^N)_{\Omega_p}$$

$$\begin{aligned}
& + \frac{\Delta t}{4\gamma} \int_{\Gamma_{fp}} (\mu_n^N)^2 + \frac{\Delta t}{4\gamma} \int_{\Gamma_{fp}} (\mu_\tau^N)^2 + \Delta t \sum_{n=0}^{N-1} \left(a_f(\mathbf{u}_f^{n+1}, \mathbf{u}_f^{n+1}) + a_p^d(\mathbf{u}_p^{n+1}, \mathbf{u}_p^{n+1}) \right) \\
& + \sum_{n=0}^{N-1} \left(\frac{\rho_p}{2} (d_t \boldsymbol{\eta}_p^{n+1} - d_t \boldsymbol{\eta}_p^n, d_t \boldsymbol{\eta}_p^{n+1} - d_t \boldsymbol{\eta}_p^n)_{\Omega_p} + \frac{\rho_f}{2} (\mathbf{u}_f^{n+1} - \mathbf{u}_f^n, \mathbf{u}_f^{n+1} - \mathbf{u}_f^n)_{\Omega_f} \right. \\
& \quad \left. + \frac{1}{2} a_p^e(\boldsymbol{\eta}_p^{n+1} - \boldsymbol{\eta}_p^n, \boldsymbol{\eta}_p^{n+1} - \boldsymbol{\eta}_p^n) + \frac{s_0}{2} (p_p^{n+1} - p_p^n, p_p^{n+1} - p_p^n)_{\Omega_p} \right) \\
& = \frac{\rho_f}{2} (\mathbf{u}_f^0, \mathbf{u}_f^0)_{\Omega_f} + \frac{\rho_p}{2} (d_t \boldsymbol{\eta}_p^0, d_t \boldsymbol{\eta}_p^0)_{\Omega_p} + \frac{1}{2} a_p^e(\boldsymbol{\eta}_p^0, \boldsymbol{\eta}_p^0) + \frac{s_0}{2} (p_p^0, p_p^0)_{\Omega_p} + \frac{\Delta t}{4\gamma} \int_{\Gamma_{fp}} (\mu_n^0)^2 + \frac{\Delta t}{4\gamma} \int_{\Gamma_{fp}} (\mu_\tau^0)^2.
\end{aligned}$$

which gives (4.10). \square

Bound (4.10) provides control on \mathbf{u}_f^n , \mathbf{u}_p^n , p_p^n , $\boldsymbol{\eta}_p^n$, and $d_t \boldsymbol{\eta}_p^n$. Bound on $\|p_p^n\|_{L^2(\Omega_f)}$ can be obtained using that $\mathbf{V}_{f,h} \times W_{f,h}$ is a stable Stokes pair satisfying the inf-sup condition [33, Lemma 4.1]

$$\forall w_f \in W_{f,h}, \quad \sup_{\mathbf{v}_f \in \mathbf{V}_{f,h}: \mathbf{v}_f|_{\Gamma_{fp}}=0} \frac{b_f(\mathbf{v}_f, w_f)}{\|\mathbf{v}_f\|_{H^1(\Omega_f)}} \geq \beta_f \|w_f\|_{L^2(\Omega_f)}. \quad (4.14)$$

Additionally, the control on p_p^n depends on s_0 , which in practice can be very small. A bound on p_p^n independent of s_0 can be obtained from the discrete Darcy inf-sup condition [10]

$$\forall w_p \in W_{p,h}, \quad \sup_{\mathbf{v}_p \in \mathbf{V}_{p,h}: \mathbf{v}_p|_{\Gamma_{fp}}=0} \frac{b_p(\mathbf{v}_p, w_p)}{\|\mathbf{v}_p\|_{H(\text{div}; \Omega_p)}} \geq \beta_p \|w_p\|_{L^2(\Omega_p)}. \quad (4.15)$$

Furthermore, we note that the Δt scaling in the terms $\Delta t \|\mu_n^N\|_{L^2(\Gamma_{fp})}^2$ and $\Delta t \|\mu_\tau^N\|_{L^2(\Gamma_{fp})}^2$ in \mathcal{E}^N , cf. (4.6), implies that the stability bound on $\|\mu_n^N\|_{L^2(\Gamma_{fp})}$ and $\|\mu_\tau^N\|_{L^2(\Gamma_{fp})}$ obtained in (4.10) scales like $\sqrt{\Delta t^{-1}}$. A stability bound on $\boldsymbol{\mu}^n$ that is optimal with respect to Δt can be obtained in the norm $\|\cdot\|_{H^{-1/2}(\Gamma_{fp})}$, which is the dual of $\|\cdot\|_{H^{1/2}(\Gamma_{fp})}$. For simplicity, we present the arguments for the quasistatic Stokes model, where the term $\rho_f(d_t \mathbf{u}_f^{n+1}, \mathbf{v}_f)_{\Omega_f}$ in (3.15) is not present. Let $\tilde{\mathcal{E}}^n$ be \mathcal{E}^n without the term $\frac{\rho_f}{2} \|\mathbf{u}_f^n\|_{L^2(\Omega_f)}^2$ and let

$$\tilde{\mathcal{D}}^n = \|\mathbf{u}_f^n\|_f^2 + \|\mathbf{u}_p^n\|_d^2 + \|p_p^n\|_{L^2(\Omega_f)}^2 + \|\boldsymbol{\mu}^{n-1}\|_{H^{-1/2}(\Gamma_{fp})}^2 + \|p_p^n\|_{L^2(\Omega_p)}^2.$$

Theorem 4.2. *The following energy inequality holds for the quasistatic Stokes version of Algorithm 1:*

$$\tilde{\mathcal{E}}^N + \Delta t \sum_{n=1}^N \tilde{\mathcal{D}}^n + \sum_{n=1}^N \mathcal{S}^n \leq C \tilde{\mathcal{E}}^0. \quad (4.16)$$

Proof. A bound on $\|p_f^n\|_{L^2(\Omega_f)}$ can be obtained from (4.14) and (3.15). Noting that the restriction $\mathbf{v}_f|_{\Gamma_{fp}} = 0$ in (4.14) eliminates all interface terms in (3.15), we obtain

$$\|p_f^{n+1}\|_{L^2(\Omega_f)} \leq C \|\mathbf{u}_f^{n+1}\|_{H^1(\Omega_f)}. \quad (4.17)$$

Similarly, (4.15) and (3.18) with $\boldsymbol{\xi}_p = 0$ imply

$$\|p_p^{n+1}\|_{L^2(\Omega_p)} \leq C \|\mathbf{u}_p^{n+1}\|_{L^2(\Omega_p)}. \quad (4.18)$$

Next, we have

$$\begin{aligned}\|\boldsymbol{\mu}^n\|_{H^{-1/2}(\Gamma_{fp})} &= \sup_{\varphi \in (H^{1/2}(\Gamma_{fp}))^d} \frac{\langle \varphi, \boldsymbol{\mu}^n \rangle_{\Gamma_{fp}}}{\|\varphi\|_{H^{1/2}(\Gamma_{fp})}} = \sup_{\varphi \in (H^{1/2}(\Gamma_{fp}))^d} \frac{\langle P_{\Lambda_h} \varphi, \boldsymbol{\mu}^n \rangle_{\Gamma_{fp}}}{\|\varphi\|_{H^{1/2}(\Gamma_{fp})}} \\ &\leq C_\Lambda \sup_{\varphi \in (H^{1/2}(\Gamma_{fp}))^d} \frac{\langle P_{\Lambda_h} \varphi, \boldsymbol{\mu}^n \rangle_{\Gamma_{fp}}}{\|P_{\Lambda_h} \varphi\|_{H^{1/2}(\Gamma_{fp})}}.\end{aligned}$$

Since $\Lambda_h = \mathbf{V}_{f,h}|_{\Gamma_{fp}}$, there exists a discrete Stokes extension $\mathbf{E}_{f,h} : \Lambda_h \rightarrow \mathbf{V}_{f,h}$ such that for each $\chi \in \Lambda_h$, $\mathbf{E}_{f,h} \chi|_{\Gamma_{fp}} = \chi$ and $\|\mathbf{E}_{f,h} \chi\|_{H^1(\Omega_f)} \leq C_{ext} \|\chi\|_{H^{1/2}(\Gamma_{fp})}$. Therefore,

$$\begin{aligned}\|\boldsymbol{\mu}^n\|_{H^{-1/2}(\Gamma_{fp})} &\leq C_\Lambda C_{ext} \sup_{\varphi \in (H^{1/2}(\Gamma_{fp}))^d} \frac{\langle \mathbf{E}_{f,h} P_{\Lambda_h} \varphi, \boldsymbol{\mu}^n \rangle_{\Gamma_{fp}}}{\|\mathbf{E}_{f,h} P_{\Lambda_h} \varphi\|_{H^1(\Omega_f)}} \leq C_\Lambda C_{ext} \sup_{\mathbf{v}_f \in \mathbf{V}_{f,h}} \frac{\langle \mathbf{v}_f, \boldsymbol{\mu}^n \rangle_{\Gamma_{fp}}}{\|\mathbf{v}_f\|_{H^1(\Omega_f)}} \\ &\leq C \left(\|\mathbf{u}_f^{n+1}\|_{H^1(\Omega_f)} + \|p_f^{n+1}\|_{L^2(\Omega_f)} \right),\end{aligned}\quad (4.19)$$

using (3.15) for the last inequality. Bound (4.16) follows from combining (4.17)–(4.19) with (4.10). \square

Remark 4.1. In the fully dynamic model, in order to control $\|p_f^{n+1}\|_{L^2(\Omega_f)}$, we need first to bound $\|d_t \mathbf{u}_f^{n+1}\|_{L^2(\Omega_f)}$, which can be done by applying the discrete time differentiation operator d_t to the entire system. We omit further details.

Remark 4.2. There is no restriction on Δt in the bounds obtained in Theorems 4.1 and 4.2, hence the non-iterative Robin-Robin method given in **Algorithm 1** is unconditionally stable.

5 Time discretization error analysis for the quasistatic model

In this section we analyze the time discretization error in the Robin-Robin method given in (3.15)–(3.16), (3.18)–(3.19), and (3.21). To this end, we consider the semidiscrete continuous in space version of the algorithm and compare its solution to the variational formulation (3.3)–(3.6). In addition, for the sake of simplicity, we focus on the quasistatic model, where the terms $\rho_f \partial_t \mathbf{u}_f$ and $\rho_p \partial_{tt} \boldsymbol{\eta}_p$ are omitted. In this section we assume that Γ_{fp} is at least C^1 .

Introducing the continuous versions of μ_n and μ_τ from (3.14),

$$\mu_n(t) := -\gamma(\partial_t \boldsymbol{\eta}_p(t) + \mathbf{u}_p(t)) \cdot \mathbf{n}_p + \boldsymbol{\sigma}_p(t) \mathbf{n}_p \cdot \mathbf{n}_p, \quad (5.1a)$$

$$\mu_\tau(t) := -\gamma \partial_t \boldsymbol{\eta}_p(t) \cdot \boldsymbol{\tau}_p + \boldsymbol{\sigma}_p(t) \mathbf{n}_p \cdot \boldsymbol{\tau}_p, \quad (5.1b)$$

the system (3.3)–(3.6) in the quasistatic case can be rewritten as

$$\begin{aligned}a_f(\mathbf{u}_f, \mathbf{v}_f) + b_f(\mathbf{v}_f, p_f) + \gamma \langle \mathbf{u}_f \cdot \mathbf{n}_f, \mathbf{v}_f \cdot \mathbf{n}_f \rangle_{\Gamma_{fp}} + \gamma \langle \mathbf{u}_f \cdot \boldsymbol{\tau}_f, \mathbf{v}_f \cdot \boldsymbol{\tau}_f \rangle_{\Gamma_{fp}} \\ = (\mathbf{f}_f, \mathbf{v}_f)_{\Omega_f} + \langle \mu_n, \mathbf{v}_f \cdot \mathbf{n}_f \rangle_{\Gamma_{fp}} + \langle \mu_\tau, \mathbf{v}_f \cdot \boldsymbol{\tau}_f \rangle_{\Gamma_{fp}}\end{aligned}\quad (5.2)$$

$$- b_f(\mathbf{u}_f, w_f) = (q_f, w_f)_{\Omega_f}, \quad (5.3)$$

$$\begin{aligned}a_p^e(\boldsymbol{\eta}_p, \boldsymbol{\xi}_p) + a_p^d(\mathbf{u}_p, \mathbf{v}_p) + \alpha b_p(\boldsymbol{\xi}_p, p_p) + b_p(\mathbf{v}_p, p_p) \\ + \gamma \langle (\mathbf{u}_p + \partial_t \boldsymbol{\eta}_p) \cdot \mathbf{n}_p, (\mathbf{v}_p + \boldsymbol{\xi}_p) \cdot \mathbf{n}_p \rangle_{\Gamma_{fp}} + \gamma \langle \partial_t \boldsymbol{\eta}_p \cdot \boldsymbol{\tau}_p, \boldsymbol{\xi}_p \cdot \boldsymbol{\tau}_p \rangle_{\Gamma_{fp}} \\ = (\mathbf{f}_p, \mathbf{v}_p)_{\Omega_p} + \langle \mu_n - 2\gamma \mathbf{u}_f \cdot \mathbf{n}_f, (\mathbf{v}_p + \boldsymbol{\xi}_p) \cdot \mathbf{n}_p \rangle_{\Gamma_{fp}} + \langle \mu_\tau - 2\gamma \mathbf{u}_f \cdot \boldsymbol{\tau}_f, \boldsymbol{\xi}_p \cdot \boldsymbol{\tau}_p \rangle_{\Gamma_{fp}}\end{aligned}\quad (5.4)$$

$$s_0(\partial_t p_p, w_p)_{\Omega_p} - \alpha b_p(\partial_t \boldsymbol{\eta}_p, w_p) - b_p(\mathbf{u}_p, w_p) = (q_p, w_p)_{\Omega_p}. \quad (5.5)$$

Let us define the error terms for $i = f, p$ as follows:

$$\mathbf{U}_i^{n+1} = \mathbf{u}_i(t_{n+1}) - \mathbf{u}_i^{n+1}, \quad P_i^{n+1} = p_i(t_{n+1}) - p_i^{n+1}, \quad \mathbf{H}_p^{n+1} = \boldsymbol{\eta}_p(t_{n+1}) - \boldsymbol{\eta}_p^{n+1}.$$

Additionally, we define a splitting error and a time discretization error operators acting on the exact solutions as follows:

$$\begin{aligned} \mathbb{S}^{n+1}(\phi) &:= \phi(t_{n+1}) - \phi(t_n), \\ \mathbb{T}^{n+1}(\phi) &:= \partial_t \phi(t_{n+1}) - d_t \phi(t_{n+1}), \end{aligned}$$

where we recall $d_t \phi(t_{n+1}) := \frac{\phi(t_{n+1}) - \phi(t_n)}{\Delta t}$. We note that the argument of \mathbb{T}^{n+1} can be either a vector or a scalar. Next, we define variations of μ_n and μ_τ with discrete time derivatives:

$$\tilde{\mu}_n(t_n) := -\gamma(d_t \boldsymbol{\eta}_p(t_n) + \mathbf{u}_p(t_n)) \cdot \mathbf{n}_p + \boldsymbol{\sigma}_p(t_n) \mathbf{n}_p \cdot \mathbf{n}_p, \quad (5.6a)$$

$$\tilde{\mu}_\tau(t_n) := -\gamma d_t \boldsymbol{\eta}_p(t_n) \cdot \boldsymbol{\tau}_p + \boldsymbol{\sigma}_p(t_n) \mathbf{n}_p \cdot \boldsymbol{\tau}_p. \quad (5.6b)$$

Consequently, it follows that

$$\mu_n(t_n) = \tilde{\mu}_n(t_n) - \gamma \mathbb{T}^n(\boldsymbol{\eta}_p) \cdot \mathbf{n}_p, \quad (5.7a)$$

$$\mu_\tau(t_n) = \tilde{\mu}_\tau(t_n) - \gamma \mathbb{T}^n(\boldsymbol{\eta}_p) \cdot \boldsymbol{\tau}_p. \quad (5.7b)$$

We define the interface error terms:

$$M_n^n := \tilde{\mu}_n(t_n) - \mu_n^n, \quad (5.8a)$$

$$M_\tau^n := \tilde{\mu}_\tau(t_n) - \mu_\tau^n. \quad (5.8b)$$

Consequently, we have

$$\begin{aligned} \mu_n(t_{n+1}) - \mu_n^n &= (\mu_n(t_{n+1}) - \mu_n(t_n)) + \mu_n(t_n) - \mu_n^n \\ &= \mathbb{S}^{n+1}(\mu_n) + \mu_n(t_n) - \tilde{\mu}_n(t_n) + \tilde{\mu}_n(t_n) - \mu_n^n \\ &= \mathbb{S}^{n+1}(\mu_n) - \gamma \mathbb{T}^n(\boldsymbol{\eta}_p) \cdot \mathbf{n}_p + M_n^n, \end{aligned} \quad (5.9)$$

and, by the same argument,

$$\mu_\tau(t_{n+1}) - \mu_\tau^n = \mathbb{S}^{n+1}(\mu_\tau) - \gamma \mathbb{T}^n(\boldsymbol{\eta}_p) \cdot \boldsymbol{\tau}_p + M_\tau^n. \quad (5.10)$$

We note that in the continuous in space case considered in this section, the update (4.3) simplifies to

$$\mu_n^{n+1} = \mu_n^n - 2\gamma((d_t \boldsymbol{\eta}_p^{n+1} + \mathbf{u}_p^{n+1}) \cdot \mathbf{n}_p + \mathbf{u}_f^{n+1} \cdot \mathbf{n}_f), \quad (5.11a)$$

$$\mu_\tau^{n+1} = \mu_\tau^n - 2\gamma(d_t \boldsymbol{\eta}_p^{n+1} \cdot \boldsymbol{\tau}_p + \mathbf{u}_f^{n+1} \cdot \boldsymbol{\tau}_f). \quad (5.11b)$$

Theorem 5.1. *Assuming that the solution to (2.2)–(2.10) is sufficiently smooth, the following error estimate holds for the quasistatic continuous in space version of Algorithm 1:*

$$\begin{aligned} \max_{1 \leq n \leq N} (\|\mathbf{H}_p^n\|_e + \|P_p^n\|_{L^2(\Omega_p)}) &+ \left(\Delta t \sum_{n=1}^N \|\mathbf{U}_f^n\|_f^2 \right)^{1/2} + \left(\Delta t \sum_{n=1}^N \|\mathbf{U}_p^n\|_d^2 \right)^{1/2} + \left(\Delta t \sum_{n=1}^N \|P_f^n\|_{L^2(\Omega_f)}^2 \right)^{1/2} \\ &+ \left(\Delta t \sum_{n=1}^N \|P_p^n\|_{L^2(\Omega_p)}^2 \right)^{1/2} + \left(\Delta t \sum_{n=1}^N \|\mathbf{M}^{n-1}\|_{H^{-1/2}(\Gamma_{fp})}^2 \right)^{1/2} = \mathcal{O}(\sqrt{T} \Delta t). \end{aligned} \quad (5.12)$$

Proof. Subtracting (3.15)–(3.16) from (5.2)–(5.3) at $t = t_{n+1}$ and applying (5.9) and (5.10) yields

$$\begin{aligned} a_f(\mathbf{U}_f^{n+1}, \mathbf{v}_f) + b_f(\mathbf{v}_f, P_f^{n+1}) &+ \gamma \langle \mathbf{U}_f^{n+1} \cdot \mathbf{n}_f, \mathbf{v}_f \cdot \mathbf{n}_f \rangle_{\Gamma_{fp}} + \gamma \langle \mathbf{U}_f^{n+1} \cdot \boldsymbol{\tau}_f, \mathbf{v}_f \cdot \boldsymbol{\tau}_f \rangle_{\Gamma_{fp}} \\ &= \langle \mu_n(t_{n+1}) - \mu_n^n, \mathbf{v}_f \cdot \mathbf{n}_f \rangle_{\Gamma_{fp}} + \langle \mu_\tau(t_{n+1}) - \mu_\tau^n, \mathbf{v}_f \cdot \boldsymbol{\tau}_f \rangle_{\Gamma_{fp}} \\ &= \langle M_n^n, \mathbf{v}_f \cdot \mathbf{n}_f \rangle_{\Gamma_{fp}} + \langle M_\tau^n, \mathbf{v}_f \cdot \boldsymbol{\tau}_f \rangle_{\Gamma_{fp}} \\ &\quad + \langle \mathbb{S}^{n+1}(\mu_n) - \gamma \mathbb{T}^n(\boldsymbol{\eta}_p) \cdot \mathbf{n}_p, \mathbf{v}_f \cdot \mathbf{n}_f \rangle_{\Gamma_{fp}} + \langle \mathbb{S}^{n+1}(\mu_\tau) - \gamma \mathbb{T}^n(\boldsymbol{\eta}_p) \cdot \boldsymbol{\tau}_p, \mathbf{v}_f \cdot \boldsymbol{\tau}_f \rangle_{\Gamma_{fp}}, \end{aligned} \quad (5.13)$$

$$- b_f(\mathbf{U}_f^{n+1}, w_f) = 0. \quad (5.14)$$

Take $\mathbf{v}_f = \mathbf{U}_f^{n+1}$ and $w_f = P_f^{n+1}$ in (5.13)–(5.14) and add them up to obtain

$$\begin{aligned} a_f(\mathbf{U}_f^{n+1}, \mathbf{U}_f^{n+1}) &+ \gamma \langle \mathbf{U}_f^{n+1} \cdot \mathbf{n}_f, \mathbf{U}_f^{n+1} \cdot \mathbf{n}_f \rangle_{\Gamma_{fp}} + \gamma \langle \mathbf{U}_f^{n+1} \cdot \boldsymbol{\tau}_f, \mathbf{U}_f^{n+1} \cdot \boldsymbol{\tau}_f \rangle_{\Gamma_{fp}} \\ &= \langle M_n^n, \mathbf{U}_f^{n+1} \cdot \mathbf{n}_f \rangle_{\Gamma_{fp}} + \langle M_\tau^n, \mathbf{U}_f^{n+1} \cdot \boldsymbol{\tau}_f \rangle_{\Gamma_{fp}} + I_1, \end{aligned} \quad (5.15)$$

where

$$I_1 := \langle \mathbb{S}^{n+1}(\mu_n) - \gamma \mathbb{T}^n(\boldsymbol{\eta}_p) \cdot \mathbf{n}_p, \mathbf{U}_f^{n+1} \cdot \mathbf{n}_f \rangle_{\Gamma_{fp}} + \langle \mathbb{S}^{n+1}(\mu_\tau) - \gamma \mathbb{T}^n(\boldsymbol{\eta}_p) \cdot \boldsymbol{\tau}_p, \mathbf{U}_f^{n+1} \cdot \boldsymbol{\tau}_f \rangle_{\Gamma_{fp}}, \quad (5.16)$$

We can manipulate (5.15) as follows:

$$a_f(\mathbf{U}_f^{n+1}, \mathbf{U}_f^{n+1}) = \frac{1}{\gamma} \langle M_n^n - \gamma \mathbf{U}_f^{n+1} \cdot \mathbf{n}_f, \gamma \mathbf{U}_f^{n+1} \cdot \mathbf{n}_f \rangle_{\Gamma_{fp}} + \frac{1}{\gamma} \langle M_\tau^n - \gamma \mathbf{U}_f^{n+1} \cdot \boldsymbol{\tau}_f, \gamma \mathbf{U}_f^{n+1} \cdot \boldsymbol{\tau}_f \rangle_{\Gamma_{fp}} + I_1.$$

By applying (4.1), we have

$$\begin{aligned} a_f(\mathbf{U}_f^{n+1}, \mathbf{U}_f^{n+1}) &= \frac{1}{4\gamma} (\|M_n^n\|_{L^2(\Gamma_{fp})}^2 - \|M_n^n - 2\gamma \mathbf{U}_f^{n+1} \cdot \mathbf{n}_f\|_{L^2(\Gamma_{fp})}^2) \\ &\quad + \frac{1}{4\gamma} (\|M_\tau^n\|_{L^2(\Gamma_{fp})}^2 - \|M_\tau^n - 2\gamma \mathbf{U}_f^{n+1} \cdot \boldsymbol{\tau}_f\|_{L^2(\Gamma_{fp})}^2) + I_1. \end{aligned} \quad (5.17)$$

For the Biot problem, subtracting (3.18)–(3.19) from (5.4)–(5.5) at $t = t_{n+1}$, we obtain

$$\begin{aligned} a_p^e(\mathbf{H}_p^{n+1}, \boldsymbol{\xi}_p) &+ a_p^d(\mathbf{U}_p^{n+1}, \mathbf{v}_p) + \alpha b_p(\boldsymbol{\xi}_p, P_p^{n+1}) + b_p(\mathbf{v}_p, P_p^{n+1}) \\ &\quad + \gamma \langle (\mathbf{U}_p^{n+1} + d_t \mathbf{H}_p^{n+1}) \cdot \mathbf{n}_p, (\mathbf{v}_p + \boldsymbol{\xi}_p) \cdot \mathbf{n}_p \rangle_{\Gamma_{fp}} + \gamma \langle \mathbb{T}^{n+1}(\boldsymbol{\eta}_p) \cdot \mathbf{n}_p, (\mathbf{v}_p + \boldsymbol{\xi}_p) \cdot \mathbf{n}_p \rangle_{\Gamma_{fp}} \\ &\quad + \gamma \langle d_t \mathbf{H}_p^{n+1} \cdot \boldsymbol{\tau}_p, \boldsymbol{\xi}_p \cdot \boldsymbol{\tau}_p \rangle_{\Gamma_{fp}} + \gamma \langle \mathbb{T}^{n+1}(\boldsymbol{\eta}_p) \cdot \boldsymbol{\tau}_p, \boldsymbol{\xi}_p \cdot \boldsymbol{\tau}_p \rangle_{\Gamma_{fp}} \\ &= \langle \mu_n(t_{n+1}) - \mu_n^n - 2\gamma \mathbf{U}_f^{n+1} \cdot \mathbf{n}_f, (\mathbf{v}_p + \boldsymbol{\xi}_p) \cdot \mathbf{n}_p \rangle_{\Gamma_{fp}} + \langle \mu_\tau(t_{n+1}) - \mu_\tau^n - 2\gamma \mathbf{U}_f^{n+1} \cdot \boldsymbol{\tau}_f, \boldsymbol{\xi}_p \cdot \boldsymbol{\tau}_p \rangle_{\Gamma_{fp}} \end{aligned} \quad (5.18)$$

$$\begin{aligned} s_0(d_t P_p^{n+1}, w_p)_{\Omega_p} &+ s_0(\mathbb{T}^{n+1}(p_p), w_p)_{\Omega_p} - \alpha b_p(d_t \mathbf{H}_p^{n+1}, w_p) - \alpha b_p(\mathbb{T}^{n+1}(\boldsymbol{\eta}_p), w_p) \\ &- b_p(\mathbf{U}_p^{n+1}, w_p) = 0. \end{aligned} \quad (5.19)$$

Letting $\mathbf{v}_p = \mathbf{U}_p^{n+1}$, $\boldsymbol{\xi}_p = d_t \mathbf{H}_p^{n+1}$, and $w_p = P_p^{n+1}$ in (5.18)–(5.19), adding them up and using (5.9) and (5.10), we have

$$\begin{aligned} a_p^e(\mathbf{H}_p^{n+1}, d_t \mathbf{H}_p^{n+1}) &+ s_0(d_t P_p^{n+1}, P_p^{n+1})_{\Omega_p} + a_p^d(\mathbf{U}_p^{n+1}, \mathbf{U}_p^{n+1}) \\ &\quad + \gamma \langle (\mathbf{U}_p^{n+1} + d_t \mathbf{H}_p^{n+1}) \cdot \mathbf{n}_p, (\mathbf{U}_p^{n+1} + d_t \mathbf{H}_p^{n+1}) \cdot \mathbf{n}_p \rangle_{\Gamma_{fp}} + \gamma \langle d_t \mathbf{H}_p^{n+1} \cdot \boldsymbol{\tau}_p, d_t \mathbf{H}_p^{n+1} \cdot \boldsymbol{\tau}_p \rangle_{\Gamma_{fp}} \\ &= \langle M_n^n - 2\gamma \mathbf{U}_f^{n+1} \cdot \mathbf{n}_f, (\mathbf{U}_p^{n+1} + d_t \mathbf{H}_p^{n+1}) \cdot \mathbf{n}_p \rangle_{\Gamma_{fp}} + \langle M_\tau^n - 2\gamma \mathbf{U}_f^{n+1} \cdot \boldsymbol{\tau}_f, d_t \mathbf{H}_p^{n+1} \cdot \boldsymbol{\tau}_p \rangle_{\Gamma_{fp}} \\ &\quad + \langle \mathbb{S}^{n+1}(\mu_n) - \gamma \mathbb{T}^n(\boldsymbol{\eta}_p) \cdot \mathbf{n}_p, (\mathbf{U}_p^{n+1} + d_t \mathbf{H}_p^{n+1}) \cdot \mathbf{n}_p \rangle_{\Gamma_{fp}} \end{aligned}$$

$$\begin{aligned}
& + \langle \mathbb{S}^{n+1}(\mu_\tau) - \gamma \mathbb{T}^n(\boldsymbol{\eta}_p) \cdot \boldsymbol{\tau}_p, d_t \mathbf{H}_p^{n+1} \cdot \boldsymbol{\tau}_p \rangle_{\Gamma_{fp}} \\
& - \gamma \langle \mathbb{T}^{n+1}(\boldsymbol{\eta}_p) \cdot \mathbf{n}_p, (\mathbf{U}_p^{n+1} + d_t \mathbf{H}_p^{n+1}) \cdot \mathbf{n}_p \rangle_{\Gamma_{fp}} - \gamma \langle \mathbb{T}^{n+1}(\boldsymbol{\eta}_p) \cdot \boldsymbol{\tau}_p, d_t \mathbf{H}_p^{n+1} \cdot \boldsymbol{\tau}_p \rangle_{\Gamma_{fp}} \\
& - s_0(\mathbb{T}^{n+1}(p_p), P_p^{n+1})_{\Omega_p} + \alpha b_p(\mathbb{T}^{n+1}(\boldsymbol{\eta}_p), P_p^{n+1}). \tag{5.20}
\end{aligned}$$

Eq. (5.20) can be rewritten as follows:

$$\begin{aligned}
& a_p^e(\mathbf{H}_p^{n+1}, d_t \mathbf{H}_p^{n+1}) + s_0(d_t P_p^{n+1}, P_p^{n+1})_{\Omega_p} + a_p^d(\mathbf{U}_p^{n+1}, \mathbf{U}_p^{n+1}) \\
& = \langle M_n^n - 2\gamma \mathbf{U}_f^{n+1} \cdot \mathbf{n}_f - \gamma(\mathbf{U}_p^{n+1} + d_t \mathbf{H}_p^{n+1}) \cdot \mathbf{n}_p, (\mathbf{U}_p^{n+1} + d_t \mathbf{H}_p^{n+1}) \cdot \mathbf{n}_p \rangle_{\Gamma_{fp}} \\
& + \langle M_\tau^n - 2\gamma \mathbf{U}_f^{n+1} \cdot \boldsymbol{\tau}_f - \gamma d_t \mathbf{H}_p^{n+1} \cdot \boldsymbol{\tau}_p, d_t \mathbf{H}_p^{n+1} \cdot \boldsymbol{\tau}_p \rangle_{\Gamma_{fp}} \\
& + \langle A_n^n, (\mathbf{U}_p^{n+1} + d_t \mathbf{H}_p^{n+1}) \cdot \mathbf{n}_p \rangle_{\Gamma_{fp}} + \langle A_\tau, d_t \mathbf{H}_p^{n+1} \cdot \boldsymbol{\tau}_f \rangle_{\Gamma_{fp}} + I_2, \tag{5.21}
\end{aligned}$$

where

$$A_n^n := \mathbb{S}^{n+1}(\mu_n) - \gamma(\mathbb{T}^n(\boldsymbol{\eta}_p) + \mathbb{T}^{n+1}(\boldsymbol{\eta}_p)) \cdot \mathbf{n}_p, \tag{5.22a}$$

$$A_\tau^n := \mathbb{S}^{n+1}(\mu_\tau) - \gamma(\mathbb{T}^n(\boldsymbol{\eta}_p) + \mathbb{T}^{n+1}(\boldsymbol{\eta}_p)) \cdot \boldsymbol{\tau}_p, \tag{5.22b}$$

$$I_2 := -s_0(\mathbb{T}^{n+1}(p_p), P_p^{n+1})_{\Omega_p} + \alpha b_p(\mathbb{T}^{n+1}(\boldsymbol{\eta}_p), P_p^{n+1}). \tag{5.22c}$$

Using (4.1), we obtain from (5.21):

$$\begin{aligned}
& a_p^e(\mathbf{H}_p^{n+1}, d_t \mathbf{H}_p^{n+1}) + s_0(d_t P_p^{n+1}, P_p^{n+1})_{\Omega_p} + a_p^d(\mathbf{U}_p^{n+1}, \mathbf{U}_p^{n+1}) \\
& = \frac{1}{4\gamma} \|M_n^n - 2\gamma \mathbf{U}_f^{n+1} \cdot \mathbf{n}_f\|_{L^2(\Gamma_{fp})}^2 - \frac{1}{4\gamma} \|M_n^n - 2\gamma \mathbf{U}_f^{n+1} \cdot \mathbf{n}_f - 2\gamma(\mathbf{U}_p^{n+1} + d_t \mathbf{H}_p^{n+1}) \cdot \mathbf{n}_p\|_{L^2(\Gamma_{fp})}^2 \\
& + \frac{1}{4\gamma} \|M_\tau^n - 2\gamma \mathbf{U}_f^{n+1} \cdot \boldsymbol{\tau}_f\|_{L^2(\Gamma_{fp})}^2 - \frac{1}{4\gamma} \|M_\tau^n - 2\gamma \mathbf{U}_f^{n+1} \cdot \boldsymbol{\tau}_f - 2\gamma d_t \mathbf{H}_p^{n+1} \cdot \boldsymbol{\tau}_p\|_{L^2(\Gamma_{fp})}^2 \\
& + \langle A_n^n, (\mathbf{U}_p^{n+1} + d_t \mathbf{H}_p^{n+1}) \cdot \mathbf{n}_p \rangle_{\Gamma_{fp}} + \langle A_\tau, d_t \mathbf{H}_p^{n+1} \cdot \boldsymbol{\tau}_p \rangle_{\Gamma_{fp}} + I_2. \tag{5.23}
\end{aligned}$$

For the second term on the right-hand side above, we have

$$\begin{aligned}
& M_n^n - 2\gamma \mathbf{U}_f^{n+1} \cdot \mathbf{n}_f - 2\gamma(\mathbf{U}_p^{n+1} + d_t \mathbf{H}_p^{n+1}) \cdot \mathbf{n}_p \\
& = \tilde{\mu}_n(t_n) - \mu_n^n - 2\gamma \mathbf{u}_f(t_{n+1}) \cdot \mathbf{n}_f - 2\gamma(\mathbf{u}_p(t_{n+1}) + \partial_t \boldsymbol{\eta}_p(t_{n+1})) \cdot \mathbf{n}_p \\
& + 2\gamma \mathbb{T}^{n+1}(\boldsymbol{\eta}_p) \cdot \mathbf{n}_p + 2\gamma \mathbf{u}_f^{n+1} \cdot \mathbf{n}_f + 2\gamma(\mathbf{u}_p^{n+1} + d_t \boldsymbol{\eta}_p^{n+1}) \cdot \mathbf{n}_p \\
& = \tilde{\mu}_n(t_n) - \mu_n^n + 2\gamma \mathbb{T}^{n+1}(\boldsymbol{\eta}_p) \cdot \mathbf{n}_p - \mu_n^{n+1} + \mu_n^n \\
& = \tilde{\mu}_n(t_n) + 2\gamma \mathbb{T}^{n+1}(\boldsymbol{\eta}_p) \cdot \mathbf{n}_p - \mu_n^{n+1} - \tilde{\mu}_n(t_{n+1}) + \tilde{\mu}_n(t_{n+1}) - \gamma \mathbb{T}^n(\boldsymbol{\eta}_p) \cdot \mathbf{n}_p + \gamma \mathbb{T}^n(\boldsymbol{\eta}_p) \cdot \mathbf{n}_p \\
& = \tilde{\mu}_n(t_{n+1}) - \mu_n^{n+1} - (\tilde{\mu}_n(t_{n+1}) - \gamma \mathbb{T}^{n+1}(\boldsymbol{\eta}_p) \cdot \mathbf{n}_p) + (\tilde{\mu}_n(t_n) - \gamma \mathbb{T}^n(\boldsymbol{\eta}_p) \cdot \mathbf{n}_p) \\
& + \gamma(\mathbb{T}^{n+1}(\boldsymbol{\eta}_p) + \mathbb{T}^n(\boldsymbol{\eta}_p)) \cdot \mathbf{n}_p \\
& = M_n^{n+1} - \mathbb{S}^{n+1}(\mu_n) + \gamma(\mathbb{T}^{n+1}(\boldsymbol{\eta}_p) + \mathbb{T}^n(\boldsymbol{\eta}_p)) \cdot \mathbf{n}_p \\
& = M_n^{n+1} - A_n^n, \tag{5.25}
\end{aligned}$$

where we have applied (5.8a), (2.8), (5.11a), (5.7a), and (5.22a). By an analogous argument, we have

$$M_\tau^n - 2\gamma \mathbf{U}_f^{n+1} \cdot \boldsymbol{\tau}_f - 2\gamma d_t \mathbf{H}_p^{n+1} \cdot \boldsymbol{\tau}_p = M_\tau^{n+1} - A_\tau^n. \tag{5.26}$$

Applying (5.25) and (5.26) to (5.23), we obtain

$$a_p^e(\mathbf{H}_p^{n+1}, d_t \mathbf{H}_p^{n+1}) + s_0(d_t P_p^{n+1}, P_p^{n+1})_{\Omega_p} + a_p^d(\mathbf{U}_p^{n+1}, \mathbf{U}_p^{n+1})$$

$$\begin{aligned}
&= \frac{1}{4\gamma} \|M_n^n - 2\gamma \mathbf{U}_f^{n+1} \cdot \mathbf{n}_f\|_{L^2(\Gamma_{fp})}^2 - \frac{1}{4\gamma} \|M_n^{n+1}\|_{L^2(\Gamma_{fp})}^2 \\
&\quad + \frac{1}{4\gamma} \|M_\tau^n - 2\gamma \mathbf{U}_f^{n+1} \cdot \boldsymbol{\tau}_f\|_{L^2(\Gamma_{fp})}^2 - \frac{1}{4\gamma} \|M_\tau^{n+1}\|_{L^2(\Gamma_{fp})}^2 \\
&\quad + \frac{1}{2\gamma} \langle A_n^n, M_n^{n+1} + 2\gamma(\mathbf{U}_p^{n+1} + d_t \mathbf{H}_p^{n+1}) \cdot \mathbf{n}_p \rangle + \frac{1}{2\gamma} \langle A_\tau^n, M_\tau^{n+1} + 2\gamma d_t \mathbf{H}_p^{n+1} \cdot \boldsymbol{\tau}_p \rangle \\
&\quad - \frac{1}{4\gamma} \|A_n^n\|_{L^2(\Gamma_{fp})}^2 - \frac{1}{4\gamma} \|A_\tau^n\|_{L^2(\Gamma_{fp})}^2 + I_2.
\end{aligned} \tag{5.27}$$

We note that, using (5.22a) and (5.22b), I_1 may be rewritten as

$$\begin{aligned}
I_1 &= \frac{1}{2\gamma} \langle A_n^n, 2\gamma \mathbf{U}_f^{n+1} \cdot \mathbf{n}_f \rangle_{\Gamma_{fp}} + \frac{1}{2\gamma} \langle A_\tau^n, 2\gamma \mathbf{U}_f^{n+1} \cdot \boldsymbol{\tau}_f \rangle_{\Gamma_{fp}} \\
&\quad + \langle \gamma \mathbb{T}^{n+1}(\boldsymbol{\eta}_p) \cdot \mathbf{n}_p, \mathbf{U}_f^{n+1} \cdot \mathbf{n}_f \rangle_{\Gamma_{fp}} + \langle \gamma \mathbb{T}^{n+1}(\boldsymbol{\eta}_p) \cdot \boldsymbol{\tau}_p, \mathbf{U}_f^{n+1} \cdot \boldsymbol{\tau}_f \rangle_{\Gamma_{fp}}.
\end{aligned}$$

Next, we combine (5.27) and (5.17) and use the above expression to get

$$\begin{aligned}
&a_p^e(\mathbf{H}_p^{n+1}, d_t \mathbf{H}_p^{n+1}) + s_0(d_t P_p^{n+1}, P_p^{n+1})_{\Omega_p} + a_f(\mathbf{U}_f^{n+1}, \mathbf{U}_f^{n+1}) + a_p^d(\mathbf{U}_p^{n+1}, \mathbf{U}_p^{n+1}) \\
&= \frac{1}{4\gamma} (\|M_n^n\|_{L^2(\Gamma_{fp})}^2 - \|M_n^{n+1}\|_{L^2(\Gamma_{fp})}^2) + \frac{1}{4\gamma} (\|M_\tau^n\|_{L^2(\Gamma_{fp})}^2 - \|M_\tau^{n+1}\|_{L^2(\Gamma_{fp})}^2) \\
&\quad + \frac{1}{2\gamma} \langle M_n^{n+1} + 2\gamma \mathbf{U}_f^{n+1} \cdot \mathbf{n}_f + 2\gamma(\mathbf{U}_p^{n+1} + d_t \mathbf{H}_p^{n+1}) \cdot \mathbf{n}_p, A_n^n \rangle_{\Gamma_{fp}} \\
&\quad + \frac{1}{2\gamma} \langle M_\tau^{n+1} + 2\gamma \mathbf{U}_f^{n+1} \cdot \boldsymbol{\tau}_f + 2\gamma d_t \mathbf{H}_p^{n+1} \cdot \boldsymbol{\tau}_p, A_\tau^n \rangle_{\Gamma_{fp}} - \frac{1}{4\gamma} \|A_n^n\|_{L^2(\Gamma_{fp})}^2 - \frac{1}{4\gamma} \|A_\tau^n\|_{L^2(\Gamma_{fp})}^2 \\
&\quad + I_2 + I_3,
\end{aligned}$$

where

$$I_3 := \langle \gamma \mathbb{T}^{n+1}(\boldsymbol{\eta}_p) \cdot \mathbf{n}_p, \mathbf{U}_f^{n+1} \cdot \mathbf{n}_f \rangle_{\Gamma_{fp}} + \langle \gamma \mathbb{T}^{n+1}(\boldsymbol{\eta}_p) \cdot \boldsymbol{\tau}_p, \mathbf{U}_f^{n+1} \cdot \boldsymbol{\tau}_f \rangle_{\Gamma_{fp}}. \tag{5.28}$$

From (5.25) and (5.26), it follows that

$$\begin{aligned}
M_n^{n+1} + 2\gamma \mathbf{U}_f^{n+1} \cdot \mathbf{n}_f + 2\gamma(\mathbf{U}_p^{n+1} + d_t \mathbf{H}_p^{n+1}) \cdot \mathbf{n}_p &= M_n^n + A_n^n, \\
M_\tau^{n+1} + 2\gamma \mathbf{U}_f^{n+1} \cdot \boldsymbol{\tau}_f + 2\gamma d_t \mathbf{H}_p^{n+1} \cdot \boldsymbol{\tau}_p &= M_\tau^n + A_\tau^n.
\end{aligned}$$

Therefore, we have

$$\begin{aligned}
&a_p^e(\mathbf{H}_p^{n+1}, d_t \mathbf{H}_p^{n+1}) + s_0(d_t P_p^{n+1}, P_p^{n+1})_{\Omega_p} + a_f(\mathbf{U}_f^{n+1}, \mathbf{U}_f^{n+1}) + a_p^d(\mathbf{U}_p^{n+1}, \mathbf{U}_p^{n+1}) \\
&= \frac{1}{4\gamma} (\|M_n^n\|_{L^2(\Gamma_{fp})}^2 - \|M_n^{n+1}\|_{L^2(\Gamma_{fp})}^2) + \frac{1}{4\gamma} (\|M_\tau^n\|_{L^2(\Gamma_{fp})}^2 - \|M_\tau^{n+1}\|_{L^2(\Gamma_{fp})}^2) \\
&\quad + \frac{1}{2\gamma} \langle M_n^n + A_n^n, A_n^n \rangle_{\Gamma_{fp}} + \frac{1}{2\gamma} \langle M_\tau^n + A_\tau^n, A_\tau^n \rangle_{\Gamma_{fp}} - \frac{1}{4\gamma} \|A_n^n\|_{L^2(\Gamma_{fp})}^2 - \frac{1}{4\gamma} \|A_\tau^n\|_{L^2(\Gamma_{fp})}^2 + I_2 + I_3 \\
&= \frac{1}{4\gamma} (\|M_n^n\|_{L^2(\Gamma_{fp})}^2 - \|M_n^{n+1}\|_{L^2(\Gamma_{fp})}^2) + \frac{1}{4\gamma} (\|M_\tau^n\|_{L^2(\Gamma_{fp})}^2 - \|M_\tau^{n+1}\|_{L^2(\Gamma_{fp})}^2) \\
&\quad + \frac{1}{2\gamma} \langle M_n^n, A_n^n \rangle_{\Gamma_{fp}} + \frac{1}{2\gamma} \langle M_\tau^n, A_\tau^n \rangle_{\Gamma_{fp}} + \frac{1}{4\gamma} \|A_n^n\|_{L^2(\Gamma_{fp})}^2 + \frac{1}{4\gamma} \|A_\tau^n\|_{L^2(\Gamma_{fp})}^2 + I_2 + I_3.
\end{aligned} \tag{5.29}$$

For the mixed terms on the right hand side, let $\mathbf{M}^n = (M_n^n, M_\tau^n)$ and $\mathbf{A}^n = (A_n^n, A_\tau^n)$. Since Γ_{fp} is assumed to be C^1 , it holds that $\mathbf{A}^n \in (H^{1/2}(\Gamma_{fp}))^d$. We have

$$\begin{aligned} \frac{1}{2\gamma} \langle M_n^n, A_n^n \rangle_{\Gamma_{fp}} + \frac{1}{2\gamma} \langle M_\tau^n, A_\tau^n \rangle_{\Gamma_{fp}} &= \frac{1}{2\gamma} \langle \mathbf{M}^n, \mathbf{A}^n \rangle_{\Gamma_{fp}} \leq \frac{1}{2\gamma} \|\mathbf{M}^n\|_{H^{-1/2}(\Gamma_{fp})} \|\mathbf{A}^n\|_{H^{1/2}(\Gamma_{fp})} \\ &\leq \frac{\epsilon}{4\gamma} \|\mathbf{M}^n\|_{H^{-1/2}(\Gamma_{fp})}^2 + \frac{1}{4\epsilon\gamma} \|\mathbf{A}^n\|_{H^{1/2}(\Gamma_{fp})}^2, \end{aligned} \quad (5.30)$$

where we have used the duality of $\|\cdot\|_{H^{-1/2}(\Gamma_{fp})}$ and $\|\cdot\|_{H^{1/2}(\Gamma_{fp})}$, as well as Young's inequality. Using the continuous version of the inf-sup condition (4.14) and (5.13), we obtain

$$\|P_f^{n+1}\|_{L^2(\Omega_f)} \leq \frac{\sqrt{C_f}}{\beta_f} \|\mathbf{U}_f^{n+1}\|_f, \quad (5.31)$$

where C_f is the continuity constant, $a_f(\mathbf{u}_f, \mathbf{v}_f) \leq C_f \|\mathbf{u}_f\|_{H^1(\Omega_f)} \|\mathbf{v}_f\|_{H^1(\Omega_f)}$. Next, similarly to (4.19), from (5.13) we have

$$\frac{1}{C_{ext}} \|\mathbf{M}^n\|_{H^{-1/2}(\Gamma_{fp})} \leq \sqrt{C_f} (1 + \gamma C_{tr}^2) \|\mathbf{U}_f^{n+1}\|_f + \|P_f^{n+1}\|_{L^2(\Omega_f)} + C_{tr} \|\mathbb{S}^{n+1}(\boldsymbol{\mu}) - \gamma \mathbb{T}^n(\boldsymbol{\eta}_p)\|_{H^{-1/2}(\Gamma_{fp})}, \quad (5.32)$$

where C_{tr} is the trace inequality constant, $\|\mathbf{v}_f\|_{H^{1/2}(\Gamma_{fp})} \leq C_{tr} \|\mathbf{v}_f\|_{H^1(\Omega_f)}$. Combining (5.31) and (5.32) implies that

$$\|\mathbf{M}^n\|_{H^{-1/2}(\Gamma_{fp})}^2 \leq \tilde{C}_f \left(\|\mathbf{U}_f^{n+1}\|_f^2 + \|\mathbf{B}^n\|_{H^{-1/2}(\Gamma_{fp})}^2 \right), \quad (5.33)$$

where $\mathbf{B}^n := \mathbb{S}^{n+1}(\boldsymbol{\mu}) - \gamma \mathbb{T}^n(\boldsymbol{\eta}_p)$. Taking $\epsilon = \frac{\gamma}{C_f}$ in (5.30) and using (5.33) results in

$$\frac{1}{2\gamma} \langle \mathbf{M}^n, \mathbf{A}^n \rangle_{\Gamma_{fp}} \leq \frac{1}{4} \|\mathbf{U}_f^{n+1}\|_f^2 + \frac{1}{4} \|\mathbf{B}^n\|_{H^{-1/2}(\Gamma_{fp})}^2 + \frac{\tilde{C}_f}{4\gamma^2} \|\mathbf{A}^n\|_{H^{1/2}(\Gamma_{fp})}^2. \quad (5.34)$$

It remains to bound I_2 and I_3 . To this end, we first note that the continuous version of the inf-sup condition (4.15) and (5.18) with $\boldsymbol{\xi}_p = 0$ imply

$$\|P_p^{n+1}\|_{L^2(\Omega_p)}^2 \leq \tilde{C}_p \|\mathbf{U}_p^{n+1}\|_d^2. \quad (5.35)$$

Now, Using the Cauchy-Schwarz and Young's inequalities, we have

$$\begin{aligned} |I_2| &\leq s_0^2 \tilde{C}_p \|\mathbb{T}^{n+1}(p_p)\|_{L^2(\Omega_p)}^2 + \frac{1}{4\tilde{C}_p} \|P_p^{n+1}\|_{L^2(\Omega_p)}^2 + \alpha^2 \tilde{C}_p \|\nabla \cdot \mathbb{T}^{n+1}(\boldsymbol{\eta}_p)\|_{L^2(\Omega_p)}^2 + \frac{1}{4\tilde{C}_p} \|P_p^{n+1}\|_{L^2(\Omega_p)}^2 \\ &\leq s_0^2 \tilde{C}_p \|\mathbb{T}^{n+1}(p_p)\|_{L^2(\Omega_p)}^2 + \alpha^2 \tilde{C}_p \|\nabla \cdot \mathbb{T}^{n+1}(\boldsymbol{\eta}_p)\|_{L^2(\Omega_p)}^2 + \frac{1}{2} \|\mathbf{U}_p^{n+1}\|_d^2, \end{aligned} \quad (5.36)$$

$$\begin{aligned} |I_3| &\leq \frac{\gamma^2}{2\epsilon} \|\mathbb{T}^{n+1}(\boldsymbol{\eta}_p)\|_{H^{-1/2}(\Gamma_{fp})}^2 + \frac{\epsilon}{2} \|\mathbf{U}_f^{n+1}\|_{H^{1/2}(\Gamma_{fp})}^2 \leq \frac{\gamma^2}{2\epsilon} \|\mathbb{T}^{n+1}(\boldsymbol{\eta}_p)\|_{H^{-1/2}(\Gamma_{fp})}^2 + \frac{\epsilon C_{tr}^2}{2c_f} \|\mathbf{U}_f^{n+1}\|_f^2 \\ &\leq \frac{\gamma^2 C_{tr}^2}{c_f} \|\mathbb{T}^{n+1}(\boldsymbol{\eta}_p)\|_{H^{-1/2}(\Gamma_{fp})}^2 + \frac{1}{4} \|\mathbf{U}_f^{n+1}\|_f^2, \end{aligned} \quad (5.37)$$

where we used the trace inequality and the coercivity bound for a_f in (4.9) and chose $\epsilon = c_f/(2C_{tr}^2)$.

Applying bounds (5.34) and (5.36)–(5.37) in (5.29), using that $a(a-b) \geq \frac{1}{2}(a^2 - b^2)$ (cf. (4.2)) for the first four terms on the left-hand side, as well as the coercivity bounds (4.9) yields

$$\frac{1}{2\Delta t} \left(\|\mathbf{H}_p^{n+1}\|_e^2 - \|\mathbf{H}_p^n\|_e^2 \right) + \frac{s_0}{2\Delta t} \left(\|P_p^{n+1}\|_{L^2(\Omega_p)}^2 - \|P_p^n\|_{L^2(\Omega_p)}^2 \right)$$

$$+ \frac{1}{2} \|\mathbf{U}_f^{n+1}\|_f^2 + \frac{1}{2} \|\mathbf{U}_p^{n+1}\|_d^2 + \frac{1}{4\gamma} \left(\|\mathbf{M}^{n+1}\|_{L^2(\Gamma_{fp})}^2 - \|\mathbf{M}^n\|_{L^2(\Gamma_{fp})}^2 \right) \leq J^n, \quad (5.38)$$

where

$$\begin{aligned} J^n := & \frac{1}{4} \|\mathbf{B}^n\|_{H^{-1/2}(\Gamma_{fp})}^2 + \frac{\tilde{C}_f}{4\gamma^2} \|\mathbf{A}^n\|_{H^{1/2}(\Gamma_{fp})}^2 + \frac{1}{4\gamma} \|\mathbf{A}^n\|_{L^2(\Gamma_{fp})}^2 + s_0^2 \tilde{C}_p \|\mathbb{T}^{n+1}(p_p)\|_{L^2(\Omega_p)}^2 \\ & + \alpha^2 \tilde{C}_p \|\nabla \cdot \mathbb{T}^{n+1}(\boldsymbol{\eta}_p)\|_{L^2(\Omega_p)}^2 + \frac{\gamma^2 C_{tr}^2}{c_f} \|\mathbb{T}^{n+1}(\boldsymbol{\eta}_p)\|_{L^2(\Gamma_{fp})}^2. \end{aligned}$$

We multiply (5.38) by Δt and sum from $n = 0$ to $m-1$, for $1 \leq m \leq N$, which yields

$$\begin{aligned} & \frac{1}{2} \|\mathbf{H}_p^m\|_e^2 + \frac{s_0}{2} \|P_p^m\|_{L^2(\Omega_p)}^2 + \frac{\Delta t}{2} \sum_{n=0}^{m-1} \|\mathbf{U}_f^{n+1}\|_f^2 + \frac{\Delta t}{2} \sum_{n=0}^{m-1} \|\mathbf{U}_p^{n+1}\|_d^2 + \frac{\Delta t}{4\gamma} \|\mathbf{M}^m\|_{L^2(\Gamma_{fp})}^2 \\ & \leq \Delta t \sum_{n=0}^{m-1} J^n + \|\mathbf{H}_p^0\|_e^2 + \frac{s_0}{2} \|P_p^0\|_{L^2(\Omega_p)}^2 + \frac{\Delta t}{4\gamma} \|\mathbf{M}^0\|_{L^2(\Gamma_{fp})}^2. \end{aligned} \quad (5.39)$$

All initial error terms above are zero. In particular, $\mathbf{H}_p^0 = 0$ and $P_p^0 = 0$ from the choice of initial numerical values, and $d_t \boldsymbol{\eta}_p(t_0) - d_t \boldsymbol{\eta}_p^0 = \mathbf{u}_{s,0} - \mathbf{u}_{s,0} = 0$ implies that $\mathbf{M}^0 = 0$. For the term J^n , which collects all time splitting and time discretization errors, assuming that the solution is sufficiently smooth, it is straightforward to show that $J^n = \mathcal{O}(\Delta t^2)$, hence $\Delta t \sum_{n=0}^{m-1} J^n = \mathcal{O}(T \Delta t^2)$. Therefore, using that (5.39) holds for all $1 \leq m \leq N$ and combining it with (5.31), (5.33), and (5.35), we obtain (5.12). \square

6 Iterative algorithm

The algorithm discussed in the previous sections solves one Stokes and one Biot problems per time step. This is a computationally efficient choice, but it introduces a splitting error. To avoid this error, one could use the iterative version of the algorithm, which at every time t^{n+1} iterates over the Stokes and Biot sub-problems until convergence. These are Richardson (also called fixed point) iterations. Let k be the index for these iterations. For ease of notation, in the description of the algorithm we will drop the time step index from the variables in the Richardson iterations, i.e., we will write ϕ^{k+1} instead of the more rigorous (and bulkier) $\phi^{n+1,k+1}$. Finally, let $d_t \varphi^{k+1} := (\varphi^{k+1} - \varphi^n)/\Delta t$ and $d_{tt} \boldsymbol{\eta}_p^{k+1} := d_t d_t \boldsymbol{\eta}_p^{k+1} = (d_t \boldsymbol{\eta}_p^{k+1} - d_t \boldsymbol{\eta}_p^n)/\Delta t$. Recalling that $d_t \boldsymbol{\eta}_p^n = (\boldsymbol{\eta}_p^n - \boldsymbol{\eta}_p^{n-1})/\Delta t$ for $n \geq 1$, we have $d_{tt} \boldsymbol{\eta}_p^{k+1} = (\boldsymbol{\eta}_p^{k+1} - 2\boldsymbol{\eta}_p^n + \boldsymbol{\eta}_p^{n-1})/\Delta t^2$, while for $n = 0$ we have $d_{tt} \boldsymbol{\eta}_p^{k+1} = ((\boldsymbol{\eta}_p^{k+1} - \boldsymbol{\eta}_p^n)/\Delta t - \mathbf{u}_{s,0})/\Delta t$.

For simplicity we present the method in the case $\gamma_{BJS} = 0$. At every time t^{n+1} , assume that \mathbf{u}_f^n , p_p^n , $\boldsymbol{\eta}_p^n$, μ_n^n , and μ_τ^n are known.

Algorithm 2.

Set $\mu_n^0 = \mu_n^n$ and $\mu_\tau^0 = \mu_\tau^n$. The following steps are performed at iteration $k+1$, $k \geq 0$:

1. Stokes problem: Find $(\mathbf{u}_f^{k+1}, p_f^{k+1})$ such that

$$\begin{aligned} & \left(\rho_f d_t \mathbf{u}_f^{k+1}, \mathbf{v}_f \right)_{\Omega_f} + a_f(\mathbf{u}_f^{k+1}, \mathbf{v}_f) + b_f(\mathbf{v}_f, p_f^{k+1}) + \gamma_f \langle \mathbf{u}_f^{k+1} \cdot \mathbf{n}_f, \mathbf{v}_f \cdot \mathbf{n}_f \rangle_{\Gamma_{fp}} \\ & + \gamma_f \langle \mathbf{u}_f^{k+1} \cdot \boldsymbol{\tau}_f, \mathbf{v}_f \cdot \boldsymbol{\tau}_f \rangle_{\Gamma_{fp}} = (\mathbf{f}_f, \mathbf{v}_f)_{\Omega_f} + \langle \mu_n^k, \mathbf{v}_f \cdot \mathbf{n}_f \rangle_{\Gamma_{fp}} + \langle \mu_\tau^k, \mathbf{v}_f \cdot \boldsymbol{\tau}_f \rangle_{\Gamma_{fp}} \end{aligned} \quad (6.1)$$

$$- b_f(\mathbf{u}_f^{k+1}, w_f) = (q_f, w_f)_{\Omega_f}. \quad (6.2)$$

2. Biot problem: Find $(\boldsymbol{\eta}_p^{k+1}, \mathbf{u}_p^{k+1}, p_p^{k+1})$ such that

$$\begin{aligned} & (\rho_p d_{tt} \boldsymbol{\eta}_p^{k+1}, \boldsymbol{\xi}_p)_{\Omega_p} + a_p^d(\mathbf{u}_p^{k+1}, \mathbf{v}_p) + a_p^e(\boldsymbol{\eta}_p^{k+1}, \boldsymbol{\xi}_p) + b_p(\mathbf{v}_p, p_p^{k+1}) + \alpha b_p(\boldsymbol{\xi}_p, p_p^{k+1}) \\ & + \gamma_p \langle (\mathbf{u}_p^{k+1} + d_t \boldsymbol{\eta}_p^{k+1}) \cdot \mathbf{n}_p, (\mathbf{v}_p + \boldsymbol{\xi}_p) \cdot \mathbf{n}_p \rangle_{\Gamma_{fp}} + \gamma_p \langle d_t \boldsymbol{\eta}_p^{k+1} \cdot \boldsymbol{\tau}_p, \boldsymbol{\xi}_p \cdot \boldsymbol{\tau}_p \rangle_{\Gamma_{fp}} \\ & = (\mathbf{f}_p, \boldsymbol{\xi}_p)_{\Omega_p} + \langle \mu_n^k - (\gamma_p + \gamma_f) \mathbf{u}_f^{k+1} \cdot \mathbf{n}_f, (\mathbf{v}_p + \boldsymbol{\xi}_p) \cdot \mathbf{n}_p \rangle_{\Gamma_{fp}} \\ & + \left\langle \mu_\tau^k - (\gamma_p + \gamma_f) \mathbf{u}_f^{k+1} \cdot \boldsymbol{\tau}_f, \boldsymbol{\xi}_p \cdot \boldsymbol{\tau}_p \right\rangle_{\Gamma_{fp}}, \end{aligned} \quad (6.3)$$

$$(s_0 d_t p_p^{k+1}, w_p)_{\Omega_p} - \alpha b_p(d_t \boldsymbol{\eta}_p^{k+1}, w_p) - b_p(\mathbf{u}_p^{k+1}, w_p) = (q_p, w_p)_{\Omega_p}. \quad (6.4)$$

3. Update:

$$\langle \mu_n^{k+1}, \chi_n \rangle_{\Gamma_{fp}} = \langle \mu_n^k - (\gamma_f + \gamma_p)((d_t \boldsymbol{\eta}_p^{k+1} + \mathbf{u}_p^{k+1}) \cdot \mathbf{n}_p + \mathbf{u}_f^{k+1} \cdot \mathbf{n}_f), \chi_n \rangle_{\Gamma_{fp}}, \quad (6.5a)$$

$$\langle \mu_\tau^{k+1}, \chi_\tau \rangle_{\Gamma_{fp}} = \langle \mu_\tau^k - (\gamma_f + \gamma_p)(d_t \boldsymbol{\eta}_p^{k+1} \cdot \boldsymbol{\tau}_p + \mathbf{u}_f^{k+1} \cdot \boldsymbol{\tau}_f), \chi_\tau \rangle_{\Gamma_{fp}}. \quad (6.5b)$$

4. Check the stopping criterion, e.g.

$$\left\| \mathbf{u}_f^{k+1} \cdot \mathbf{n}_f - \mathbf{u}_f^k \cdot \mathbf{n}_f \right\|_{L^2(\Gamma_{fp})} < \epsilon \quad (6.6)$$

where ϵ is a given stopping tolerance. If not satisfied, repeat steps 1–4. If satisfied, set $\mathbf{u}_f^{n+1} = \mathbf{u}_f^{k+1}$, $p_f^{n+1} = p_f^{k+1}$, $\boldsymbol{\eta}_p^{n+1} = \boldsymbol{\eta}_p^{k+1}$, $\mathbf{u}_p^{n+1} = \mathbf{u}_p^{k+1}$, $p_p^{n+1} = p_p^{k+1}$, and $\boldsymbol{\mu}^{n+1} = \boldsymbol{\mu}^{k+1}$.

End of Algorithm 2.

We next show that the above algorithm converges.

Theorem 6.1. For **Algorithm 2** with $\gamma_f = \gamma_p = \gamma$ it holds that as $k \rightarrow \infty$, $\mathbf{u}_f^{k+1} \rightarrow \mathbf{u}_f^{n+1}$ in \mathbf{V}_f , $p_f^{k+1} \rightarrow p_f^{n+1}$ in W_f , $\boldsymbol{\eta}_p^{k+1} \rightarrow \boldsymbol{\eta}_p^{n+1}$ in \mathbf{X}_p , $\mathbf{u}_p^{k+1} \rightarrow \mathbf{u}_p^{n+1}$ in \mathbf{V}_p , $p_p^{k+1} \rightarrow p_p^{n+1}$ in W_p , and $\boldsymbol{\mu}^{k+1} \rightarrow \boldsymbol{\mu}^{n+1}$ in $(L^2(\Gamma_{fp}))^2$.

Proof. Let $\bar{\mathbf{u}}_f^{k+1} := \mathbf{u}_f^{k+1} - \mathbf{u}_f^k$ for $k \geq 1$ with a similar notation for the rest of the variables. Subtracting (6.1)–(6.5b) for $k+1$ and k results in the equations in the Stokes region

$$\begin{aligned} & \frac{1}{\Delta t} \left(\rho_f \bar{\mathbf{u}}_f^{k+1}, \mathbf{v}_f \right)_{\Omega_f} + a_f(\bar{\mathbf{u}}_f^{k+1}, \mathbf{v}_f) + b_f(\mathbf{v}_f, \bar{p}_f^{k+1}) + \gamma \langle \bar{\mathbf{u}}_f^{k+1} \cdot \mathbf{n}_f, \mathbf{v}_f \cdot \mathbf{n}_f \rangle_{\Gamma_{fp}} \\ & + \gamma \langle \bar{\mathbf{u}}_f^{k+1} \cdot \boldsymbol{\tau}_f, \mathbf{v}_f \cdot \boldsymbol{\tau}_f \rangle_{\Gamma_{fp}} = \langle \bar{\mu}_n^k, \mathbf{v}_f \cdot \mathbf{n}_f \rangle_{\Gamma_{fp}} + \langle \bar{\mu}_\tau^k, \mathbf{v}_f \cdot \boldsymbol{\tau}_f \rangle_{\Gamma_{fp}} \end{aligned} \quad (6.7)$$

$$- b_f(\bar{\mathbf{u}}_f^{k+1}, w_f) = 0, \quad (6.8)$$

and in the Biot region

$$\begin{aligned} & \frac{1}{\Delta t^2} \left(\rho_p \bar{\boldsymbol{\eta}}_p^{k+1}, \boldsymbol{\xi}_p \right)_{\Omega_p} + a_p^d(\bar{\mathbf{u}}_p^{k+1}, \mathbf{v}_p) + a_p^e(\bar{\boldsymbol{\eta}}_p^{k+1}, \boldsymbol{\xi}_p) + b_p(\mathbf{v}_p, \bar{p}_p^{k+1}) + \alpha b_p(\boldsymbol{\xi}_p, \bar{p}_p^{k+1}) \\ & + \gamma \left\langle \left(\bar{\mathbf{u}}_p^{k+1} + \frac{1}{\Delta t} \bar{\boldsymbol{\eta}}_p^{k+1} \right) \cdot \mathbf{n}_p, (\mathbf{v}_p + \boldsymbol{\xi}_p) \cdot \mathbf{n}_p \right\rangle_{\Gamma_{fp}} + \gamma \left\langle \frac{1}{\Delta t} \bar{\boldsymbol{\eta}}_p^{k+1} \cdot \boldsymbol{\tau}_p, \boldsymbol{\xi}_p \cdot \boldsymbol{\tau}_p \right\rangle_{\Gamma_{fp}} \\ & = \langle \bar{\mu}_n^k - 2\gamma \bar{\mathbf{u}}_f^{k+1} \cdot \mathbf{n}_f, (\mathbf{v}_p + \boldsymbol{\xi}_p) \cdot \mathbf{n}_p \rangle_{\Gamma_{fp}} + \left\langle \bar{\mu}_\tau^k - 2\gamma \bar{\mathbf{u}}_f^{k+1} \cdot \boldsymbol{\tau}_f, \boldsymbol{\xi}_p \cdot \boldsymbol{\tau}_p \right\rangle_{\Gamma_{fp}}, \end{aligned} \quad (6.9)$$

$$\frac{1}{\Delta t}(s_0 \bar{p}_p^{k+1}, w_p)_{\Omega_p} - \alpha b_p \left(\frac{1}{\Delta t} \bar{\boldsymbol{\eta}}_p^{k+1}, w_p \right) - b_p(\bar{\mathbf{u}}_p^{k+1}, w_p) = 0, \quad (6.10)$$

as well as the updates

$$\langle \bar{\mu}_n^{k+1}, \chi_n \rangle_{\Gamma_{fp}} = \left\langle \bar{\mu}_n^k - 2\gamma \left(\left(\frac{1}{\Delta t} \bar{\boldsymbol{\eta}}_p^{k+1} + \bar{\mathbf{u}}_p^{k+1} \right) \cdot \mathbf{n}_p + \bar{\mathbf{u}}_f^{k+1} \cdot \mathbf{n}_f \right), \chi_n \right\rangle_{\Gamma_{fp}}, \quad (6.11a)$$

$$\langle \bar{\mu}_{\tau}^{k+1}, \chi_{\tau} \rangle_{\Gamma_{fp}} = \left\langle \bar{\mu}_{\tau}^k - 2\gamma \left(\frac{1}{\Delta t} \bar{\boldsymbol{\eta}}_p^{k+1} \cdot \boldsymbol{\tau}_p + \bar{\mathbf{u}}_f^{k+1} \cdot \boldsymbol{\tau}_f \right), \chi_{\tau} \right\rangle_{\Gamma_{fp}}. \quad (6.11b)$$

Taking $\mathbf{v}_f = \bar{\mathbf{u}}_f^{k+1}$, $w_f = \bar{p}_f^{k+1}$, $\mathbf{v}_p = \bar{\mathbf{u}}_p^{k+1}$, $w_p = \bar{p}_p^{k+1}$, and $\boldsymbol{\xi}_p = \frac{1}{\Delta t} \bar{\boldsymbol{\eta}}_p^{k+1}$ and following the argument in the proof of Theorem 4.1, we obtain

$$\begin{aligned} & \sum_{k=1}^M \left(\frac{\rho_f}{\Delta t} (\bar{\mathbf{u}}_f^{k+1}, \bar{\mathbf{u}}_f^{k+1})_{\Omega_f} + \frac{\rho_p}{\Delta t^2} (\bar{\boldsymbol{\eta}}_p^{k+1}, \bar{\boldsymbol{\eta}}_p^{k+1})_{\Omega_p} + \frac{1}{\Delta t} a_p^e(\bar{\boldsymbol{\eta}}_p^{k+1}, \bar{\boldsymbol{\eta}}_p^{k+1}) + \frac{s_0}{\Delta t} (\bar{p}_p^{k+1}, \bar{p}_p^{k+1})_{\Omega_p} \right. \\ & \quad \left. + a_f(\bar{\mathbf{u}}_f^{k+1}, \bar{\mathbf{u}}_f^{k+1}) + a_p^d(\bar{\mathbf{u}}_p^{k+1}, \bar{\mathbf{u}}_p^{k+1}) \right) + \frac{1}{4\gamma} \int_{\Gamma_{fp}} (\bar{\mu}_n^{M+1})^2 + \frac{1}{4\gamma} \int_{\Gamma_{fp}} (\bar{\mu}_{\tau}^{M+1})^2 \\ & \leq \frac{1}{4\gamma} \int_{\Gamma_{fp}} (\bar{\mu}_n^1)^2 + \frac{1}{4\gamma} \int_{\Gamma_{fp}} (\bar{\mu}_{\tau}^1)^2, \end{aligned}$$

which implies that the series

$$\begin{aligned} & \sum_{k=1}^{\infty} \left(\frac{\rho_f}{\Delta t} (\bar{\mathbf{u}}_f^{k+1}, \bar{\mathbf{u}}_f^{k+1})_{\Omega_f} + \frac{\rho_p}{\Delta t^2} (\bar{\boldsymbol{\eta}}_p^{k+1}, \bar{\boldsymbol{\eta}}_p^{k+1})_{\Omega_p} + \frac{1}{\Delta t} a_p^e(\bar{\boldsymbol{\eta}}_p^{k+1}, \bar{\boldsymbol{\eta}}_p^{k+1}) + \frac{s_0}{\Delta t} (\bar{p}_p^{k+1}, \bar{p}_p^{k+1})_{\Omega_p} \right. \\ & \quad \left. + a_f(\bar{\mathbf{u}}_f^{k+1}, \bar{\mathbf{u}}_f^{k+1}) + a_p^d(\bar{\mathbf{u}}_p^{k+1}, \bar{\mathbf{u}}_p^{k+1}) \right) \end{aligned}$$

is convergent. Therefore $\bar{\mathbf{u}}_f^k \rightarrow 0$ in \mathbf{V}_f , $\bar{\boldsymbol{\eta}}_p^k \rightarrow 0$ in \mathbf{X}_p , $\bar{\mathbf{u}}_p^k \rightarrow 0$ in $(L^2(\Omega_p))^d$, and $\bar{p}_p^k \rightarrow 0$ in W_p . Using the inf-sup condition (4.14), we conclude from (6.7) that $\bar{p}_f^k \rightarrow 0$ in W_f .

Next, taking $w_p = \nabla \cdot \bar{\mathbf{u}}_p^{k+1}$ in (6.10) implies that $\nabla \cdot \bar{\mathbf{u}}_p^k \rightarrow 0$ in $L^2(\Omega_p)$. Also, the convergence $\bar{\mathbf{u}}_p^k \cdot \mathbf{n}_p \rightarrow 0$ in $L^2(\Gamma_{fp})$ follows from $\bar{\mathbf{u}}_p^k \rightarrow 0$ in $(L^2(\Omega_p))^d$ and the discrete trace-inverse inequality $\|\mathbf{v}_p \cdot \mathbf{n}_p\|_{L^2(\Gamma_{fp})} \leq Ch^{-1/2} \|\mathbf{v}_p\|_{L^2(\Omega_p)}$ for $\mathbf{v}_p \in \mathbf{V}_p$. Therefore $\bar{\mathbf{u}}_p^k \rightarrow 0$ in \mathbf{V}_p .

Finally, since $\boldsymbol{\Lambda}_h = \mathbf{V}_{f,h}|_{\Gamma_{fp}}$, we can take $\mathbf{v}_f = \mathbf{E}_{f,h} \bar{\boldsymbol{\mu}}^k$ in (6.7), where $\mathbf{E}_{f,h}$ is the continuous discrete Stokes extension utilized in (4.19), which implies

$$\|\bar{\boldsymbol{\mu}}^k\|_{L^2(\Gamma_{fp})}^2 \leq C(\|\bar{\mathbf{u}}_f^{k+1}\|_{H^1(\Omega_f)} + \|\bar{p}_f^{k+1}\|_{L^2(\Omega_f)}) \|\bar{\boldsymbol{\mu}}^k\|_{H^{1/2}(\Gamma_{fp})}.$$

Thus, using that $\|\bar{\boldsymbol{\mu}}^k\|_{H^{1/2}(\Gamma_{fp})} \leq Ch^{-1/2} \|\bar{\boldsymbol{\mu}}^k\|_{L^2(\Gamma_{fp})}$, we conclude that $\bar{\boldsymbol{\mu}}^k \rightarrow 0$ in $(L^2(\Gamma_{fp}))^2$. \square

Remark 6.1. *The proof of Theorem 6.1 establishes convergence of the iterative algorithm, but does not provide convergence rate. We refer the reader to [4, 5, 20], where such rates are established for related Robin-Robin schemes applied to simplified FSI or FPSI models using fixed point iteration arguments. In the numerical section we present a test on the effect of the Robin parameter on the rate of convergence.*

6.1 Monolithic scheme

Using the convergence established in Theorem 6.1, we can take $k \rightarrow \infty$ in (6.1)–(6.5b) to conclude that the limit functions satisfy the following fully coupled fully implicit scheme: find $(\mathbf{u}_f^{n+1}, p_f^{n+1}) \in \mathbf{V}_{f,h} \times W_{f,h}$, $(\boldsymbol{\eta}_p^{n+1}, \mathbf{u}_p^{n+1}, p_p^{n+1}) \in \mathbf{X}_{p,h} \times \mathbf{V}_{p,h} \times W_{p,h}$, and $\boldsymbol{\mu}_n^{n+1} \in \boldsymbol{\Lambda}_h$ such that for all $(\mathbf{v}_f, w_f) \in \mathbf{V}_{f,h} \times W_{f,h}$, $(\boldsymbol{\xi}_p, \mathbf{v}_p, w_p) \in \mathbf{X}_{p,h} \times \mathbf{V}_{p,h} \times W_{p,h}$, and $\boldsymbol{\chi} \in \boldsymbol{\Lambda}_h$,

$$\begin{aligned} & \left(\rho_f d_t \mathbf{u}_f^{n+1}, \mathbf{v}_f \right)_{\Omega_f} + a_f(\mathbf{u}_f^{n+1}, \mathbf{v}_f) + b_f(\mathbf{v}_f, p_f^{n+1}) + \gamma \langle \mathbf{u}_f^{n+1} \cdot \mathbf{n}_f, \mathbf{v}_f \cdot \mathbf{n}_f \rangle_{\Gamma_{fp}} \\ & + \gamma \langle \mathbf{u}_f^{n+1} \cdot \boldsymbol{\tau}_f, \mathbf{v}_f \cdot \boldsymbol{\tau}_f \rangle_{\Gamma_{fp}} = (\mathbf{f}_f, \mathbf{v}_f)_{\Omega_f} + \langle \mu_n^{n+1}, \mathbf{v}_f \cdot \mathbf{n}_f \rangle_{\Gamma_{fp}} + \langle \mu_\tau^{n+1}, \mathbf{v}_f \cdot \boldsymbol{\tau}_f \rangle_{\Gamma_{fp}}, \end{aligned} \quad (6.12)$$

$$- b_f(\mathbf{u}_f^{n+1}, w_f) = (q_f, w_f)_{\Omega_f}, \quad (6.13)$$

$$\begin{aligned} & (\rho_p d_{tt} \boldsymbol{\eta}_p^{n+1}, \boldsymbol{\xi}_p)_{\Omega_p} + a_p^e(\boldsymbol{\eta}_p^{n+1}, \boldsymbol{\xi}_p) + a_p^d(\mathbf{u}_p^{n+1}, \mathbf{v}_p) + \alpha b_p(\boldsymbol{\xi}_p, p_p^{n+1}) + b_p(\mathbf{v}_p, p_p^{n+1}) \\ & + \gamma \langle (\mathbf{u}_p^{n+1} + d_t \boldsymbol{\eta}_p^{n+1}) \cdot \mathbf{n}_p, (\mathbf{v}_p + \boldsymbol{\xi}_p) \cdot \mathbf{n}_p \rangle_{\Gamma_{fp}} + \gamma \langle d_t \boldsymbol{\eta}_p^{n+1} \cdot \boldsymbol{\tau}_p, \boldsymbol{\xi}_p \cdot \boldsymbol{\tau}_p \rangle_{\Gamma_{fp}} \\ & = (\mathbf{f}_p, \boldsymbol{\xi}_p)_{\Omega_p} + \langle \mu_n^{n+1} - 2\gamma \mathbf{u}_f^{n+1} \cdot \mathbf{n}_f, (\mathbf{v}_p + \boldsymbol{\xi}_p) \cdot \mathbf{n}_p \rangle_{\Gamma_{fp}} \\ & + \left\langle \mu_\tau^{n+1} - 2\gamma \mathbf{u}_f^{n+1} \cdot \boldsymbol{\tau}_f, \boldsymbol{\xi}_p \cdot \boldsymbol{\tau}_p \right\rangle_{\Gamma_{fp}}, \end{aligned} \quad (6.14)$$

$$s_0(d_t p_p^{n+1}, w_p)_{\Omega_p} - \alpha b_p(d_t \boldsymbol{\eta}_p^{n+1}, w_p) - b_p(\mathbf{u}_p^{n+1}, w_p) = (q_p, w_p)_{\Omega_p}, \quad (6.15)$$

$$\langle (d_t \boldsymbol{\eta}_p^{n+1} + \mathbf{u}_p^{n+1}) \cdot \mathbf{n}_p + \mathbf{u}_f^{n+1} \cdot \mathbf{n}_f, \chi_n \rangle_{\Gamma_{fp}} = 0, \quad (6.16)$$

$$\langle d_t \boldsymbol{\eta}_p^{n+1} \cdot \boldsymbol{\tau}_p + \mathbf{u}_f^{n+1} \cdot \boldsymbol{\tau}_f, \chi_\tau \rangle_{\Gamma_{fp}} = 0. \quad (6.17)$$

We note that the Robin data variables μ_n^{n+1} and μ_τ^{n+1} play the role of Lagrange multipliers to impose weakly the velocity continuity conditions (2.8) and (2.10) in (6.16)–(6.17). In addition, since the Stokes solution satisfies weakly the Robin boundary conditions

$$\gamma \mathbf{u}_f^{n+1} \cdot \mathbf{n}_f + (\boldsymbol{\sigma}_f^{n+1} \mathbf{n}_f) \cdot \mathbf{n}_f = \mu_n^{n+1} \quad \text{and} \quad \gamma \mathbf{u}_f^{n+1} \cdot \boldsymbol{\tau}_f + (\boldsymbol{\sigma}_f^{n+1} \mathbf{n}_f) \cdot \boldsymbol{\tau}_f = \mu_\tau^{n+1}$$

and the Biot solution satisfies weakly the Robin boundary conditions

$$\begin{aligned} & \gamma (\mathbf{u}_p^{n+1} + d_t \boldsymbol{\eta}_p^{n+1}) \cdot \mathbf{n}_p + (\boldsymbol{\sigma}_p^{n+1} \mathbf{n}_p) \cdot \mathbf{n}_p = \mu_n^{n+1} - 2\gamma \mathbf{u}_f^{n+1} \cdot \mathbf{n}_f, \\ & \gamma d_t \boldsymbol{\eta}_p^{n+1} \cdot \boldsymbol{\tau}_p + (\boldsymbol{\sigma}_p^{n+1} \mathbf{n}_p) \cdot \boldsymbol{\tau}_p = \mu_\tau^{n+1} - 2\gamma \mathbf{u}_f^{n+1} \cdot \boldsymbol{\tau}_f, \\ & \gamma (\mathbf{u}_p^{n+1} + d_t \boldsymbol{\eta}_p^{n+1}) \cdot \mathbf{n}_p - p_p^{n+1} = \mu_n^{n+1} - 2\gamma \mathbf{u}_f^{n+1} \cdot \mathbf{n}_f, \end{aligned}$$

it follows that conditions

$$\boldsymbol{\sigma}_f^{n+1} \mathbf{n}_f + \boldsymbol{\sigma}_p^{n+1} \mathbf{n}_p = \mathbf{0} \quad \text{and} \quad -(\boldsymbol{\sigma}_f^{n+1} \mathbf{n}_f) \cdot \mathbf{n}_f = p_p^{n+1}$$

are satisfied weakly, i.e., the balance of stress conditions (2.9) hold weakly for the solution of the method.

To the best of our knowledge, the fully implicit scheme (6.12)–(6.17) has not been studied in the literature. The argument above proves existence of a solution. We next establish uniqueness and stability. To this end, we define a modified energy term

$$\widehat{\mathcal{E}}^n = \frac{\rho_f}{2} \|\mathbf{u}_f^n\|_{L^2(\Omega_f)}^2 + \frac{\rho_p}{2} \|d_t \boldsymbol{\eta}_p^n\|_{L^2(\Omega_p)}^2 + \frac{1}{2} \|\boldsymbol{\eta}_p^n\|_e^2 + \frac{s_0}{2} \|p_p^n\|_{L^2(\Omega_p)}^2,$$

which is the energy term \mathcal{E}^n from (4.6) without the terms involving μ_n^n and μ_τ^n . Again for simplicity we let $\mathbf{f}_f = \mathbf{f}_p = q_f = q_p = 0$.

Theorem 6.2. *The method (6.12)–(6.17) has a unique solution satisfying the energy equality*

$$\widehat{\mathcal{E}}^N + \Delta t \sum_{n=1}^N \mathcal{D}^n + \sum_{n=1}^N \mathcal{S}^n \leq \widehat{\mathcal{E}}^0. \quad (6.18)$$

Proof. We take $\mathbf{v}_f = \mathbf{u}_f^{n+1}$, $w_f = p_f^{n+1}$, $\mathbf{v}_p = \mathbf{u}_p^{n+1}$, $w_p = p_p^{n+1}$, $\boldsymbol{\xi}_p = d_t \boldsymbol{\eta}_p^{n+1}$, $\chi_n = \mu_n^{n+1}$, and $\chi_\tau = \mu_\tau^{n+1}$ in (6.12)–(6.17) and sum the equations. In a way similar to (4.11) and (4.13), we obtain

$$\begin{aligned} & (\rho_f d_t \mathbf{u}_f^{n+1}, \mathbf{u}_f^{n+1})_{\Omega_f} + a_f(\mathbf{u}_f^{n+1}, \mathbf{u}_f^{n+1}) + (\rho_p d_{tt} \boldsymbol{\eta}_p^{n+1}, d_t \boldsymbol{\eta}_p^{n+1})_{\Omega_p} + a_p^e(\boldsymbol{\eta}_p^{n+1}, d_t \boldsymbol{\eta}_p^{n+1}) \\ & + a_p^d(\mathbf{u}_p^{n+1}, \mathbf{u}_p^{n+1}) + s_0(d_t p_p^{n+1}, p_p^{n+1})_{\Omega_p} \leq 0, \end{aligned}$$

We remark that all terms involving μ_n^{n+1} and μ_τ^{n+1} cancel out. Then (6.18) follows by using (4.2), multiplying by Δt , and summing over n .

The energy balance (6.18) implies uniqueness for \mathbf{u}_f^n , $\boldsymbol{\eta}_p^n$, \mathbf{u}_p^n , and p_p^n . Uniqueness for p_f^n and $\boldsymbol{\mu}^n$ follows from the argument used to establish that $\bar{p}_f^k \rightarrow 0$ and $\bar{\boldsymbol{\mu}}^k \rightarrow 0$ in the proof of Theorem 6.1. \square

Remark 6.2. *As noted above, the monolithic scheme (6.12)–(6.17) is new. The scheme warrants further studies. Since the Lagrange multiplier is based on Robin transmission conditions, the method may be more robust in the regime of large added-mass-effect when the system is preconditioned with subdomain solves compared to monolithic schemes based on Dirichlet or Neumann transmission conditions. This is a possible topic of future research.*

7 Numerical results

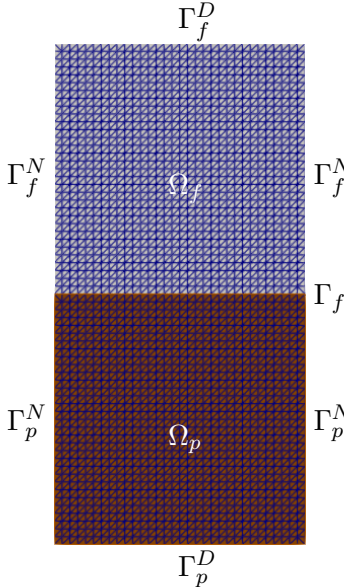
This section presents results from two numerical tests in two dimensions. We start with checking the convergence rates in time for the Robin-Robin algorithm (3.15)–(3.21), its iterative version (6.1)–(6.6), and the monolithic scheme (6.12)–(6.17). The convergence test is also used to assess the robustness of the Robin-Robin algorithm in both the non-iterative and iterative versions to changes in the value of the Robin parameter. Next, we consider a simplified blood flow problem to illustrate the behavior of the methods for a computationally challenging choice of physical parameters.

All results have been obtained with FreeFem++ [31], using triangular grids. For spatial discretization we use the following finite element spaces: the Taylor-Hood continuous $\mathcal{P}_2 - \mathcal{P}_1$ elements for the velocity–pressure pair in the Stokes problem, the Raviart-Thomas $\mathcal{RT}_1 - \mathcal{P}_1^{dc}$ elements for the Darcy velocity and pressure, and continuous \mathcal{P}_2 elements for the structure displacement and the trace function μ .

7.1 Example 1: convergence test

In order to check the convergence rates in time, we consider an analytical solution in domains $\Omega_f = (0, 1) \times (0, 1)$ and $\Omega_p = (0, 1) \times (-1, 0)$ with interface $\Gamma_{fp} = (0, 1) \times \{0\}$ over time interval $(0, 1]$. We take $\Gamma_f^D = (0, 1) \times \{1\}$, $\Gamma_f^N = \{0\} \times (0, 1) \cup \{1\} \times (0, 1)$, $\Gamma_p^D = \tilde{\Gamma}_p^D = (0, 1) \times \{-1\}$, and $\Gamma_p^N = \tilde{\Gamma}_p^N = \{0\} \times (-1, 0) \cup \{1\} \times (-1, 0)$. See the computational domain in Figure 2 (left) and the analytical solution in Figure 2 (right). We note that the analytical solution satisfies the appropriate interface conditions on Γ_{fp} .

The model parameters are set as follows: $\mu_f = 1$, $\rho_f = 1$, $\rho_p = 1$, $\mu_p = 1$, $\lambda_p = 1$, $s_0 = 1$, $K = \mathcal{I}_{2 \times 2}$, $\alpha = 1$, $\gamma_{BJS} = 0$, $\gamma_f = \gamma_p = \gamma = 1$. The forcing terms $\mathbf{f}_f, q_f, \mathbf{f}_p$ and q_p are found by plugging the



$$\begin{aligned}
& \mathbf{u}_f = \pi \cos(\pi t) \begin{pmatrix} -3x + \cos(y) \\ y + 1 \end{pmatrix}, \\
& p_f = \exp(t) \sin(\pi x) \cos\left(\frac{\pi y}{2}\right) + 2\pi \cos(\pi t), \\
& p_p = \exp(t) \sin(\pi x) \cos\left(\frac{\pi y}{2}\right), \\
& \mathbf{u}_p = -\frac{1}{\mu_f} K \nabla p_p, \\
& \boldsymbol{\eta}_p = \sin(\pi t) \begin{pmatrix} -3x + \cos(y) \\ y + 1 \end{pmatrix}.
\end{aligned}$$

Figure 2: Example 1, left: computational domain and mesh; right: analytical solution.

analytical solution in (2.3)–(2.7). Similarly, appropriate data for the Dirichlet and Neumann boundary conditions and initial conditions are derived from the exact solution.

The structured mesh used in the convergence study, obtained by setting the mesh size h to $1/32$, is shown in Figure 2 (left). The choice of the mesh size is so that the spatial discretization error does not affect the convergence rates in time.

For the time convergence study, we consider the time interval $[0, 1]$ and a sequence of progressively smaller time steps: $\Delta t = 0.2, 0.1, 0.05, 0.025, 0.0125$. Table 1 reports numerical errors for the Stokes, Biot, and auxiliary interface variables in the space-time norms bounded in the analysis, as well as the corresponding convergence rates in time for the non-iterative Robin-Robin algorithm. We note that the error for the interface variable $\boldsymbol{\mu}$ is reported in the $L^2(\Gamma_{fp})$ norm, which is stronger, but easier to compute than the $H^{-1/2}(\Gamma_{fp})$ norm that appears in the analysis. As the time step gets smaller, we observe that the rate of convergence approaches one (i.e., the expected rate) for all variables. Furthermore, Tables 2 and 3 report the errors and rates for the iterative Robin-Robin algorithm and the monolithic scheme, respectively. We also present the results from the iterative Robin-Robin algorithm with a fixed number of 10 iterations at each time step in Table 4. First order convergence in time is observed for all variables for all methods. To ease the comparison for selected variables, namely \mathbf{u}_f , \mathbf{u}_p , $\boldsymbol{\eta}_p$, Figure 3 (first row) shows the convergence plots. We see that, as one would expect, the errors in the iterative Robin-Robin algorithm are indistinguishable from the errors in the monolithic scheme (identical for the number of digits reported in the tables), while the errors in the non-iterative Robin-Robin method are slightly larger. We recall that, in the case of the iterative algorithm, the increased accuracy comes with an increased computational cost, since every time step requires the solution of multiple Stokes and Biot problems; see the last column in Table 2 for the average number of iterations required to satisfy the stopping criterion (6.6), with the maximum number of iterations set to 100. However, we also observe from Table 4 and Figure 3 (first row) that even not running the iterative scheme to convergence, but only taking a small number of iterations (10), also gives results very close to the monolithic scheme.

Δt	$\ e_{\mathbf{u}_f}\ _{L^\infty(H^1(\Omega_f))}$		$\ e_{p_f}\ _{L^2(L^2(\Omega_f))}$		$\ e_{\mathbf{u}_p}\ _{L^2(H(div;\Omega_p))}$		$\ e_{p_p}\ _{L^\infty(L^2(\Omega_p))}$	
0.2	1.663e+00	Rate	1.706e+00	Rate	1.800e+00	Rate	3.112e-01	Rate
0.1	9.071e-01	0.87	8.999e-01	0.92	1.046e+00	0.78	1.827e-01	0.72
0.05	4.768e-01	0.92	4.640e-01	0.95	5.825e-01	0.84	1.023e-01	0.83
0.025	2.449e-01	0.96	2.360e-01	0.97	3.113e-01	0.90	5.497e-02	0.89
0.0125	1.247e-01	0.97	1.191e-01	0.98	1.617e-01	0.94	2.855e-02	0.94

Δt	$\ e_{\boldsymbol{\eta}_p}\ _{L^\infty(H^1(\Omega_p))}$		$\ e_{\partial_t \boldsymbol{\eta}_p}\ _{L^\infty(L^2(\Omega_p))}$		$\ e_\mu\ _{L^\infty(L^2(\Gamma_{fp}))}$	
0.2	1.966e+00	Rate	1.578e+00	Rate	2.369e+00	Rate
0.1	1.183e+00	0.73	8.996e-01	0.81	1.311e+00	0.85
0.05	6.675e-01	0.82	4.808e-01	0.90	6.857e-01	0.93
0.025	3.589e-01	0.89	2.491e-01	0.94	3.479e-01	0.97
0.0125	1.868e-01	0.94	1.270e-01	0.97	1.745e-01	0.99

Table 1: Example 1, numerical errors and convergence rates in time for the non-iterative Robin-Robin algorithm.

Δt	$\ e_{\mathbf{u}_f}\ _{L^\infty(H^1(\Omega_f))}$		$\ e_{p_f}\ _{L^2(L^2(\Omega_f))}$		$\ e_{\mathbf{u}_p}\ _{L^2(H(div;\Omega_p))}$		$\ e_{p_p}\ _{L^\infty(L^2(\Omega_p))}$	
0.2	1.233e+00	Rate	1.537e+00	Rate	1.730e+00	Rate	2.855e-01	Rate
0.1	6.481e-01	0.92	7.809e-01	0.97	1.005e+00	0.78	1.700e-01	0.74
0.05	3.331e-01	0.96	3.936e-01	0.98	5.602e-01	0.84	9.646e-02	0.81
0.025	1.686e-01	0.98	1.977e-01	0.99	2.998e-01	0.90	5.169e-02	0.90
0.0125	8.473e-02	0.99	9.911e-02	0.99	1.559e-01	0.94	2.686e-02	0.94

Δt	$\ e_{\boldsymbol{\eta}_p}\ _{L^\infty(H^1(\Omega_p))}$		$\ e_{\partial_t \boldsymbol{\eta}_p}\ _{L^\infty(L^2(\Omega_p))}$		$\ e_\mu\ _{L^\infty(L^2(\Gamma_{fp}))}$		# iter
0.2	1.520e+00	Rate	1.553e+00	Rate	1.853e+00	Rate	96.60
0.1	8.827e-01	0.78	8.933e-01	0.79	9.848e-01	0.91	89.20
0.05	4.938e-01	0.83	4.803e-01	0.89	5.123e-01	0.94	76.50
0.025	2.659e-01	0.89	2.497e-01	0.94	2.625e-01	0.96	65.45
0.0125	1.388e-01	0.93	1.276e-01	0.96	1.337e-01	0.97	55.10

Table 2: Example 1, numerical errors and convergence rates in time for the iterative Robin-Robin algorithm. The last column reports the average number of iterations required to satisfy the stopping criterion (6.6).

7.1.1 Robustness to the Robin parameter γ

In this subsection, we study the robustness of the Robin-Robin schemes to the value of γ , which is obviously a key parameter. All the parameters are set as previously, with the exception of $\gamma = \gamma_f = \gamma_p$, which will take different values. In practice, it is reasonable to set γ so that the magnitudes of the velocity and stress terms in the Robin combination are comparable. While these can be inferred from the physical data and/or preliminary simulation results, some degree of robustness to γ is desirable.

First, we consider the non-iterative Robin-Robin scheme and the effect of γ on the numerical errors. Figure 4 shows the convergence plots for \mathbf{u}_f , \mathbf{u}_p , $\boldsymbol{\eta}_p$ for $\gamma = 0.001, 0.01, 0.1, 1, 10, 100$. For all variables, we observe first order convergence for $\gamma = 0.01, 0.1, 1, 10$, with the rates approaching first order as $\Delta t \rightarrow 0$ for $\gamma = 100$. However, the convergence rate deteriorates for $\gamma = 0.001$. The different variables exhibit somewhat different sensitivity to γ , with \mathbf{u}_f being slightly more sensitive than \mathbf{u}_p and $\boldsymbol{\eta}_p$. The general trend is that the errors are similar for $\gamma \in [0.01, 10]$ and the errors increase if γ is too small or too

Δt	$\ e_{\mathbf{u}_f}\ _{L^\infty(H^1(\Omega_f))}$		$\ e_{p_f}\ _{L^2(L^2(\Omega_f))}$		$\ e_{\mathbf{u}_p}\ _{L^2(H(div;\Omega_p))}$		$\ e_{p_p}\ _{L^\infty(L^2(\Omega_p))}$	
0.2	1.233e+00	Rate	1.537e+00	Rate	1.730e+00	Rate	2.855e-01	Rate
0.1	6.481e-01	0.92	7.809e-01	0.97	1.005e+00	0.78	1.700e-01	0.74
0.05	3.331e-01	0.96	3.936e-01	0.98	5.602e-01	0.84	9.646e-02	0.81
0.025	1.686e-01	0.98	1.977e-01	0.99	2.998e-01	0.90	5.169e-02	0.90
0.0125	8.473e-02	0.99	9.911e-02	0.99	1.559e-01	0.94	2.686e-02	0.94

Δt	$\ e_{\boldsymbol{\eta}_p}\ _{L^\infty(H^1(\Omega_p))}$		$\ e_{\partial_t \boldsymbol{\eta}_p}\ _{L^\infty(L^2(\Omega_p))}$		$\ e_\mu\ _{L^\infty(L^2(\Gamma_{fp}))}$	
0.2	1.520e+00	Rate	1.553e+00	Rate	1.865e+00	Rate
0.1	8.827e-01	0.78	8.933e-01	0.79	9.887e-01	0.91
0.05	4.938e-01	0.83	4.803e-01	0.89	5.130e-01	0.94
0.025	2.659e-01	0.89	2.497e-01	0.94	2.626e-01	0.96
0.0125	1.388e-01	0.93	1.276e-01	0.96	1.337e-01	0.97

Table 3: Example 1, numerical errors and convergence rates in time for the monolithic scheme.

Δt	$\ e_{\mathbf{u}_f}\ _{L^\infty(H^1(\Omega_f))}$		$\ e_{p_f}\ _{L^2(L^2(\Omega_f))}$		$\ e_{\mathbf{u}_p}\ _{L^2(H(div;\Omega_p))}$		$\ e_{p_p}\ _{L^\infty(L^2(\Omega_p))}$	
0.2	1.240e+00	Rate	1.537e+00	Rate	1.731e+00	Rate	2.862e-01	Rate
0.1	6.491e-01	0.93	7.807e-01	0.97	1.006e+00	0.78	1.704e-01	0.74
0.05	3.325e-01	0.96	3.934e-01	0.98	5.603e-01	0.84	9.659e-02	0.81
0.025	1.676e-01	0.98	1.974e-01	0.99	2.995e-01	0.90	5.162e-02	0.90
0.0125	8.365e-02	1.00	9.866e-02	1.00	1.554e-01	0.94	2.662e-02	0.94

Δt	$\ e_{\boldsymbol{\eta}_p}\ _{L^\infty(H^1(\Omega_p))}$		$\ e_{\partial_t \boldsymbol{\eta}_p}\ _{L^\infty(L^2(\Omega_p))}$		$\ e_\mu\ _{L^\infty(L^2(\Gamma_{fp}))}$		# iter
0.2	1.512e+00	Rate	1.553e+00	Rate	1.828e+00	Rate	10.00
0.1	8.877e-01	0.78	8.933e-01	0.79	9.658e-01	0.92	10.00
0.05	4.903e-01	0.83	4.803e-01	0.89	5.020e-01	0.94	10.00
0.025	2.637e-01	0.89	2.497e-01	0.94	2.583e-01	0.95	10.00
0.0125	1.373e-01	0.94	1.276e-01	0.96	1.324e-01	0.96	10.00

Table 4: Example 1, numerical errors and convergence rates in time for the iterative Robin-Robin algorithm with 10 iterations per time step.

large. We note that for the range $\gamma \in [0.01, 10]$ the magnitudes of the velocity and stress terms in the Robin combination are comparable. The increase in errors for extreme values of γ can be explained from the theoretical estimate, which has terms proportional to both γ^2 , cf. (5.37) and $1/\gamma^2$, cf. (5.34). We conjecture that the reason for the reduced convergence rate with $\gamma = 0.001$ is that velocity continuity is not properly enforced by the Robin transmission conditions. We finally note that both the converged iterative scheme and the iterative scheme with 10 iterations give smaller errors and recover first order convergence in time for the extreme values $\gamma = 0.001, 100$, see the second and third rows in Figure 3. Moreover, in Figure 5 we present the convergence plots for $\mathbf{u}_f, \mathbf{u}_p, \boldsymbol{\eta}_p$ with $\gamma = 0.001, 0.01, 0.1, 1, 10, 100$ for the iterative method with 10 iterations and note that the sensitivity to γ is significantly reduced compared to the non-iterative method.

Next, we consider the iterative scheme and the effect of γ on the number of iterations. We take the same values of γ used above, i.e., $\gamma = 0.001, 0.01, 0.1, 1, 10, 100$. Table 5 lists the average number of iterations needed for convergence for each γ value. We observe that, for a given value of γ , the average number of iterations required to satisfy the stopping criterion (6.6) per time step decreases as the time step size is reduced. On the other hand, for a given time step the average number of iterations varies

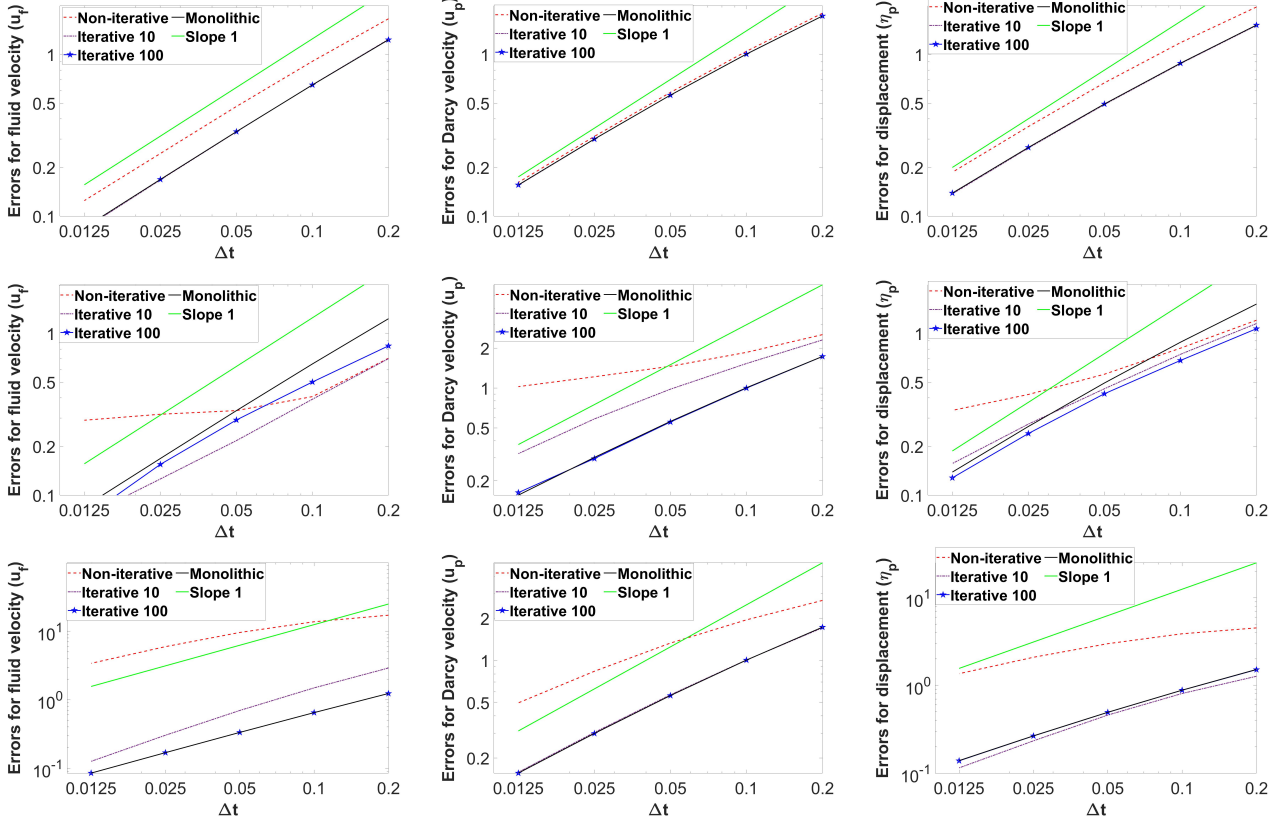


Figure 3: Example 1, convergence plots for fluid velocity \mathbf{u}_f (left), Darcy velocity \mathbf{u}_p (center), and displacement $\boldsymbol{\eta}_p$ (right) for $\gamma = 1$ (first row), $\gamma = 0.001$ (second row), and $\gamma = 100$ (third row) computed by the non-iterative and iterative Robin-Robin methods and the monolithic method.

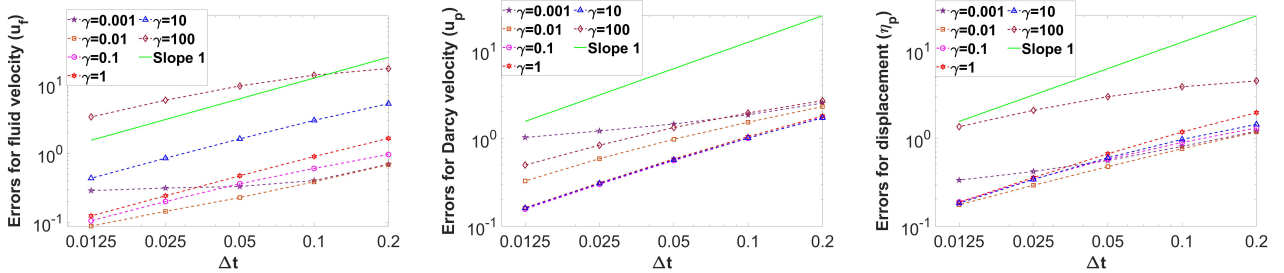


Figure 4: Example 1, convergence plots for fluid velocity \mathbf{u}_f (left), Darcy velocity \mathbf{u}_p (center) and displacement $\boldsymbol{\eta}_p$ (right) for the non-iterative Robin-Robin algorithm for different values of γ .

considerably with γ , with $\gamma = 0.1$ being the “optimal” value. This value is in the range $[0.01, 10]$ of values for γ that resulted in smaller time discretization errors for the non-iterative scheme. We conclude that values of γ in the “optimal” range, where the magnitudes of the velocity and stress terms in the Robin combination are comparable, result in both smaller errors in the non-iterative scheme and faster convergence in the iterative scheme.

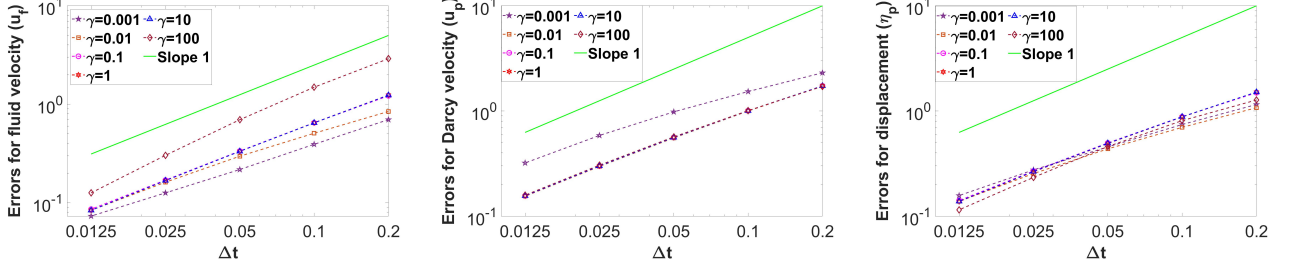


Figure 5: Example 1, convergence plots for fluid velocity \mathbf{u}_f (left), Darcy velocity \mathbf{u}_p (center) and displacement $\boldsymbol{\eta}_p$ (right) for the iterative Robin-Robin algorithm with 10 iterations per time step for different values of γ .

Δt	$\gamma = 0.001$	$\gamma = 0.01$	$\gamma = 0.1$	$\gamma = 1$	$\gamma = 10$	$\gamma = 100$
0.2	100.00	94.40	26.80	96.60	49.00	99.80
0.1	100.00	86.70	20.20	89.20	43.70	93.90
0.05	100.00	54.20	17.05	76.50	39.20	67.65
0.025	76.20	23.675	12.60	65.45	34.97	46.525
0.0125	31.45	13.3375	8.72	55.10	30.96	32.325

Table 5: Example 1, average number of iterations required to satisfy the stopping criterion (6.6) per time step of the iterative Robin-Robin scheme for different values of γ .

7.2 Example 2: blood flow test

In this example, we test the behavior of the method for a computationally challenging choice of physical parameters. We consider a benchmark on modeling blood flow through a section of an idealized artery. The Stokes equations model the blood flow in the lumen of the artery and the Biot equations model the arterial wall. Let R and L be the radius and length of the artery, respectively. The fluid domain is $\Omega_f = (0, L) \times (-R, R)$. Its top and bottom boundaries are in contact with the poroelastic arterial wall of thickness r_p . See the computational domain in Figure 6 (left).

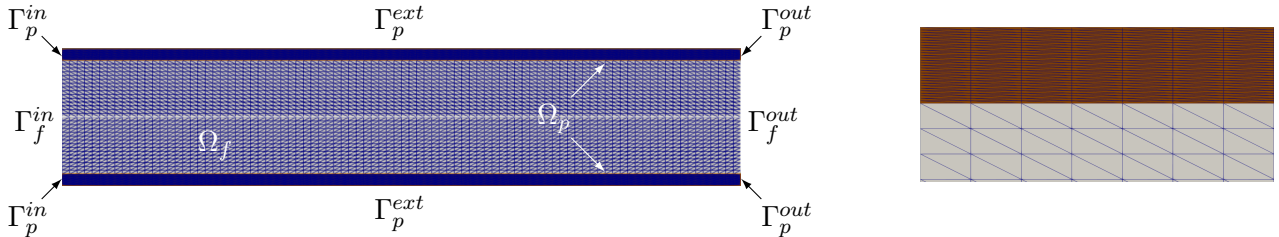


Figure 6: Example 2, left: computational domain and mesh; right: zoomed-in view of the mesh at the fluid-structure interface.

Since this is a 2D problem representing a slice of a 3D problem, we add an extra term to (2.5) to account for the fact that the 2D structure is actually part of a 3D cylindrical tube:

$$\rho_p \partial_{tt} \boldsymbol{\eta}_p - \nabla \cdot \boldsymbol{\sigma}_p + \beta \boldsymbol{\eta}_p = \mathbf{f}_p \quad \text{in } \Omega_p \times (0, T],$$

where ρ_p is the fluid density in the poroelastic region. The additional term (i.e., the last term at the left-hand side) comes from the axially symmetric two dimensional formulation, accounting for the recoil

due to the circumferential strain [4]. The body force terms \mathbf{f}_f and \mathbf{f}_p and external source q_p are set to zero.

Let $\Gamma_f^{in} = \{(0, y) | -R < y < R\}$ and $\Gamma_f^{out} = \{(L, y) | -R < y < R\}$ be the inlet and outlet boundaries of the fluid domain, respectively. Following [34, 38, 46], we prescribe the normal stress at both inlet and outlet:

$$\boldsymbol{\sigma}_f \mathbf{n}_f^{in} = -p_{in}(t) \mathbf{n}_f, \quad \text{on } \Gamma_f^{in} \times (0, T]; \quad \boldsymbol{\sigma}_f \mathbf{n}_f^{out} = \mathbf{0}, \quad \text{on } \Gamma_f^{out} \times (0, T]; \quad (7.1)$$

where \mathbf{n}_f^{in} and \mathbf{n}_f^{out} are the respective outward unit normals and

$$p_{in}(t) = \begin{cases} \frac{P_{\max}}{2} \left(1 - \cos \left(\frac{2\pi t}{T_{\max}} \right) \right), & \text{if } t \leq T_{\max}; \\ 0, & \text{if } t > T_{\max}, \end{cases} \quad (7.2)$$

with $P_{\max} = 13,334 \text{ dyn/cm}^2$ and $T_{\max} = 0.003 \text{ s}$. flow distribution and pressure field are often unknown, they are common in blood flow models. In a system in rest state, this inlet boundary condition generates a pressure pulse that travels through the fluid and poroelastic structure domains. We set the end of the time interval of interest to $T = 0.021 \text{ s}$ to avoid the pressure pulse reaching the outlet boundary.

With similar notation, we denote with $\Gamma_p^{in} = \{(0, y) | -R - r_p < y < R \text{ or } R < y < R + r_p\}$ and $\Gamma_p^{out} = \{(L, y) | -R - r_p < y < R \text{ or } R < y < R + r_p\}$ the inlet and outlet boundaries of the poroelastic structure, respectively. We assume that the poroelastic structure is fixed at the inlet and outlet boundaries:

$$\boldsymbol{\eta}_p = \mathbf{0}, \quad \text{on } \Gamma_p^{in} \cup \Gamma_p^{out} \times (0, T], \quad (7.3)$$

and for the Darcy velocity we impose the following drained boundary condition:

$$\mathbf{u}_p = \mathbf{0}, \quad \text{on } \Gamma_p^{in} \cup \Gamma_p^{out} \times (0, T]. \quad (7.4)$$

Let $\Gamma_p^{ext} = \{(x, y) | 0 < x < L, y = -R - r_p \text{ or } y = R + r_p\}$ be the external structure boundary. Following [46], therein we impose:

$$\begin{aligned} (\boldsymbol{\sigma}_e \mathbf{n}_p) \cdot \mathbf{n}_p &= 0, & \text{on } \Gamma_p^{ext} \times (0, T], \\ \boldsymbol{\eta}_p \cdot \boldsymbol{\tau}_p &= 0, & \text{on } \Gamma_p^{ext} \times (0, T], \\ p_p &= 0, & \text{on } \Gamma_p^{ext} \times (0, T]. \end{aligned} \quad (7.5)$$

To save computational time, we halve the domain in Figure 6 (left) along the horizontal symmetry axis, denoted with Γ_f^{sym} , and impose the following symmetry conditions therein:

$$\begin{aligned} \mathbf{u}_f \cdot \mathbf{n}_f &= 0, & \text{on } \Gamma_f^{sym} \times (0, T], \\ (\boldsymbol{\sigma}_f \mathbf{n}_f) \cdot \boldsymbol{\tau}_f &= 0, & \text{on } \Gamma_f^{sym} \times (0, T]. \end{aligned} \quad (7.6)$$

The geometric and physical parameters for this test are summarized Table 6. The physical parameters are chosen within the range of physical values for arterial blood flow.

Remark 7.1. *The physical parameters in Table 6 present several computational challenges. The closeness of the fluid density ρ_f and poroelastic wall density ρ_p may lead to the so-called added-mass-effect, which causes stability and convergence issues for classical Neumann-Dirichlet methods [5, 20]. The small values of permeability K and storativity s_0 may lead to poroelastic locking. The high stiffness of the arterial wall due to large Lamé parameters λ_p and μ_p results in large stress along the interface and affects the choice of the Robin parameter γ .*

Parameter	Symbol	Units	Reference value
Radius	R	cm	0.5
Length	L	cm	6
Poroelastic wall thickness	r_p	cm	0.1
Poroelastic wall density	ρ_p	g/cm ³	1.1
Fluid density	ρ_f	g/cm ³	1.0
Dyn. viscosity	μ_f	g/cm-s	0.035
Spring coeff.	β	dyn/cm ⁴	4×10^6
Mass storativity	s_0	cm ² /dyn	10^{-3}
Permeability	K	cm ²	$diag(1, 1) \times 10^{-6}$
Lamé coeff.	μ_p	dyn/cm ²	5.575×10^5
Lamé coeff.	λ_p	dyn/cm ²	1.7×10^6
BJS coeff.	α_{BJS}		1
Biot-Willis constant	α		1

Table 6: Example 2, geometric and physical parameters.

The computational mesh is shown in Figure 6 (left), with a zoomed-in view around the fluid-structure interface in Figure 6 (right). The time step is set to $\Delta t = 10^{-4}$ s. Regarding the choice of the Robin parameter γ , the $O(10^6)$ values of λ_p and β indicate that the stress is several orders of magnitude larger than the velocity, suggesting a large value of γ . With estimated magnitudes $O(1)$ for the interface velocity and $O(10^3)$ for the interface stress, obtained from a preliminary computation, we set $\gamma_f = \gamma_p = \gamma = 1000$ in order to balance the two terms in the Robin combination. We later test the robustness of the non-iterative method for different values of γ .

Figure 7 shows the fluid pressure p_f and Darcy pressure p_p in their corresponding domains computed by the Robin-Robin scheme in the non-iterative version and the monolithic scheme at three different times. We clearly see the propagation of the pressure wave and an excellent qualitative match in the pressures computed by the two methods. Figure 8 shows the velocity fields \mathbf{u}_f and \mathbf{u}_p computed by the same two schemes at the same times used in Figure 7. Again, we see a great qualitative match in the solutions computed by the two methods. The faint lines that can be seen along the horizontal symmetry line in the plots in Figure 7 and 8 are due to the fact that we have solved the problem on half of the domain and mirrored the results in Paraview to show the entire vessel.

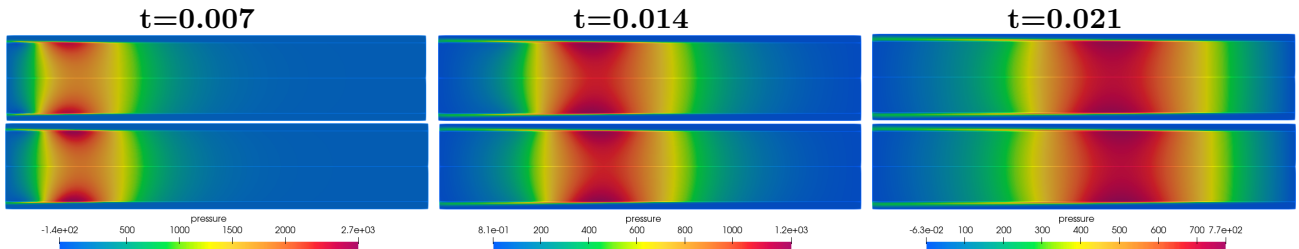


Figure 7: Example 2, fluid and Darcy pressure computed by the non-iterative Robin-Robin scheme (top) and the monolithic scheme (bottom) at times $t = 0.007, 0.014, 0.021$ s (from left to right).

To further compare the solutions given by the different methods, Figure 9 displays the fluid pressure, vertical fluid velocity, vertical Darcy velocity, and vertical structure displacement along the interface computed at different times by the non-iterative and iterative Robin-Robin methods, and the monolithic

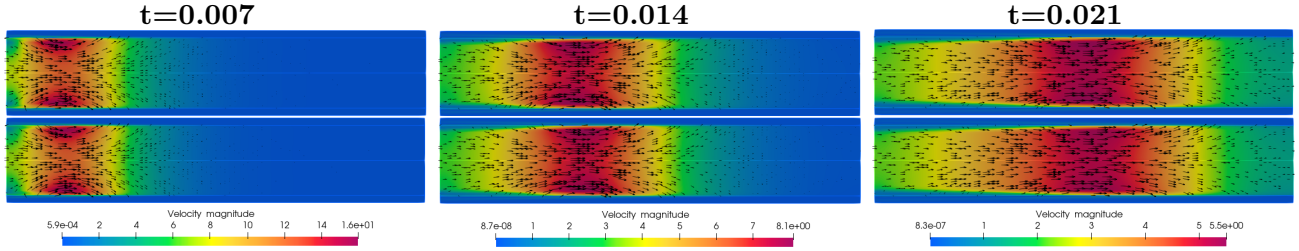


Figure 8: Example 2, fluid and Darcy velocity computed by the non-iterative Robin-Robin scheme (top) and the monolithic scheme (bottom) at times $t = 0.007, 0.014, 0.021$ s (from left to right). The arrows represent the velocity vectors and the color represents the velocity magnitudes.

method. We see that the curves given by the iterative Robin-Robin method and the monolithic method overlap. There is a slight difference with the curves given by the non-iterative Robin-Robin method, which becomes less noticeable as time passes. It seems that initially the lack of iterations in the Robin-Robin method slows down the wave. Overall, we conclude that the non-iterative Robin-Robin method provides accuracy comparable to the other two methods.

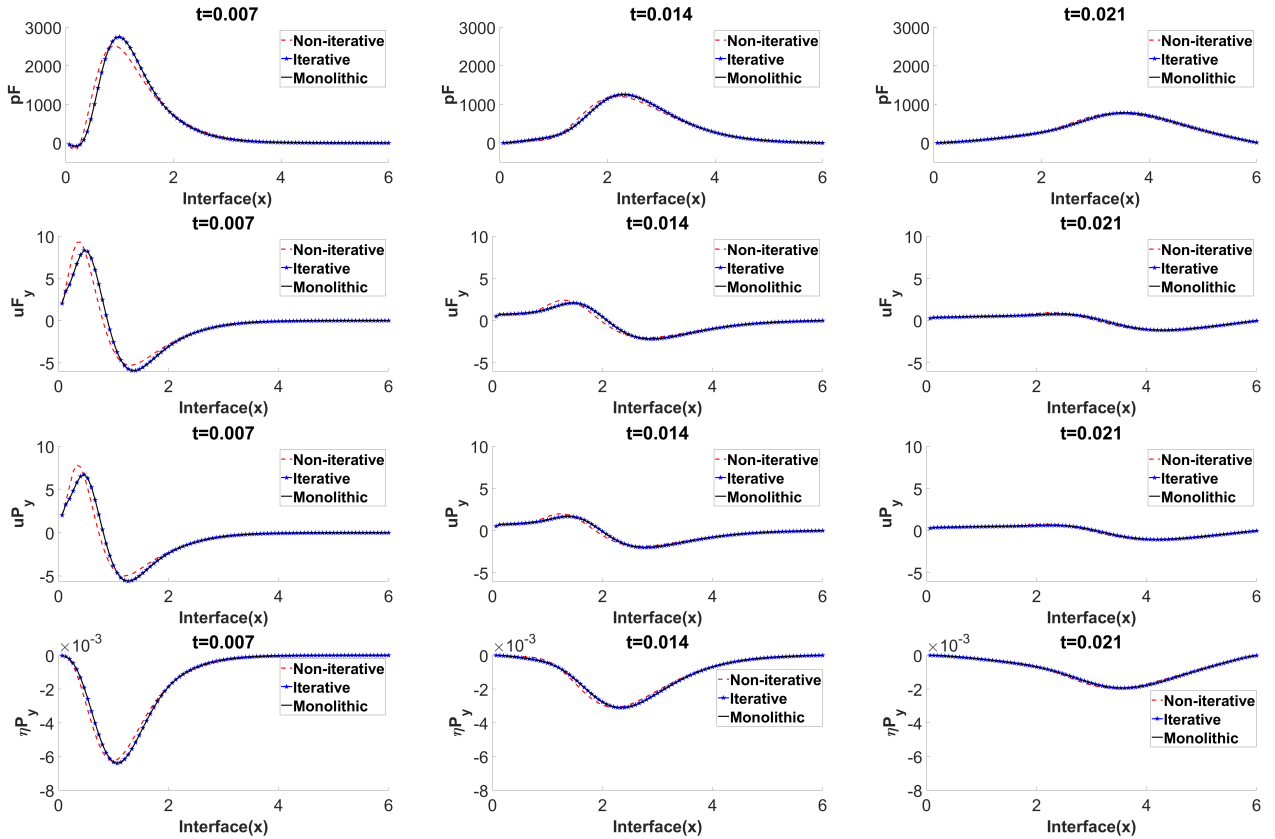


Figure 9: Example 2, fluid pressure (first row), vertical fluid velocity (second row), vertical Darcy velocity (third row), vertical structure displacement (fourth row) along the interface computed by the Robin-Robin method in the non-iterative and iterative versions, and the monolithic method at times $t = 0.007, 0.014, 0.021$ s (from left to right).

Finally, we test the robustness of the non-iterative Robin-Robin method to the Robin parameter γ . Figure 10 shows the solution along the interface for $\gamma = 10, 100, 500, 1000, 2000$. The curves for $\gamma = 100, 500, 1000$ are very similar and the curves for $\gamma = 2000$ deviate from them slightly. The curves for $\gamma = 10$ are significantly different. As in the previous example, we conclude that there is a range of values of γ , for which the two terms in the Robin combination are of comparable magnitudes, that produce accurate results. Values outside of this range may result in reduction in accuracy, especially values of γ that are too small.

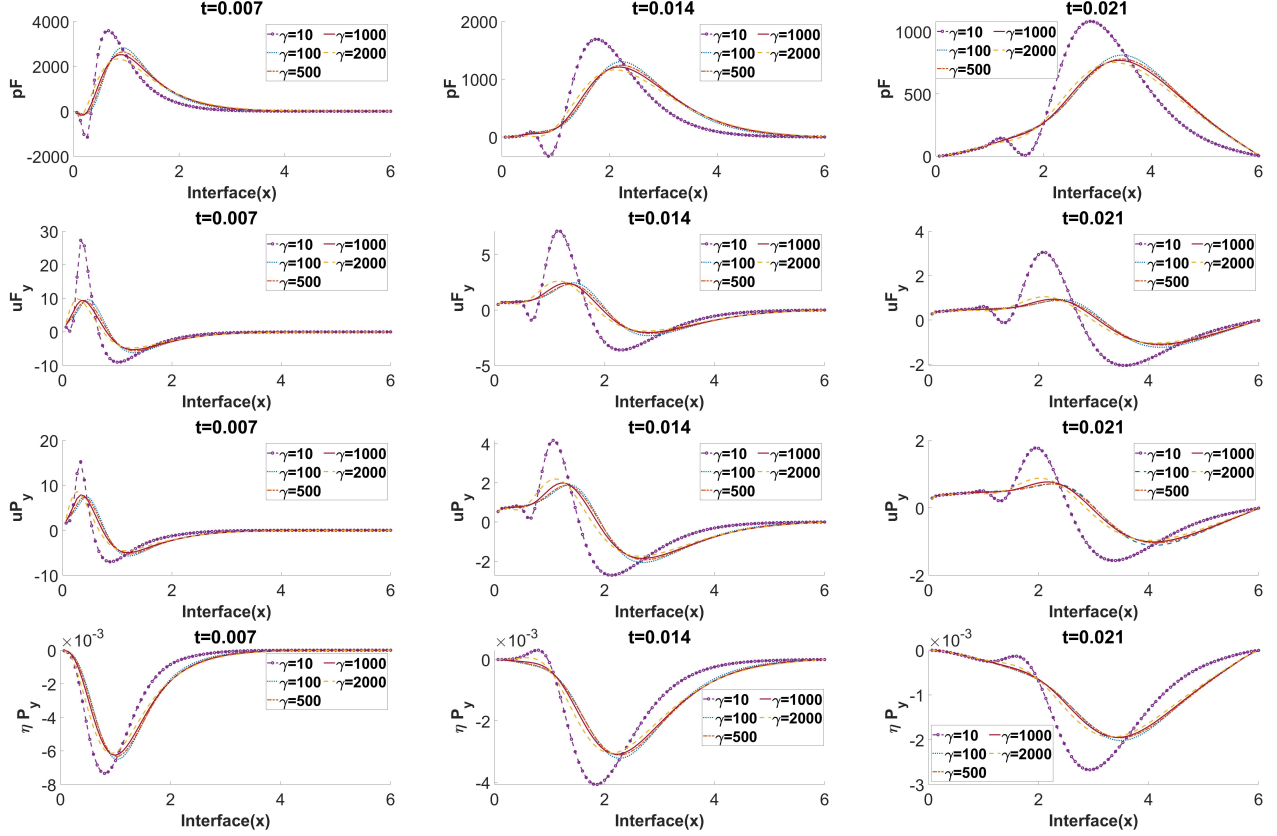


Figure 10: Example 2, fluid pressure (first row), vertical fluid velocity (second row), vertical Darcy velocity (third row), vertical structure displacement (fourth row) along the interface computed by the Robin-Robin method in the non-iterative version at times $t = 0.007, 0.014, 0.021$ s (from left to right) for different values of γ .

8 Conclusions

We developed an iterative and a non-iterative splitting methods for the Stokes-Biot model based on Robin-Robin transmission conditions. The methods utilize an auxiliary interface variable that models the Robin data. It is used to handle properly the insufficient regularity of the normal stress on the interface. With a suitable choice of negative norm for this variable, we established unconditional stability and first order convergence in time for the non-iterative scheme. To the best of our knowledge, this is the first such result in the literature in a general setting for Robin-Robin methods for both fluid-structure

interaction and fluid-poroelastic structure interaction. We further studied the iterative version of the method and established convergence to a new monolithic scheme. We presented two sets of numerical experiments to illustrate the behavior of the methods. In the first example, based on a given analytical solution, we verified the first order time discretization rates and the convergence of the iterative scheme. We also studied the robustness to the Robin parameter γ . For extreme values of γ (too small or too large), for which the accuracy of the non-iterative method deteriorates, we found that employing just a small number of iterations helps to recover optimal rates of convergence. The second example, based on a blood flow modeling benchmark, illustrated the applicability of the methods for computationally challenging physical parameters in the regimes of added-mass-effect and poroelastic locking.

References

- [1] I. Ambartsumyan, V. J. Ervin, T. Nguyen, and I. Yotov. A nonlinear Stokes-Biot model for the interaction of a non-Newtonian fluid with poroelastic media. *ESAIM Math. Model. Numer. Anal.*, 53(6):1915–1955, 2019.
- [2] I. Ambartsumyan, E. Khattatov, T. Nguyen, and I. Yotov. Flow and transport in fractured poroelastic media. *GEM Int. J. Geomath.*, 10(1):1–34, 2019.
- [3] I. Ambartsumyan, E. Khattatov, I. Yotov, and P. Zunino. A Lagrange multiplier method for a Stokes-Biot fluid-poroelastic structure interaction model. *Numer. Math.*, 140(2):513–553, 2018.
- [4] S. Badia, F. Nobile, and C. Vergara. Fluid-structure partitioned procedures based on Robin transmission conditions. *J. Comput. Phys.*, 227(14):7027–7051, 2008.
- [5] S. Badia, A. Quaini, and A. Quarteroni. Coupling Biot and Navier-Stokes equations for modelling fluid-poroelastic media interaction. *J. Comput. Phys.*, 228(21):7986–8014, 2009.
- [6] J. W. Banks, W. D. Henshaw, and D. W. Schwendeman. An analysis of a new stable partitioned algorithm for FSI problems. Part I: Incompressible flow and elastic solids. *J. Comput. Phys.*, 269:108–137, 2014.
- [7] G. Beavers and D. Joseph. Boundary conditions at a naturally impermeable wall. *J. Fluid Mech.*, 30:197–207, 1967.
- [8] M. Biot. General theory of three-dimensional consolidation. *J. Appl. Phys.*, 12:155–164, 1941.
- [9] L. Bociu, S. Canic, B. Muha, and J. T. Webster. Multilayered poroelasticity interacting with Stokes flow. *SIAM J. Math. Anal.*, 53(6):6243–6279, 2021.
- [10] D. Boffi, F. Brezzi, and M. Fortin. *Mixed finite element methods and applications*, volume 44. Springer, 2013.
- [11] W. M. Boon, M. Hornkjøl, M. Kuchta, K.-A. Mardal, and R. Ruiz-Baier. Parameter-robust methods for the Biot-Stokes interfacial coupling without Lagrange multipliers. *J. Comput. Phys.*, 467:Paper No. 111464, 25, 2022.
- [12] M. Bukač, I. Yotov, R. Zakerzadeh, and P. Zunino. Partitioning strategies for the interaction of a fluid with a poroelastic material based on a Nitsche’s coupling approach. *Comput. Methods Appl. Mech. Eng.*, 292:138–170, 2015.

- [13] M. Bukač. A loosely-coupled scheme for the interaction between a fluid, elastic structure and poroelastic material. *J. Comput. Phys.*, 313:377–399, 2016.
- [14] M. Bukač, I. Yotov, and P. Zunino. An operator splitting approach for the interaction between a fluid and a multilayered poroelastic structure. *Numer. Methods Partial Differential Equations*, 31(4):1054–1100, 2015.
- [15] M. Bukač, I. Yotov, and P. Zunino. Dimensional model reduction for flow through fractures in poroelastic media. *ESAIM Math. Model. Numer. Anal.*, 51(4):1429–1471, 2017.
- [16] E. Burman, R. Durst, M. Fernández, and J. Guzmán. Loosely coupled, non-iterative time-splitting scheme based on Robin-Robin coupling: unified analysis for parabolic/parabolic and parabolic/hyperbolic problems. *J. Numer. Math.*, 31(1):59–77, 2023.
- [17] E. Burman, R. Durst, M. A. Fernández, and J. Guzmán. Fully discrete loosely coupled Robin-Robin scheme for incompressible fluid-structure interaction: stability and error analysis. *Numer. Math.*, 151(4):807–840, 2022.
- [18] E. Burman, R. Durst, and J. Guzmán. Stability and error analysis of a splitting method using Robin-Robin coupling applied to a fluid-structure interaction problem. *Numer. Methods Partial Differential Equations*, 38(5):1396–1406, 2022.
- [19] S. Caucao, T. Li, and I. Yotov. A multipoint stress-flux mixed finite element method for the Stokes-Biot model. *Numer. Math.*, 152(2):411–473, 2022.
- [20] P. Causin, J. F. Gerbeau, and F. Nobile. Added-mass effect in the design of partitioned algorithms for fluid-structure problems. *Comput. Methods Appl. Mech. Engrg.*, 194(42-44):4506–4527, 2005.
- [21] A. Cesmelioglu. Analysis of the coupled Navier-Stokes/Biot problem. *J. Math. Anal. Appl.*, 456(2):970–991, 2017.
- [22] A. Cesmelioglu and P. Chidyagwai. Numerical analysis of the coupling of free fluid with a poroelastic material. *Numer. Methods Partial Differential Equations*, 36(3):463–494, 2020.
- [23] A. Cesmelioglu, H. Lee, A. Quaini, K. Wang, and S.-Y. Yi. Optimization-based decoupling algorithms for a fluid-poroelastic system. In *Topics in numerical partial differential equations and scientific computing*, volume 160 of *IMA Vol. Math. Appl.*, pages 79–98. Springer, New York, 2016.
- [24] A. Cesmelioglu, J. J. Lee, and S. Rhebergen. Hybridizable discontinuous Galerkin methods for the coupled Stokes-Biot problem. *Comput. Math. Appl.*, 144:12–33, 2023.
- [25] P. G. Ciarlet. *The finite element method for elliptic problems*, volume Vol. 4 of *Studies in Mathematics and its Applications*. North-Holland Publishing Co., Amsterdam-New York-Oxford, 1978.
- [26] M. Discacciati, A. Quarteroni, and A. Valli. Robin-Robin domain decomposition methods for the Stokes-Darcy coupling. *SIAM J. Numer. Anal.*, 45(3):1246–1268 (electronic), 2007.
- [27] M. A. Fernández. Incremental displacement-correction schemes for incompressible fluid-structure interaction. *Numer. Math.*, 123(1):21–65, 2013.
- [28] G. Gigante and C. Vergara. On the stability of a loosely-coupled scheme based on a Robin interface condition for fluid-structure interaction. *Comput. Math. Appl.*, 96:109–119, 2021.

- [29] V. Girault, D. Vassilev, and I. Yotov. Mortar multiscale finite element methods for Stokes-Darcy flows. *Numer. Math.*, 127(1):93–165, 2014.
- [30] G. Guidoboni, R. Glowinski, N. Cavallini, and S. Canic. Stable loosely-coupled-type algorithm for fluid-structure interaction in blood flow. *J. Comput. Phys.*, 228(18):6916–6937, 2009.
- [31] F. Hecht. New development in freefem++. *J. Numer. Math.*, 20(3-4):251–265, 2012.
- [32] H. Kunwar, H. Lee, and K. Seelman. Second-order time discretization for a coupled quasi-Newtonian fluid-poroelastic system. *Internat. J. Numer. Methods Fluids*, 92(7):687–702, 2020.
- [33] W. J. Layton, F. Schieweck, and I. Yotov. Coupling fluid flow with porous media flow. *SIAM J. Numer. Anal.*, 40(6):2195–2218 (2003), 2002.
- [34] T. Li, S. Caucao, and I. Yotov. An augmented fully mixed formulation for the quasistatic Navier–Stokes–Biot model. *IMA J. Numer. Anal.*, 44(2):1153–1210, 06 2023.
- [35] T. Li and I. Yotov. A mixed elasticity formulation for fluid–poroelastic structure interaction. *ESAIM Math. Model. Numer. Anal.*, 56(1):01–40, 2022.
- [36] M. Lukáčová-Medvid'ová, G. Rusnáková, and A. Hundertmark-Zaušková. Kinematic splitting algorithm for fluid-structure interaction in hemodynamics. *Comput. Methods Appl. Mech. Engrg.*, 265:83–106, 2013.
- [37] M. A. Murad, J. N. Guerreiro, and A. F. D. Loula. Micromechanical computational modeling of secondary consolidation and hereditary creep in soils. *Comput. Methods Appl. Mech. Engrg.*, 190(15-17):1985–2016, 2001.
- [38] C. Parrow and M. Bukač. A Robin-Robin strongly coupled partitioned method for fluid-poroelastic structure interaction. *J. Numer. Math.*, doi:10.1515/jnma-2024-0057, 2025.
- [39] A. Quarteroni and A. Valli. *Domain decomposition methods for partial differential equations*. Oxford Science Publications, 1999.
- [40] R. Ruiz-Baier, M. Taffetani, H. D. Westermeyer, and I. Yotov. The Biot-Stokes coupling using total pressure: formulation, analysis and application to interfacial flow in the eye. *Comput. Methods Appl. Mech. Engrg.*, 389:Paper No. 114384, 30, 2022.
- [41] P. G. Saffman. On the boundary condition at the surface of a porous media. *Stud. Appl. Math.*, 2:93–101, 1971.
- [42] A. Seboldt and M. Bukač. A non-iterative domain decomposition method for the interaction between a fluid and a thick structure. *Numer. Methods Partial Differential Equations*, 37(4):2803–2832, 2021.
- [43] A. Seboldt, O. Oyekole, J. Tambača, and M. Bukač. Numerical modeling of the fluid-porohyperelastic structure interaction. *SIAM J. Sci. Comput.*, 43(4):A2923–A2948, 2021.
- [44] R. E. Showalter. Poroelastic filtration coupled to Stokes flow. In *Control theory of partial differential equations*, volume 242 of *Lect. Notes Pure Appl. Math.*, pages 229–241. Chapman & Hall/CRC, Boca Raton, FL, 2005.

- [45] S. Čanić, Y. Wang, and M. Bukač. A next-generation mathematical model for drug-eluting stents. *SIAM J. Appl. Math.*, 81(4):1503–1529, 2021.
- [46] X. Wang and I. Yotov. A Lagrange multiplier method for the fully dynamic Navier-Stokes-Biot system. arXiv:2503.12240 [math.NA], 2024.